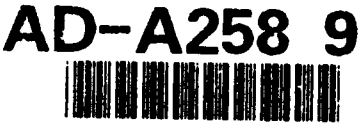

AFIT/GA/ENY/92D-13

PASSIVE DAMPING OF A SOLAR ARRAY

THESIS

Mark A. Scharpen
Lt, USAF

AFIT/GA/ENY/92D-13

Approved for public release; distribution unlimited

AFIT/GA/ENY/92D-13

PASSIVE DAMPING OF A SOLAR ARRAY

THESIS

Presented to the Faculty of the School of Engineering
of the Air Force Institute of Technology
Air University
In Partial Fulfillment of the
Requirements for the Degree of
Master of Science in Astronautical Engineering

Mark A. Scharpen, B. S.
Lt, USAF

December 1992

Preface

This thesis contains elements of theory, design, *and* experimentation. You will find that it is organized in a rather atypical manner. In writing the paper, I tried to communicate my thought processes as they occurred, for a report is supposed to reflect the work that was done. There are several places in the report where it appears that I got sidetracked because peripheral excursions sometimes span several pages. Please bear with these parts of the paper because I feel they have a necessary place in helping show you why I did what I did.

Many people have made this effort possible for me. For about eight months, my wife Holly had to endure many nights without me as I was at school most every weeknight trying to understand what has been a difficult subject area to learn. Few people can complete a concerted effort of this length without someone behind them to give continual encouragement, make several "dine-and-dash" dinners, clean up after them, and be a source of inspiration. Holly has been all of these for me and I am most grateful. Thank you, Holly, for your unwavering faith in me.

Dr. Peter J. Torvik, my thesis advisor, has been extremely helpful to me. He is truly a master of this subject, and his timely advice and valuable counsel saved me countless hours pursuing academic dead ends. I am grateful for his time and for taking an interest in me.

Any student who uses a laboratory knows the value of knowledgeable and experienced technicians. I am thankful to Mr. Jay Anderson for providing me with training on how to use the modal analysis hardware and software. Mr. Andy Mills and Mr. Mark Derriso are appreciated for all of the footwork they did for me, hunting down parts and supplies I would have never found on my own.

Finally, the men of the AFIT Model Fabrication Shop, Mr. Joe Hofele and Mr. Jack Tiffany in particular, are some of the finest craftsmen I have ever met. Their expertise and suggestions resulted in providing me with a test apparatus and damping device of exceedingly high quality. Thank you for giving me a superior effort.

Mark A. Scharpen

Table of Contents

List of Figures

List of Tables

List of Symbols

Symbol	Definition
a_i -	comparison function coefficients
$a_i, b_i, c_i, d_i, e_i, k_i$ -	dummy coefficients for Mindlin and Goodman's method
b -	width of a sandwich beam (in.)
b_1 -	wide sandwich beam width (in.)
b_2 -	slim sandwich beam width (in.)
dx -	differential slice of a structure or beam (in.)
f_i -	time-dependent moment (lb.in.)
g -	shear parameter = $\sqrt{\frac{G}{Et_1t_2}}$ (in.$^{-1}$)
g_i -	comparison function for the ith boundary condition
h -	long lever length (in.)
q_o -	distributed load (lb./in.)
q_i -	coefficients of Appendix B
s -	short lever length (in.)
t_i -	thickness of the ith layer (in.)
u_o -	longitudinal displacement of the substrate at the interface of the viscoelastic layer (in.)
u_i -	longitudinal displacement of the ith layer (in.)
w -	transverse displacement (in.)
B_o -	a parameter defined as $\sqrt{\frac{E_3 t_2 t_3}{G^*}}$ (in.)
B_i -	operator for boundary conditions in Chapter 5
C -	coefficient of the modal expansion in Chapter 5
D -	volume specific energy dissipated per cycle (lb.in.)

D_s - energy dissipated in a system per cycle of oscillation (lb. in.)

E_i - Young's modulus of the i^{th} elastic layer

FE - finite element

G^* - viscoelastic layer complex shear modulus (psi)

G' - viscoelastic layer real shear modulus (psi)

G'' - viscoelastic layer loss shear modulus (psi)

G_i - shear modulus of the i^{th} layer (psi)

G_{ni} - coefficient of spatial solution orthogonalized with respect to $M[g_i(x)]$

G_{ni}^* - coefficient of spatial solution orthogonalized with respect to $L[g_i(x)]$

Hz - hertz (sec^{-1})

I - imaginary part of the square root of q_8 in Appendix B

L_1 - characteristic length of a constraining layer segment in Chapter 4 (in.)

$L[x]$ - stiffness operator

$M[x]$ - mass operator

M_b - maximum moment applied to the ends of a sandwich beam during a vibration cycle

$N_n(t)$ - generalized force for the n^{th} generalized coordinate

P - load (lb.)

P_o - maximum load due to maximum truss deflection for a given cycle of vibration (lb.)

R - real part of the square root of q_8 in Appendix B

SB - sandwich beam

$T_n(t)$ - assumed temporal solution of the sixth-order differential equation

U - elastic strain energy (lb. in.)

U_{nom} - nominal strain energy equal to the maximum strain energy in an element of a constraining layer if it was strained by ε_o (lb.in.)

V_n - mass normalized coefficient of the n^{th} term in a modal expansion

Y - geometric parameter = $\frac{Et_1(t_1+t_2)^2}{2D}$

β - eigenvalue

δ - variation symbol

δ_{mn} - Kronecker delta

ε_o - uniform extensional strain in the substrate

γ - shear strain (rad)

$\dot{\gamma}$ - rate of change of shear strain (sec^{-1})

γ_b - shear strain due to bending (rad)

γ_s - shear strain due to axial loading (rad)

η - loss factor

η_s - system loss factor

η_v - viscoelastic material loss factor

λ - $= \sqrt{\sqrt{\frac{G}{Et_1t_2}}} = \sqrt{g}$ ($in.^{-1/2}$)

ν - poisson's ratio

θ, ϕ - angles (rad)

ρ - mass density $\left(\frac{lb.sec^2}{in.^4}\right)$

σ - normal stress (psi)

τ - shear stress (psi)

ω - frequency (sec^{-1})

ω_{SB} - mode 1 frequency of the sandwich beam(sec^{-1})

ω_T - mode 1 frequency of the truss (sec^{-1})

ζ - damping ratio ($\eta = 2\zeta$)

Δ - displacement (in.)

$\frac{\partial^i}{\partial x^i}$ - i^{th} derivative (also given by "primes")

Abstract

This study was an attempt to conceptualize, design, build, and test a constrained layer damping device that uses mechanical advantage to increase the damping of transient vibration of a five-bay planar truss. The aluminum truss was clamped to a fixed support and simulated a solar array. A conventional constrained layer treatment was designed, built, and tested to serve as a benchmark for comparison. For the conventional treatment, Plunkett and Lee's segmented constraining layer technique was used.

The improved device, two three-layer sandwich beams spanning the two bays nearest the built-in end, were supported several inches away from the truss plane by a series of levers that were designed to impart a combined shear and bending load to the beam ends. Mindlin and Goodman's method was used to solve a sixth-order, homogeneous differential equation of motion with time-dependent boundary conditions.

Experimental results showed that the sandwich beam device did not exceed the loss factors of the conventional treatment for any of the first four out-of-plane bending modes. However, measurable levels of system damping were achieved for all modes of interest, particularly at the mode whose frequency coincided with that of the sandwich beams.

PASSIVE DAMPING OF A SOLAR ARRAY

I. Introduction

Background

Developments in propulsion technology have now made it possible to send large structures into space. The field of large, flexible space structures is one of growing interest (the NASA space station Freedom program is one example of the need for research in this area). For the purposes of this paper, large can be arbitrarily defined as anything larger than the space shuttle. Space structures are typically designed to be as light as possible, so an increase in mass most likely means an increase in size. This increase in size brings with it a host of new challenges for design engineers. A primary area of concern is the control of vibration. Increasing size and mass creates vibration modes which can be very low in frequency. The seriousness of this problem is amplified by ever more demanding mission requirements such as optical pointing accuracies, spacecraft shape control (of a parabolic mirror, for example), and settling times after slewing maneuvers. Furthermore, low natural frequencies, in general, cause relatively large deflections, which give rise to high maximum stresses. Consequently, vibration suppression is a major area of concern.

By virtue of their placement and function on a space structure, solar arrays typically are problem areas for vibration control. They are usually long and thin, having low natural frequencies and sometimes high modal densities. The shape of a solar array lends itself to control by means of constrained-layer damping. The technology of constrained layer damping is well-developed, and its use in space structures is desirable because passive damping is relatively simple, reliable, lightweight, and does not require power. In addition, it is inherently stable and is an excellent complement to active damping. Finally, passive damping is a good post-fabrication fix for vibration problems that were not anticipated in the design phase. These characteristics show that passive damping is a reasonable, practical means of controlling resonance in structures.

For structures that are already in service, the effectiveness of constrained layer damping treatments is limited. Ideally, the maximum effectiveness can be achieved by redesigning

the structure so that damping treatments can be placed in the most advantageous locations. Obviously, this is not always an option because, for a complex structure, it is cost-prohibitive. The inability to optimally locate the damping material on a given structure provided the impetus for this research.

Problem

Problem Statement: *With passive means and by using an optimized conventional constrained-layer damping treatment as a benchmark, design, build, and test an alternative damping treatment that provides more energy dissipation per unit mass than the conventional treatment. Specifically, the loss factor of the improved treatment must exceed that of the classical treatment for the lowest six vibration modes.*

A truss structure was fabricated to serve as the test article. Operationally, the truss supports photovoltaic solar cells that, for the purpose of this research, were massless, rigid, and incapable of dissipating energy. Naturally, modifications to the truss cannot interfere with the operation of the solar cells.

Since additional payload can cost up to several thousand dollars per pound, the best way of damping a structure may not be the simplest or the cheapest. A reliable, easily manufacturable design that significantly reduces the amount of added weight can be worth the added complexity.

As stated earlier, the damping material in a conventional constrained-layer treatment is not located optimally. From basic strength of materials theory, the maximum shear forces occur on the neutral surface of a rectangular, prismatic beam. Hence, a sandwich configuration (Figure 1.1) is optimal.

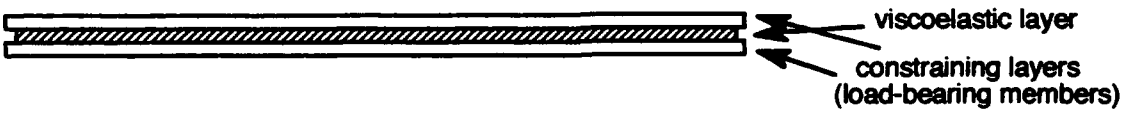

Figure 1.1 Sandwich Beam

Designing an optimal damping treatment requires an examination of how strain energy is distributed throughout a structure. Since strain energy is a function of stress and strain, it will vary throughout a member in bending. In general, an optimum damping treatment is tailored to exploit areas of high strain energy. For example, the strain energy in a cantilever beam in its fundamental mode is a maximum at the built-in end.

Torvik and Lazan [1] have investigated the possibility of moving the damping treatment further away from the neutral surface of the beam as a means of gaining mechanical advantage to increase the shear deformations in the viscoelastic. The author conducted research in this area with emphasis on a different mechanism: *bending* of the viscoelastic layer. See Figure 1.2 below.

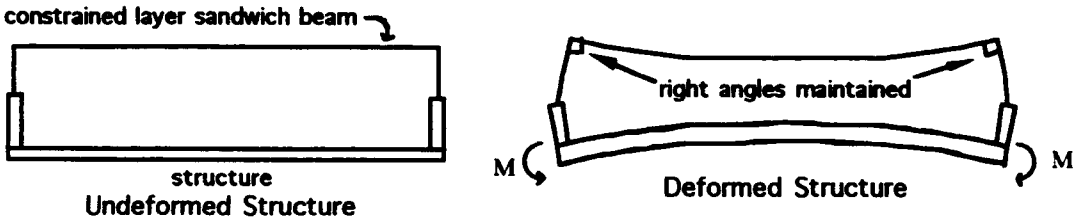

Figure 1.2 Deformation of Structure

The device is very simple: when the structure bends, the relative rotation of the levers causes a displacement at their ends, which in turn causes the sandwich beam to undergo direct and bending shear. Any dimension in the design can be optimized for a given material and/or frequency. It was presumed that the added bonus of shear due to moment would significantly increase the effectiveness of the damping treatment.

Review of the Literature

The application of viscoelastic damping treatments is well documented. Torvik's tutorial work [2] contains not only an extensive investigation of various analysis and design techniques, but also a thorough look at the historical developments in constrained layer damping over the years from 1957 to 1980. Soovere and Drake [3,4] have compiled perhaps the most comprehensive work ever written on material damping. Their Damping Design Guide is full of design procedures, case histories, and analysis techniques.

The development of the theory of sandwich beams occurred over a period of about twenty years. E. M. Kerwin [5] is regarded as the first person to derive an expression for damping in a constrained layer configuration. Ungar [6] developed energy expressions of Kerwin's analysis in 1962. DiTaranto [7] was credited with deriving a differential equation of motion for a three layer sandwich beam in 1965. The general boundary conditions for DiTaranto's equation were developed by Mead and Markus [8] in 1969. Yan and Dowell [9] followed in 1974 by generalizing the analysis to asymmetric sandwich beams. Rao

[10,11], among others, added the effects of shear layer extension and inertia in order to develop an analysis technique for short sandwich beams. The author sought to apply this body of knowledge to a modified geometric configuration that increases the effectiveness of the damping layer.

Much research has been conducted in finding more efficient ways of applying damping treatments to structures. Whittier [12] investigated various configurations involving spacers in 1958, as did Torvik and Lazan [1] in the mid-1960's. In 1965, Metherell and Sokol [13] examined the effects of anchoring the ends in various ways. In 1970, Plunkett and Lee [14] explored the effect of optimizing the length of the constraining layers in an effort to increase the strain in the damping layers. It was the author's intention to investigate the effect of pulling on the ends of the beam shown in Figure 1.3, and optimize this configuration for the solar array truss.

Figure 1.3 Viscoelastic Sandwich Beam With Combined Shear Force and Moment

Research in this area of increasing mechanical advantage for gains in damping loss factor has generally been fruitful. Some configurations, although innovative in theory, have been difficult to fabricate because of material cost and odd geometry. One of the challenges of this study was to design a practical damping treatment that was easy to make and relatively simple to analyze. The reason why simplicity is desirable is because this treatment was not only designed, but built and tested as well.

In the past fifteen years, the study of viscoelastic material behavior has been extended by Torvik and Bagley [16] to include the use of fractional-order derivative models that predict elastomer material response. The author did not use this analysis technique.

Scope

The experimental nature of this project means that a large portion of time was spent in testing. Therefore, no deliberate attempt was made to reach a theoretical breakthrough regarding the analysis of sandwich beams.

This project was an interdisciplinary study with many variables. Consequently, some areas of the design process were treated more rigorously than others. Since the problem was defined arbitrarily, there is no real reason for some of the constraints to exist other than that they helped define a practical apparatus to experiment with.

There are, of course, many ways to use mechanical advantage to increase damping. The proposed sandwich beam was chosen for investigation primarily because it is simple. Other configurations can probably be used effectively as well, but even a simple device like the sandwich beam can present difficult analysis issues when unusual geometries are present.

A logical approach was used to reduce the problem to a workable level of complexity. The five-bay truss was designed for easy handling and predictable finite element analysis. The specified range of problem frequencies was arbitrarily defined to be low. Considering only a small number of modes to be dangerous in a given vibration problem is a common way of reducing complexity. Time constraints prohibited more than one new damping design to be built and tested. Impact testing was chosen for collecting data because it is a quick, simple and accurate way of determining natural frequencies and modes.

The basic goal of the author's research was to show that greater damping efficiency can be achieved by judiciously choosing where and how to apply a damping treatment to a structure. Only the proposed treatment and a conventional damping treatment were tested.

The effectiveness of the damping treatments was judged by the modal loss factors. Impact testing allowed several test runs to be averaged. Averaging served to minimize the effect of noise and was less susceptible to error than a single test. Five to ten test runs provided sufficiently reliable data. In addition, every effort was made to insure that three significant figures of accuracy could be obtained for all measurements. Fortunately, accurate calibration of the test equipment was done and this level of precision was possible.

Assumptions

In order to reduce the problem to a manageable size, some simplifying assumptions were made for the analysis. In addition, although the operational environment of the solar array will be a given earth orbit (assume the proposed orbit is geostationary), practical considerations precluded the use of the following design constraints such as near-vacuum pressures, large, rapid temperature swings, steady state temperatures well below 0°C, and zero-g effects.

The first assumption was that the truss could not be scrapped and redesigned. Replacing the structure is cost-prohibitive. Next, the modification must have been producible from "off the shelf" materials. Composite materials were not used for the constraining layers. The assumed operating temperature for design purposes was the laboratory temperature (60-85°F).

The analysis and design of the sandwich beams proceeded with the following assumptions: Young's modulus of the viscoelastic material is small compared to that of the structure and constraining layers; material thicknesses remain constant throughout all deformations; the bonds between the different layers are perfect (so that forces could be considered to be distributed over the entire area); and published viscoelastic material property data are accurate.

Approach

The research project was divided into the following major steps:

1.) Design a test article that is simple enough to characterize quickly.

2.) Calibrate the test equipment.

3.) Conduct a coarse-mesh finite element (FE) analysis. Refine the model and analyze again.

4.) Characterize the actual structure when received. Find frequencies, mode shapes, and modal loss factors.

5.) Establish test conditions in order to obtain design constraints (testing temperature is one example of a test condition).

6.) Design a conventional constrained-layer treatment. Explore different techniques and optimize the design.

7.) Use the theoretical results obtained from the conventional treatment as a benchmark to establish design specifications for the improved treatment. Design the improved treatment with the constraint that it must be able to be removed.

8.) Produce design drawings for the AFIT Model Fabrication Shop and have both treatments built.

9.) Install the improved treatment first, and then characterize the improved damped system.

10.) Remove improved treatment and apply the conventional treatment.

11.) Characterize the system again.

12.) Write a lab report that includes a comparison of the both sets of results. Discuss uncertainty, acknowledge unfairness in the comparison, and propose further improvements.

13.) Write the report.

Sequence of Presentation

This project is a bold undertaking whose approach and schedule had no precedent. Therefore, the order of presentation is similar to the order of the research. Since no design was predetermined at the outset of the analysis, a chapter was needed to include some general ideas on improving a conventional constrained layer treatment. Chapter three explains how the test article was designed and characterized (modes and frequencies determined). The next chapter includes the analysis and design of the conventional damping treatment. In Chapter five, a theory is developed for analyzing the proposed improved damping treatment, a sandwich beam subjected to time-dependent boundary conditions. Expressions for the shear strain and loss factor follow in this section. Finally, the design of the improved treatment, and construction and testing of both treatments is discussed.

II. Improving On A Conventional Constrained Layer Damping Treatment

In researching the many different applications of constrained layer damping, it became evident that many treatments possess the same problem: uniform treatments are applied over distances where strains change, sometimes dramatically. Designing variable-thickness layers for uniform stress is possible, but fabricating such a treatment is a non-trivial matter. Given the constraints regarding the manufacture of constrained layer damping treatments, compromises must be made when choosing lengths and thicknesses. This unfortunate fact warrants a careful look into how constrained layer damping can be made more effective.

The amount of energy dissipated per cycle of vibration per unit volume is

$$D = \int_0^{\frac{2\pi}{\omega}} \tau\dot{\gamma}\, dt \tag{2.1}$$

where

τ = shear stress,

$\dot{\gamma}$ = rate of shear strain, and

ω = natural frequency of the vibrating structure .

The natural frequency of a given structure will change a relatively small amount with the addition of mass and/or stiffness. It is a parameter of which we have relatively little control unless major changes are made to the structure. The shear stress is a forced condition based on geometric deformations. On the other hand, the rate of shear strain is based on the rate of change of the structure's shape. The distribution of strain, and thus strain energy, is certainly not uniform for any structure unless it is exceedingly basic (a simply supported beam with circular curvature is one important example). Therefore, the value of shear strain in a structure depends a great deal on where we look. It is possible to exploit large shear strains by carefully choosing where and how to install a damping device. If we assume that the operating environment of the structure cannot be changed, we then look to design a damping treatment with two important characteristics: *the ability to generate high rates of shear strain, and the ability to evenly distribute high strains over significant areas.* In this way, we can obtain maximum effectiveness from a uniform coverage. Clearly, the mechanism to employ is *strain amplification by mechanical advantage.*

Any given structure has many vibration modes and corresponding natural frequencies. It is important to identify structural modes that a.) have the possibility of being excited (by

movement of the structure, rotation of an on-board motor, or some other type of forcing function), and b.) have the possibility of causing damage if a resonance condition goes unchecked. For most metals, very high frequency vibrations are dissipated by natural acoustic radiation. In space, this range of frequencies is a problem because there is no medium in which to transfer energy. For this paper, high frequencies will not be considered a problem. In general, frequencies too low to acoustically radiate yet too high to visually observe are typically dismissed because every material has, to some extent, a material loss factor (albeit small) which causes energy dissipation in a short time simply because the period of oscillation is short. An important exception to this case is the operation of a slightly unbalanced motor maintaining a given rate of rotation. Barring this exception, the frequencies typically considered to be of concern are the lowest ones. There are three major reasons for this:

1.) Movement of a structure is a common occurrence and tends to excite low modes,
2.) Low frequency modes produce the largest displacements and stresses.
3.) By virtue of their relatively long periods of vibration, low modes have the longest settling times. This becomes a problem when performance specifications require a short settling time.

These facts emphasize the need to control low modes.

The geometry of a complex structure will most likely have one or more regions of relatively high strains. For this paper, the structure of interest is a two-dimensional truss that simulates a solar array. Because the energy-collecting cells it holds are most likely brittle, the array is designed to prohibit movement in the plane (shear and bending). However, out-of-plane bending and torsion modes generally have low frequencies and relatively large displacements. The movement of the structure in these modes allows several ways of using mechanical advantage to increase damping. A few novel ideas were proposed, but some of them would require a considerable support structure. Most of the design effort in this project centered around trying to exploit a large *distance* change between two points during a typical structural deformation.

Generating bending in some kind of sandwich beam-like addition seemed to offer the most versatile design possibilities. It then became apparent that, since this "improved" treatment would most likely be attached at discrete points, the most fundamental concern was getting as much displacement or rotation out of the attachment points as possible. With a possible solution at hand, the focus became, "What will this improved treatment be compared to?" At this point, the course of action for the project was defined. The research would proceed through the following phases:

1.) Design of a realistic test article. It needed to be easy to make, relatively simple to analyze, and easy to modify.

2.) Second, two unknown parameters had to be determined as constraints for an improved design: maximum weight addition and a target system loss factor. The only reasonable way to find these two numbers was to design a conventional constrained layer treatment.

3.) Once the weight and loss factor are determined, conceptualize, design, and analyze an improved damping treatment.

4.) Finally, the two designs need to be built and tested. At that point, results can be compared and any testing biases acknowledged.

Once the general sequence of research was determined, it was time to proceed to the design of the test article; the solar array truss.

III. Design of the Test Article

The inspiration for the test article originated from the observation of the Passive and Active Control of Space Structures (PACOSS) Representative System Article (RSA) data [16]. Martin Marietta's data on the low frequency modal identification showed that 159 out of the structure's lowest 210 modes (all below 10 Hz) were solar array modes. Since the thrust of the proposed research was the design and testing of a damping treatment, designing a structure with this kind of modal density would needlessly complicate matters. Since the number of system modes decreases geometrically with decreasing complexity, the best way to avoid high modal density is to make it with fewer members. In addition, most arrays are attached to a space structure with a single shaft which allows rotation about their longitudinal axis for the purpose of pointing the array with a minimum amount of energy. Converting the single support point to two attached beams serves to "shift" the torsional vibration modes to higher frequencies.

Since the test article is supposed to be a preexisting structure, every effort was made to make it as realistic as possible. However, some desirable features needed to be designed in to make laboratory work easier. For example, low frequencies are visually observable, and being able to actually see the various modes helps give one a "feel" for what is happening. Additionally, an abundant material such as aluminum makes procurement and fabrication easy. Furthermore, some FE analysis was planned, so a high level of idealization was desired. Fully clamped ends, rectangular, prismatic cross-sections, and welded connections were convenient attributes that allowed easy finite element modeling.

Using these considerations, the final design for the test article was determined. The article is a two-dimensional, five bay truss whose dimensions are listed on the following diagram. For an oblique close-up view of the clamped area, the reader is referred to Chapter 6.

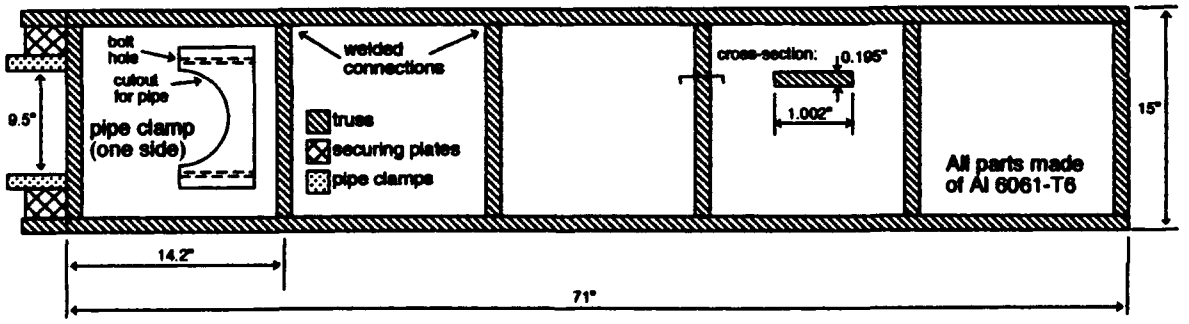

Figure 3.1 Test Article With Dimensions

The long members are continuous beams whose cross-section is detailed on the figure. The cross-members are made of the same cross-section and are butt jointed and welded to the long members. The weld bead extends a small distance (about 1/16") into the long members and was ground smooth to their edge. The cantilever connection points consist of two pipe clamps made from 0.500" plate aluminum. They were secured to a 6.75" outer diameter, 6.25" inner diameter steel tube. There is a thin aluminum strip (.040") that lines the inside of each clamp in order to insure a very snug fit. Finally, the securing plates depicted in the figure are the same thickness as the truss cross-section and have the purpose of stiffening up the clamped end. The pipe only had about ten inches of clearance for clamping. Thus the reason for the complicated connection points. The pipe is itself a cross-member in one of PACOSS's three suspension supports. These supports are about 20 feet high and are secured to the cement floor with several large bolts. In addition, each support has a few hundred pounds of lead on their bottoms to further secure the supports. The transmission of energy through the supports to the truss is only possible at high frequencies (greater than about 200 Hz) and can be accomplished by striking the support with a metal object. However, no amount of human force applied to the support caused the truss to move in any way.

From this point on, the solar array will be referred to as the "truss."

Characterization of the Truss

Once the truss was received and mounted, its modal frequencies needed to be determined. First, the equipment needed to be calibrated over the range of frequencies of interest. The most important consideration in calibrating the equipment was making sure the trials were repeatable. The goal of the testing was to determine the ratio of output voltage (acceleration) to input voltage (impact force) across the frequency spectrum. This transfer function would be used to determine modal frequencies and damping ratios.

Summary of Equipment Used

The accelerometer, a Kistler PeizoBEAM™ (model 8632A5), was calibrated with respect to a standard accelerometer calibrated by the National Bureau of Standards. The output voltage was calibrated at 100 Hz and measured 99 mV/g. The force transducer

(Kistler model 9712A5) was calibrated at 840 mV/lb$_f$. The computer software used was Tektronix TekSTAR™ version 2.2. This software has an averaging feature whereby several response measurements can be averaged to smooth out data. Simple "boxcar" windowing was used to obtain data. The software also includes a feature where the user can choose the number of samples per trial, up to a maximum of 4096. Choosing the frequency band of 0-20 Hz and running the trial for 4096 samples made for a 71.1 second trial. The effect of the 60 Hz noise spikes was kept to a negligible level by choosing the maximum number of samples per trial. The reason why this noise had to be kept to a minimum was because the spikes caused the polynomial curve fitter (a feature of the SMS-StarStruct™ software package for manipulating data) to form less abrupt modal peaks (an indication of higher damping).

Summary of Truss Dynamics

Once the equipment was calibrated, the accelerometer was mounted to the truss. In order to fully characterize the dynamic response of the truss, the accelerometer had to be mounted at more than one location. For example, the second out-of-plane bending mode has a node at about 0.8L. This location happened to coincide with a cross member, making it possible to excite the fundamental mode almost exclusively. The tip of the truss was an excellent accelerometer location for recording all modes, and a large number of excitation-response configurations had the accelerometer at the truss tip.

For each data point, ten trials were averaged and the corresponding spectral transfer function was saved as a TekSTAR data file. Then the modal peaks were curve fit using the SMS StarStruct software. The output was given in percent damping, so the value had to be doubled to obtain the modal loss factor (according to $\eta = 2\zeta$).

Some modes were quite close to one another in frequency, and determining the mode type was done by moving the accelerometer to a different location. For example, placing the accelerometer on the longitudinal centerline of the truss should yield a response devoid of torsional modes. Then, by moving the accelerometer off the centerline, all of the new peaks ought to represent torsional modes. A more complete characterization that includes the undamped loss factors appears in Appendix A, but the frequencies of the modes of interest are listed below.

Mode	Frequency (Hz)	Mode Type
1	1.05	Out-of-Plane Bending 1
2	6	Bending 2
3	7.4	Torsion 1
4	16.5	Bending 3
5	22	In-Plane Bending 1
6	22.5	Torsion 2
7	31.8	Bending 4

Table 3.1 Experimental Modes and Frequencies

A finite element model was constructed for comparison. An accurate FE model was needed because analysis of the distribution of strain energy would be used in designing the improved damping treatment. Since the structure was designed to be easily idealized, modeling was quick and simple. The input dimensions were accurate to four significant figures on cross-sectional area and the area moments of inertia, and to within three figures on distances. The modal analysis on the FE model produced the following results:

Mode	Frequency (Hz)	Mode Type
1	0.955	Out-of-Plane Bending 1
2	5.94	Bending 2
3	7.98	Torsion 1
4	16.5	Bending 3
5	23.2	In-Plane Bending 1
6	24.2	Torsion 2
7	31.7	Bending 4

Table 3.2 Finite Element Model Modes and Frequencies

These results compare favorably to the actual structure, which suggests that the model is a good one. In addition, an accurate model allows one to iterate through a number of proposed improvements quickly, and thus saving a great deal of time. Without a usable model, the improved treatment would have had to have been made adjustable in order to iterate to an optimum configuration.

Once the test article was measured and its modal frequencies determined, the next step was the design of the conventional treatment.

IV. Conventional Constrained Layer Treatment - Analysis and Design

The purpose of analyzing and designing a conventional constrained layer damping treatment was to obtain two key design constraints for the improved treatment: the maximum weight and the target modal loss factors.

An extensive review of the earlier literature (1970 and previous) was conducted in order to find an analysis technique suited to the problem. Most analyses on this subject can be derived from E. M. Kerwin's 1959 paper [5]. Two methods of analysis were chosen for this project: Torvik's variational development [17], and Plunkett and Lee's approach which assumes constant strain in the substrate [14]. Torvik's 1989 paper, using the calculus of variations, is a good teaching tool because of its elegance and because the boundary conditions are a natural by-product of the mathematics. However, after finding the expression for the loss factor and substituting in the truss's dimensions, it was determined that a constraining layer length of 71" (the length of the long truss members) was too long. For this reason, the method of Plunkett and Lee was chosen as the theoretical basis for the conventional design. The development of the loss factor by the variational technique appears in Appendix B.

The theory of Plunkett and Lee is repeated here for convenience. They hypothesized that there exists an optimum length constraining layer segment which gives maximum damping for a given viscoelastic material and a given frequency. Their explanation of this hypothesis is the following:

> If the constraining layer is very long, the shear stress near the ends induces the same axial strain in it as in the basic structure; thus there is no shear in the viscoelastic layer away from the ends and the damping is small. If the length of each element of the constraining layer is very short, it exerts no constraint on the underlying viscoelastic layer, there is little shear strain, and the damping is small. At some finite value for the lengths of the elements of the constraining layer, the damping is a maximum. [14: 151]

Plunkett and Lee's theory is based on the following assumptions:

1.) All energy dissipation in the viscoelastic layer is attributable to shear strain.

2.) The constrained and constraining layers have small thicknesses with respect to the substrate. This assumption a.) makes bending stiffnesses in the constraining layer negligible with respect to the structure, and b.) allows us to analyze the constraining layer as if it were in tension only, and the viscoelastic layer as if it were in shear only.

3.) The viscoelastic material behaves linearly throughout the range of operating strains and can be characterized by its shear modulus, the complex value

$$G^* = G' + iG'' = G'(1 + i\eta_v) \tag{4.1}$$

where

G' = the elastic shear modulus,

G'' = the loss shear modulus, and

η_v = the material loss factor $= \frac{G''}{G'}$.

4.) The constraining layer and the substrate are elastic and dissipate no energy. This is a fairly good assumption since aluminum has a structural damping factor of $\eta_S \approx 0.0005$.

5.) Poisson effects are negligible.

6.) The axial strain is uniform at the interface of the substrate and the viscoelastic layer. For a beam, this assumption implies circular curvature. Even in deformations where this assumption is not explicitly the case, the strain in the substrate will approach a constant value as the segment length gets small.

7.) The shear strain in the viscoelastic layer is constant through the thickness.

8.) The normal strain in the constraining layer is assumed uniform through the thickness.

9.) Young's moduli of the constraining layer and substrate are much greater the shear modulus of the viscoelastic layer.

Suppose we have a given constraining layer segment like the one in figure 4.1.

Figure 4.1 Depiction of Constraining Layer Segment With Free Body Diagram of Slice dx

The equilibrium equation for the differential element dx is

$$\frac{\partial \sigma}{\partial x} t_2 = \tau \tag{4.2}$$

Using assumption 7, the constitutive relations for the constraining layer and the viscoelastic layer are

$$\sigma = E\varepsilon_x = E\frac{\partial u}{\partial x} \tag{4.3}$$

and

$$\tau^* = G^*\gamma^* = G^*\left(\frac{u^* - u_o}{t_2}\right), \tag{4.4}$$

respectively. Assuming constant strain in the substrate,

$$u_o = \varepsilon_o x \tag{4.5}$$

Substituting eqs. (4.3), (4.4), and (4.5) into (4:1) gives

$$t_3 E_3 \frac{\partial^2 u^*}{\partial x^2} = G^*\left(\frac{u^* - u_o}{t_2}\right)$$

or

$$\frac{t_2 t_3 E_3}{G^*}\frac{\partial^2 u^*}{\partial x^2} - u^* = -\varepsilon_o x \tag{4.6}$$

For future convenience, use Plunkett's notation to define

$$B_o^* = \sqrt{\frac{t_2 t_3 E_3}{G^*}} \tag{4.7}$$

The boundary conditions for any single constraining layer segment are

$$\left.\frac{\partial u^*}{\partial x}\right|_{-1/2}^{1/2} = 0 \tag{4.8}$$

The general solution of this equation is

$$u^*(x) = \varepsilon_o \left[x - B_o^* \frac{\sinh\left(\frac{x}{B_o^*}\right)}{\cosh\left(\frac{L_1}{2B_o^*}\right)} \right] \tag{4.9}$$

Now, using assumption 7 again, the energy dissipated per cycle per unit width and length is

$$dD = \pi t_2 G'' |\gamma^*|^2 \tag{4.10}$$

where

$$|\gamma^*| = \sqrt{(\gamma')^2 + (\gamma'')^2}$$

Using the relation

$$\gamma^* = \left(\frac{u^* - u_o}{t_2} \right) \tag{4.11}$$

gives

$$dD = \pi t_2 G'' \left| \frac{1}{t_2} \left[\varepsilon_o \left(x - B_o^* \frac{\sinh\left(\frac{x}{B_o^*}\right)}{\cosh\left(\frac{L_1}{2B_o^*}\right)} \right) - \varepsilon_o x \right] \right|^2 = \pi \frac{\varepsilon_o^{\,2}}{t_2} G''\left(B_o^*\right)^2 \left| \frac{\sinh\left(\frac{x}{B_o^*}\right)}{\cosh\left(\frac{L_1}{2B_o^*}\right)} \right|^2 \tag{4.12}$$

Integrating D over the length of the constraining layer gives the energy dissipated per cycle per unit width.

$$D = 2\pi \varepsilon_o^{\,2} t_3 E_3 B_o^* \left[\frac{\sinh\left(\frac{L_1}{B_o^*}\cos\frac{\eta_v}{2}\right)\sin\frac{\eta_v}{2} - \sin\left(\frac{L_1}{B_o^*}\sin\frac{\eta_v}{2}\right)\cos\frac{\eta_v}{2}}{\cosh\left(\frac{L_1}{B_o^*}\cos\frac{\eta_v}{2}\right) + \cos\left(\frac{L_1}{B_o^*}\sin\frac{\eta_v}{2}\right)} \right] \tag{4.13}$$

We now define a nominal energy U_{nom} which equals the maximum strain energy in an element of the constraining layer if it was strained by ε_o as

$$U_{nom} = \frac{1}{2}\varepsilon_o^2 E_3 t_3 L_1 \tag{4.14}$$

We can nondimensionalize D by dividing by U_{nom}. Define a dimensionless loss coefficient η_1 as

$$\eta_1 = \frac{D}{U_{nom}} = 4\pi \frac{B_o^*}{L_1}\left[\frac{\sinh\left(\frac{L_1}{B_o^*}\cos\frac{\eta_v}{2}\right)\sin\frac{\eta_v}{2} - \sin\left(\frac{L_1}{B_o^*}\sin\frac{\eta_v}{2}\right)\cos\frac{\eta_v}{2}}{\cosh\left(\frac{L_1}{B_o^*}\cos\frac{\eta_v}{2}\right) + \cos\left(\frac{L_1}{B_o^*}\sin\frac{\eta_v}{2}\right)}\right] \tag{4.15}$$

This value is found to be a maximum at $L_1/B_O = 3.28$. Therefore, the optimum length $L_1 = 3.28B_O$.

Plunkett and Lee used a cantilever beam coated on both sides (the same configuration used here) as an application of their theory. Their analysis of the cantilever beam follows.

Consider the deformations of a cantilever beam subjected to sinusoidal flexural oscillation. The strain at the interface is

$$\varepsilon_o = -\frac{t_1}{2}\frac{\partial^2 w}{\partial x^2} \tag{4.16}$$

where

t_1 = thickness of the substrate

$\frac{\partial^2 w}{\partial x^2}$ = curvature of beam

Assuming the damping treatment is applied from 0 to L, the energy dissipated per cycle in the system D_s is

$$D_s = 2\int_0^L \frac{D}{L_1}\,dx \tag{4.17}$$

where the 2 comes from treating both sides of the beam. Substituting,

$$D_s = 2\int_0^L \frac{\eta_1 U_{nom}}{L_1}\,dx$$
$$= \eta_h E_3 t_3 \left(\frac{t_1^2}{4}\right)\int_0^L \left(\frac{\partial^2 w}{\partial x^2}\right)^2 dx \tag{4.18}$$

The maximum strain energy in the system is

$$U_s = \left(\frac{E_1 t_1^3}{24}\right)\int_0^L \left(\frac{\partial^2 w}{\partial x^2}\right)^2 dx \tag{4.19}$$

The system loss factor η_S is then

$$\eta_s = \frac{D_s}{2\pi U_s} = \frac{\frac{\eta_h E_3 t_1^2 t_3}{4}\int_0^L \left(\frac{\partial^2 w}{\partial x^2}\right)^2 dx}{\frac{2\pi E_1 t_1^3}{24}\int_0^L \left(\frac{\partial^2 w}{\partial x^2}\right)^2 dx} \tag{4.20}$$

Assuming a given segment length is much less than a wavelength and the treatment is applied over the entire length of the beam, the integrals are identically equal at all locations x. For $E_1 = E_3$,

$$\eta_s = \eta_h \frac{3t_3}{\pi t_1}$$
$$= \frac{12 t_3 B_o^*}{t_1 L_1}\left[\frac{\sinh\left(\frac{L_1}{B_o^*}\cos\frac{\eta_v}{2}\right)\sin\frac{\eta_v}{2} - \sin\left(\frac{L_1}{B_o^*}\sin\frac{\eta_v}{2}\right)\cos\frac{\eta_v}{2}}{\cosh\left(\frac{L_1}{B_o^*}\cos\frac{\eta_v}{2}\right) + \cos\left(\frac{L_1}{B_o^*}\sin\frac{\eta_v}{2}\right)}\right] \tag{4.21}$$

A parametric study was conducted on a spreadsheet to find the optimum configuration of thicknesses and segment length. Since G^* is dependent on frequency, each mode will exhibit a different optimum length of segment. Any given length, then, will have different loss factors for each mode. A graph comparing the theoretical loss factor and segment length was constructed for a number of candidate configurations. Figure 4.2 is one example of such a graph. The curves for the higher modes are less

accurate because the assumption that the segment length is much shorter than the wavelength is no longer valid.

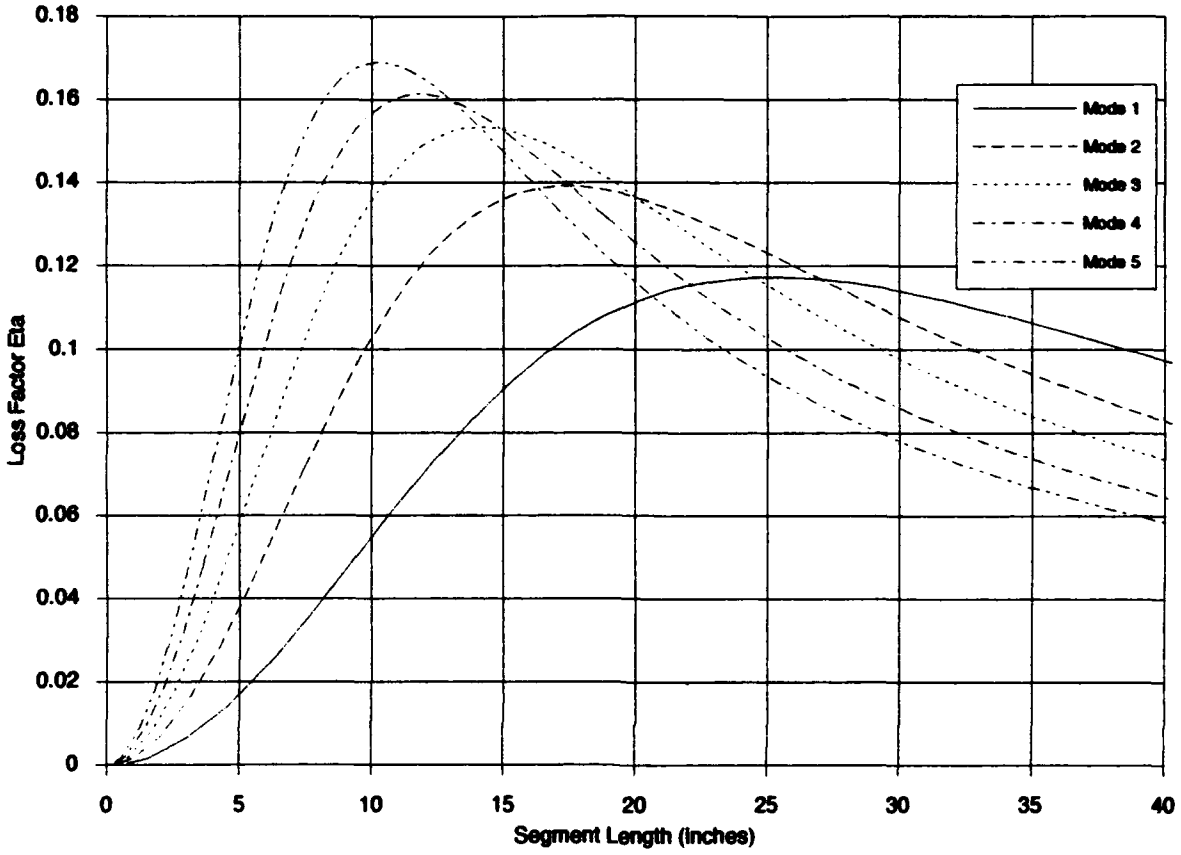

Figure 4.2 Theoretical Loss Factor vs. Segment Length for 032005 ISD 112

Before a configuration was chosen, a short laboratory experiment was conducted to verify whether or not this theory would match the results of an actual experiment. Three identical 11" Al 6061-T6 beams with cross-section 0.126" x 0.75" were used to perform a number of tests, each test having a different segment length. Each test consisted of collecting data on several sets of trials. The damping material was a 0.002" thick 3M ISD 112 viscoelastic layer with a 0.005" thick type 1100 dead soft aluminum constraining layer. Each segment length was tested by means of conducting ten impact trials averaged into a single frequency response function (FRF), which was then curve fit for the damping ratio. The damping ratio (in percent damping) was then multiplied by two to obtain the experimental system loss factor. Each set of ten impact trials produced two data points (for modes 1 and 2), which were plotted in Figure 4.3. The details of this "mini-experiment" and the tabulated data can be found in Appendix C.

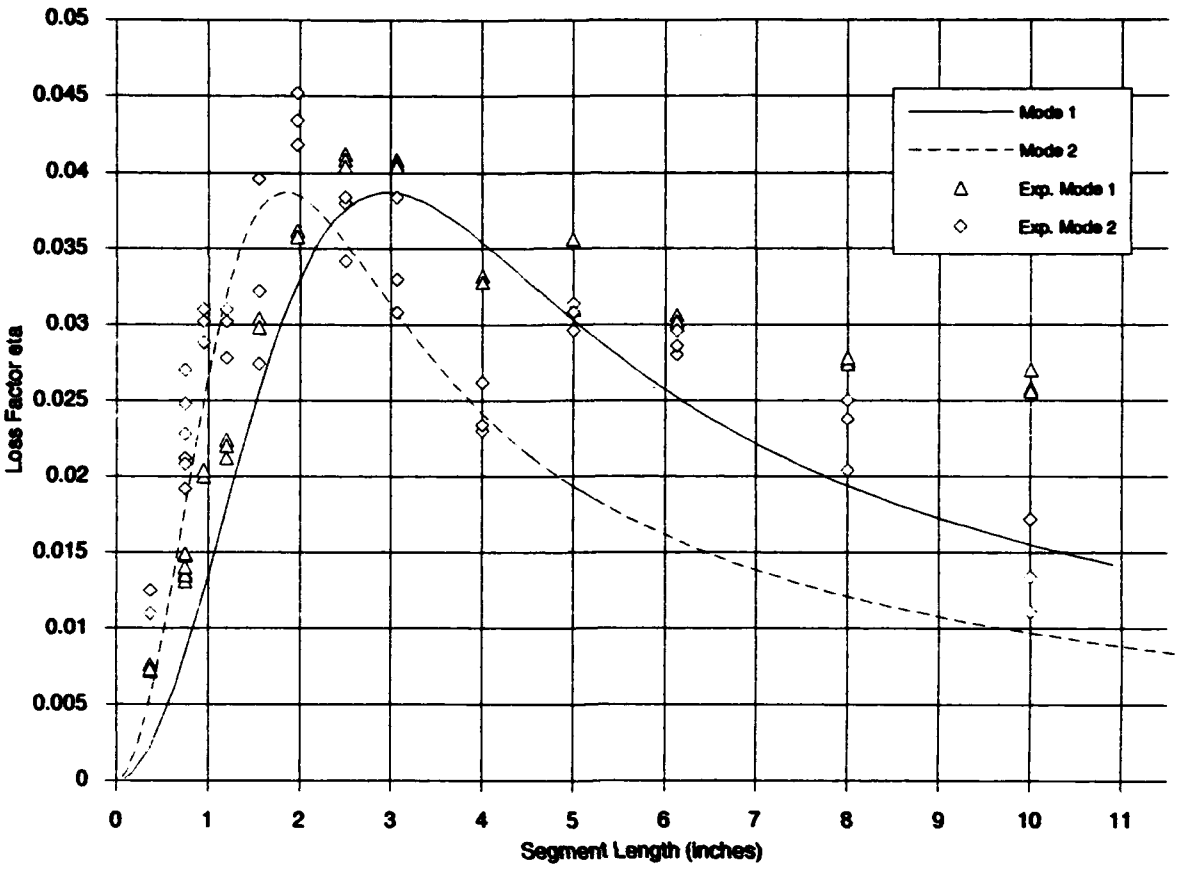

Figure 4.3 11" Beam Experimental Data With Theoretical Curves

Mantena, Gibson, and Hwang [18] ran a similar experiment with 3M ISD 112 and concluded that the dead soft aluminum backing (theoretically assumed to have negligible energy dissipation) had a significant material loss factor. 3M does not test ISD 112 with the aluminum backing, so loss data was not available. If the material loss factor is indeed significant, the experimental loss factor would be higher, particularly for long segment lengths (where strain in the constraining layer is close to strain in the substrate over a considerable distance). This phenomenon would explain why the long segment lengths gave considerably higher damping than the theory. Based on the data above, it was concluded that Plunkett and Lee's theory *is* verifiable. Furthermore, by eliminating as much uncertainty as is reasonably possible, obtaining repeatable data is possible.

Once the preceding experiment was finished, a configuration was chosen. Several factors were considered in the decision. Within reason, the potential loss factor is limited only by the constraining layer thickness. Hence, a restriction was placed on the weight of the entire treatment. A maximum weight of one pound (about $^1/_4$ of the truss's weight)

was arbitrarily chosen. The limit on the constraining layer thickness, then, is about $^1/_{32}$" (0.032"). Aluminum of this thickness is produced in sheet form. The added uncertainty of using the dead soft aluminum backing precluded its use (even though it would be advantageous to have another energy-dissipating component). Therefore, bare ISD 112 was selected. Table 4.1 shows the change in optimum length for varying t_2 (while all other parameters are held constant). As observed from Table 4.1, if the segment length is allowed to vary with varying t_2, then the loss factor is only *indirectly* dependent on t_2. It would be advantageous, then, to select the thinnest t_2 because it is the lightest. In addition, the table shows how the segment length decreases with decreasing t_2. Intuitively, since the distribution of strain along a cantilever beam varies, decreasing the segment length (to a reasonably small length) should give an overall higher damping factor. If the strain decreases monotonically (as in mode 1 vibration), shorter segments will better exploit the concentrations of strain and give rise to higher damping because energy dissipation is proportional to the square of the shear strain. Besides, one of the initial assumptions was that the segment length is much smaller than a wavelength. Theoretically, then, the optimum value of L_1 is probably small. Unfortunately, a configuration with a small segment length would require a viscoelastic layer of vanishing thickness. The following are nominal pararameters used to construct Table 4.1 (η_1 was determined from the other parameters):

$t_1 = 0.195"$, $E = 10^7$ psi, $G = 23$ psi, $\eta_v = 0.61$, $w = L_1/B_o = 3.28$, $\eta_1 = 0.7495$

t_2	t_3	L_1	t_2/t_3	η_{sys}
0.002	0.032	15.987	0.0625	0.1174551
0.004	0.032	22.608	0.125	0.1174551
0.005	0.032	25.277	0.1563	0.1174551
0.007	0.032	29.908	0.2188	0.1174551
0.009	0.032	33.912	0.2813	0.1174551
0.01	0.032	35.747	0.3125	0.1174551
0.012	0.032	39.159	0.375	0.1174551
0.015	0.032	43.781	0.4688	0.1174551

Table 4.1 Example of Relationship Between L_1 and t_2 for Nominal Parameters

Another unfortunate fact is that the contact surfaces sandwiching the viscoelastic must have some nonzero value of average surface roughness to enable adequate bonding of the ISD 112. The problem of surface roughness could not be ignored because its value on both the truss and the constraining layer is on the order of the thinnest available t_2

(0.002" is 3M's thinnest layer). This roughness was deliberately exacerbated by sanding the surfaces to insure a good bond. Since the shear stresses are so sensitive in this region of values of t_2, it was decided that selecting $t_2 = 0.002$" would be unwise. However, this effect can be diminished markedly by going to the next thinnest available layer. Consequently, a viscoelastic layer thickness $t_2 = 0.005$" was chosen.

According to Figure 4.2, the optimum segment length differs for each mode. The mode 1 optimum segment length of 25.3 in. would be a poor choice because the effectiveness of that length at higher modes is low. As the graph indicates, a much better choice of length is somewhere between the peaks for modes 1 and 2. In order to obtain higher damping in the higher modes, a length of 18" was chosen. As you can see, this length is closer to the mode 2 peak, but the relative insensitivity of the mode 1 curve to changes in length in this region justifies the choice. Therefore, the final configuration for the conventional treatment is the following:

Constraining Layer Thickness $t_1 = 0.032$"
Viscoelastic Layer Thickness $t_2 = 0.005$"
Constraining Layer Length $L_1 = 18.0$"

Based on Figure 4.2, the expected values of η for modes 1 and 2 are:

weight = 0.96 lb.
Mode 1: η = 0.11
Mode 2: η = 0.14

These expected values became inequality design constraints for the improved damping treatment.

V. Improved Damping Treatment

The major goal of devising an improved damping treatment for a cantilevered structure is exploiting regions of high strain energy. For low frequency vibration modes, this region is the built-in end. Somehow, a damping treatment must be designed so that strain energy is "channeled" into an attached device. Unless this device contacts the structure over a large area (like a conventional treatment), it will have to be secured to the structure at *discrete* points. This observation leads one to consider which point properties are important. The two properties which are useful in this case are *displacements* and *forces*. If we assume that mode 1 and possibly mode 2 are problem frequencies, then we can reduce the problem to a reasonable level of complexity. At this point, it appeared that the goal of the thesis statement (obtaining higher modal loss factors of the first *six* vibration modes) made for a design problem whose solution would be too complex. For the improved treatment, it was decided to design such that only mode 1 would be considered. This concession is not an admission of defeat; rather, it is a practical reduction of the problem in order to obtain a solution. By designing to damp mode 1 vibration most effectively, modes 2 through 6 may in fact have higher damping as well.

It should be noted here that mode 3 is the fundamental torsion mode. This mode will not be taken into consideration for the design. However, it will be tested and compared with the conventional treatment.

As stated in Chapter 1, a sandwich beam offers the advantage of locating the viscoelastic material in the region of the beam cross-section having the maximum shear stress (the neutral surface). Additionally, it is possible to generate large bending deflections with relatively small forces. In a conventional treatment, the major cause of shear strain in the viscoelastic layer is attributable to the extension of the substrate at the interface, whereas the causes of shear strain in a sandwich beam are *both* the longitudinal extension of the constraining layers *and* the relative motion of the top and bottom interfaces of the viscoelastic layer due to bending. Considering these facts, it seems necessary then to connect this sandwich beam in such a way that these purportedly large bending deflections will have enough physical space to occur. Therefore, some sort of support structure will be needed to hold the sandwich beam away from the truss.

With a weight constraint on the design, minimizing the weight of any "non-damping" parts is of crucial importance. However, in order to generate bending in a

sandwich beam, forces from the truss (which will be felt as a *combination* of axial forces and end moments by the sandwich beam) will have to be transmitted through the support structure to the sandwich beam. Therefore, we need a *lightweight* support structure that can resist the applied forces as rigidly as possible, for any deformation in the support structure will likely cause a decrease in damping.

The next question is one of how to generate large bending deflections in a sandwich beam. If the sandwich beam needs to feel end moments, then we must look to optimize the product of force and distance. The following configuration was considered to be the most practical for the given problem.

Consider a rigid rod positioned vertically with a pivot on the bottom (the lower lever of Figure 5.2 illustrates this setup). When the bottom point rotates a small amount θ, all points on the lever will rotate, and all points except the pivot will displace some amount according to $\Delta = x\theta$. Now, place the pivot somewhere on the truss (like the location depicted in Figure 5.1). Assuming the truss will vibrate in a given way regardless of what is connected to it, we can theoretically generate as much displacement Δ as we want. Unfortunately, several factors limit the practical maximum length h. If a resisting force P is applied at the tip of the lever, the angle θ will be reduced (for a static case, this reduction in θ can be found by summing moments about the pivot). Furthermore, the resisting force P will cause some bending deflection in the lever to further reduce the displacement. Finally, the longer the lever, the heftier it must be to rigidly transmit the desired displacements to the sandwich beam, and in consequence less weight is available for the damper. Assuming some optimum length can be found, consider how this "displacement-generating" lever can be connected to the truss.

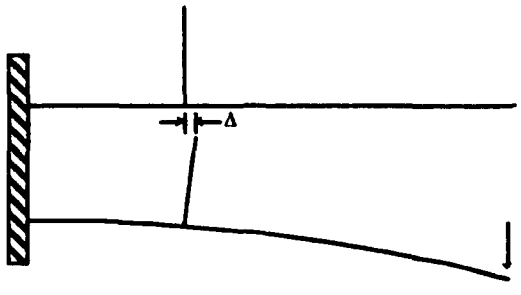

Figure 5.1 Illustration of Lever Tip Movement

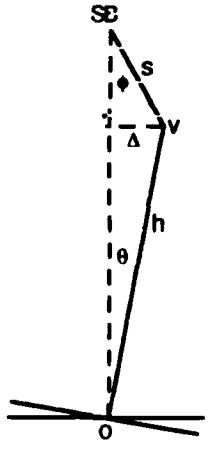

Figure 5.2 Two Lever Concept

The cross-members of the truss provide an adequate securing location for the levers. However, an increase in distance between two points does not solve the problem of how to generate bending. Consequently, a second set of levers was proposed for placement at the lever tips (refer again to figure 5.2). The additional lever is then rigidly attached perpendicular to the sandwich beam end. Figure 5.3 below illustrates this configuration.

As point o (connected to the truss) rotates by an angle θ, point v displaces some distance $\Delta = h\theta$. This distance is approximately equal to $s\phi$ (for small ϕ). By choosing the ratio of h/s, it is possible to control the ratio of θ/ϕ. Care must be taken to avoid a configuration where ϕ becomes too large (it will be shown later that the limits of the truss's deflection will prevent ϕ from becoming too large).

In Figure 5.3, the connection of levers h and s is a pin joint, and the short levers and sandwich beam maintain a right angle orientation with respect to each other throughout the vibration cycle . In addition, assume the pin joint is frictionless.

Placing this setup on the truss, we have the following situation.

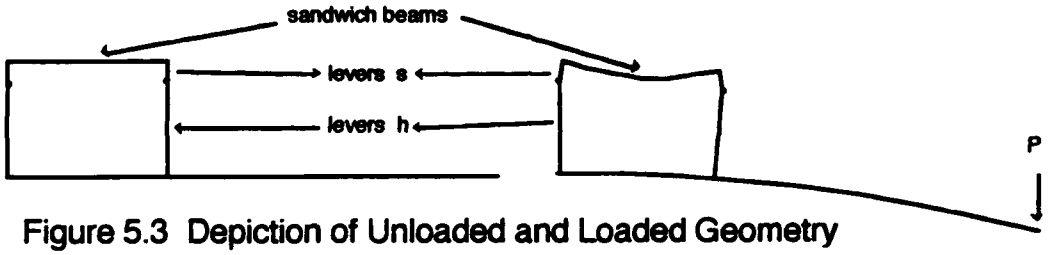

Figure 5.3 Depiction of Unloaded and Loaded Geometry

In addition to bending, it is possible to generate *direct* shear strains in the viscoelastic layer. Consider the following diagram of a sandwich beam.

Figure 5.4 Exploded View of Sandwich Beam
(Viscoelastic layer thickness greatly exaggerated)

If the left lever is connected to the bottom sandwich plate and the right lever connected to the top plate, the load P will become a shear load that the viscoelastic layer must resist for equilibrium.

By equipollency and assuming small ϕ, the direct loads P produce corresponding moments (equal to the product of P and s) at the end of the sandwich beam. Therefore, the sandwich beam is in a state of combined loading (axial and bending). We will

assume that the displacement equation for any individual layer of the sandwich beam is the superposition of displacements due to each separate loading. This assumption will be shown to be valid (for small deflections) in spite of beam-column effects that occur during the compressive half-cycle of oscillation. Since the levers will move back and forth when the truss vibrates, both loadings will be sinusoidal in time according to

$$P(t) = P_o \sin \omega_T t \quad \text{and} \quad M(t) = P_o s \sin \omega_T t \tag{5.1}$$

where

P_o = the maximum load P due to maximum truss deflection for a given cycle
ω_T = the mode 1 natural frequency of the truss

We will assume the natural frequency of the truss is minimally affected by the addition of the damping device. For this reason, changes in the viscoelastic material properties are considered to be negligible. Although the direct load is time-dependent, the natural frequencies of longitudinal vibration can be safely assumed to be much greater than any truss frequency of interest, so a static loading analysis is in order. However, the natural frequencies of *transverse* vibration cannot generally be assumed to be much greater than ω_T, so a dynamic analysis is required.

The sequence of the sandwich beam analysis will be as follows:

- develop the displacement equations for a three layer sandwich beam in direct shear
- determine the effect of the lever geometry on the dynamic bending analysis
    - statically analyze an eccentrically loaded beam-column
    - discuss asymmetric phenomena
- develop the homogeneous differential equation of motion for a three-layer sandwich beam (most of this development is in appendix D)
- establish boundary conditions for the solution of the equation of motion
- solve the differential equation for the displacement $w(x,t)$
- determine shear strains and system loss factors.

Displacement Equations for a Three Layer Sandwich Beam In Direct Shear

Consider a slice dx of the beam of unit width illustrated in figure 5.5. Assume there is no shearing strain in the elastic members and that the viscoelastic layer has no axial strain. Assume also that the shear strain is distributed uniformly through the viscoelastic thickness and the axial stress is uniformly distributed through the thickness

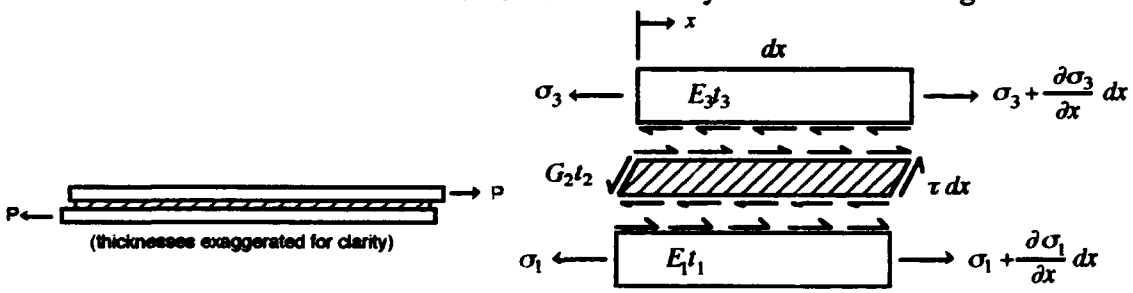

Figure 5.5 Typical Sandwich Beam and a Differential Slice dx

of the constraining layers. We will prescribe the constraining layers to be made of the same material and have the same thickness. Finally assume that Young's modulus of the elastic layers is much greater than the shear modulus of the viscoelastic.

Looking at the differential slice depicted in figure 5.5, we can sum the forces in the upper and lower constraining layers to obtain

$$t_1 \frac{\partial \sigma_1}{\partial x} dx + \tau dx = 0 \quad \text{and} \quad t_3 \frac{\partial \sigma_3}{\partial x} dx - \tau dx = 0 \tag{5.2}$$

respectively. The shear strain in the viscoelastic layer γ (assuming γ is small) is

$$\gamma = \left(\frac{u_3 - u_1}{t_2} \right) \tag{5.3}$$

Using the stress-strain constitutive relations,

$$\tau = G\gamma = G\left(\frac{u_3 - u_1}{t_2} \right) \quad \text{and} \quad \sigma_i = E_i \varepsilon_i = E_i \frac{\partial u_i}{\partial x} \tag{5.4}$$

Substitution of (5.4) into (5.2) gives

$$E_1 t_1 \frac{\partial^2 u_1}{\partial x^2} - G\left(\frac{u_1 - u_3}{t_2}\right) = 0 \quad \text{and} \quad E_3 t_3 \frac{\partial^2 u_3}{\partial x^2} + G\left(\frac{u_1 - u_3}{t_2}\right) = 0 \tag{5.5}$$

Rearranging (5.5), we obtain

$$\frac{\partial^2 u_1}{\partial x^2} - \frac{G}{E_1 t_1 t_2}(u_1 - u_3) = 0 \quad \text{and} \quad \frac{\partial^2 u_3}{\partial x^2} + \frac{G}{E_3 t_3 t_2}(u_1 - u_3) = 0 \tag{5.6}$$

For convenience, let

$$\frac{\partial^2}{\partial x^2} u_i = u_i'' \tag{5.7}$$

and, since $t_3 = t_1$, let

$$\frac{G}{E_1 t_1 t_2} = \frac{G}{E_3 t_3 t_2} = \frac{g}{2} \tag{5.8}$$

The set of two homogeneous, coupled differential equations is then

$$\begin{aligned} u_1'' - \frac{g}{2}(u_1 - u_3) &= 0 \\ u_3'' + \frac{g}{2}(u_1 - u_3) &= 0 \end{aligned} \tag{5.9}$$

Subtracting the second equation from the first yields

$$\left(u_1'' - u_3''\right) - g(u_1 - u_3) = 0 \tag{5.10}$$

Let $\Delta = u_1 - u_3$ and $\Delta'' = u_1'' - u_3''$ to simplify (5.10) to

$$\Delta'' - g\Delta = 0 \tag{5.11}$$

The solution to (5.11) is

$$\Delta(x) = A \sinh \lambda x + B \cosh \lambda x \tag{5.12}$$

where A and B are constants and

$$\lambda = \sqrt{g} \tag{5.13}$$

The boundary conditions for this problem are

$$\Delta(0) = \Delta(L) = \varepsilon \tag{5.14}$$

where ε is some difference in the end displacements with respect to each other. This quantity will be determined later. Solving the left boundary condition,

$$\Delta(0) = B = \varepsilon \quad \Rightarrow \quad \Delta(x) = A \sinh \lambda x + \varepsilon \cosh \lambda x \tag{5.15}$$

Using the right boundary condition,

$$\begin{aligned} &\Delta(L) = A \sinh \lambda L + \varepsilon \cosh \lambda L = \varepsilon \\ \Rightarrow \quad &A = \varepsilon \left[\frac{(1 - \cosh \lambda L)}{\sinh \lambda L} \right] = -\varepsilon \tanh \frac{\lambda L}{2} \end{aligned} \tag{5.16}$$

The expression for Δ becomes

$$\Delta(x) = \varepsilon \left(-\tanh \frac{\lambda L}{2} \sinh \lambda x + \cosh \lambda x \right) \tag{5.17}$$

Since $\Delta = u_1 - u_3$,

$$u_1'' - \frac{g}{2} \Delta = 0 \tag{5.18}$$

We can arbitrarily set $u_1(0)$ to zero. This defines the boundary conditions for the solution of u_1 as

$$u_1(0) = 0 \quad \text{and} \quad u_1'(L) = 0 \tag{5.19}$$

Substituting (5.17) into (5.18) gives

$$u_1'' = \frac{g\varepsilon}{2}\left[-\tanh\frac{\lambda L}{2}\sinh\lambda x + \cosh\lambda x\right] \tag{5.20}$$

Integration of this expression yields

$$u_1' = \frac{g\varepsilon}{2\lambda}\left[-\tanh\frac{\lambda L}{2}\cosh\lambda x + \sinh\lambda x\right] + C_1 \tag{5.21}$$

Using the right boundary condition,

$$\begin{aligned} u_1'(L) = 0 \;\Rightarrow\; & \frac{g\varepsilon}{2\lambda}\left[-\tanh\frac{\lambda L}{2}\cosh\lambda L + \sinh\lambda L\right] + C_1 = 0 \\ & C_1 = -\frac{g\varepsilon}{2\lambda}\left[-\tanh\frac{\lambda L}{2}\cosh\lambda L + \sinh\lambda L\right] \end{aligned} \tag{5.22}$$

Therefore,

$$u_1' = \frac{g\varepsilon}{2\lambda}\left[-\tanh\frac{\lambda L}{2}\cosh\lambda x + \sinh\lambda x\right] - \frac{g\varepsilon}{2\lambda}\left[-\tanh\frac{\lambda L}{2}\cosh\lambda L + \sinh\lambda L\right] \tag{5.23}$$

Integrating once again, we obtain

$$u_1(x) = \frac{g\varepsilon}{2\lambda^2}\left[-\tanh\frac{\lambda L}{2}\sinh\lambda x + \cosh\lambda x\right] - \frac{g\varepsilon}{2\lambda}\left[-\tanh\frac{\lambda L}{2}\cosh\lambda L + \sinh\lambda L\right]x + C_2 \tag{5.24}$$

The left boundary condition gives

$$u_1(0) = 0 \;\Rightarrow\; C_2 = -\frac{g\varepsilon}{2\lambda^2} \tag{5.25}$$

Consequently, the expression for u_1 is

$$u_1(x) = \frac{g\varepsilon}{2\lambda^2}\left[-\tanh\frac{\lambda L}{2}\sinh\lambda x + \cosh\lambda x\right] - \frac{g\varepsilon}{2\lambda}\left[-\tanh\frac{\lambda L}{2}\cosh\lambda L + \sinh\lambda L\right]x - \frac{g\varepsilon}{2\lambda^2} \tag{5.26}$$

To find u_3, we use the relation $u_3 = u_1 - \Delta$ to get

$$u_3(x) = u_1(x) - \Delta$$

$$= \left(\frac{g\varepsilon}{2\lambda^2} - \varepsilon\right)\left[-\tanh\frac{\lambda L}{2}\sinh\lambda x + \cosh\lambda x\right] - \frac{g\varepsilon}{2\lambda}\left[-\tanh\frac{\lambda L}{2}\cosh\lambda L + \sinh\lambda L\right]x - \frac{g\varepsilon}{2\lambda^2} \tag{5.27}$$

We now need to find the unknown quantity ε in terms of known quantities. Differentiating $u_3(x)$ gives

$$u_3'(x) = -\lambda\varepsilon\left(-\tanh\frac{\lambda L}{2}\cosh\lambda x + \sinh\lambda x\right) \tag{5.28}$$

At this point, we prescribe right boundary condition $u_3'(L)$ to be

$$u_3'(L) = \frac{P}{AE} \tag{5.29}$$

where $A = t_1$ for a unit width.

Substitution into $u_3'(x)$ gives the value of ε as

$$\varepsilon = -\frac{P}{\lambda AE}\left[-\tanh\frac{\lambda L}{2}\cosh\lambda L + \sinh\lambda L\right]^{-1} \tag{5.30}$$

Substitution of ε into the expressions for $u_1(x)$ and $u_3(x)$ gives

$$u_1(x) = \frac{P}{2\sqrt{g}AE}\left\{\frac{1 - \left[-\tanh\frac{\sqrt{g}L}{2}\sinh\sqrt{g}x + \cosh\sqrt{g}x\right]}{-\tanh\frac{\sqrt{g}L}{2}\cosh\sqrt{g}L + \sinh\sqrt{g}L}\right\} + \frac{Px}{2AE} \tag{5.31}$$

$$u_3(x) = \frac{P}{2\sqrt{g}AE}\left\{\frac{\left[-\tanh\frac{\sqrt{g}L}{2}\sinh\sqrt{g}x + \cosh\sqrt{g}x\right] + 1}{-\tanh\frac{\sqrt{g}L}{2}\cosh\sqrt{g}L + \sinh\sqrt{g}L}\right\} + \frac{Px}{2AE} \tag{5.32}$$

What we are really interested in, however, is the magnitude of $u_1 - u_3$. This expression is

$$u_1(x) - u_3(x) = \frac{P}{\sqrt{g}AE}\left\{\frac{-\tanh\frac{\sqrt{g}L}{2}\sinh\sqrt{g}x + \cosh\sqrt{g}x}{-\tanh\frac{\sqrt{g}L}{2}\cosh\sqrt{g}L + \sinh\sqrt{g}L}\right\} \tag{5.33}$$

For the given set of parameters, the difference of u_1 - u_3 is illustrated in figure 5.6.

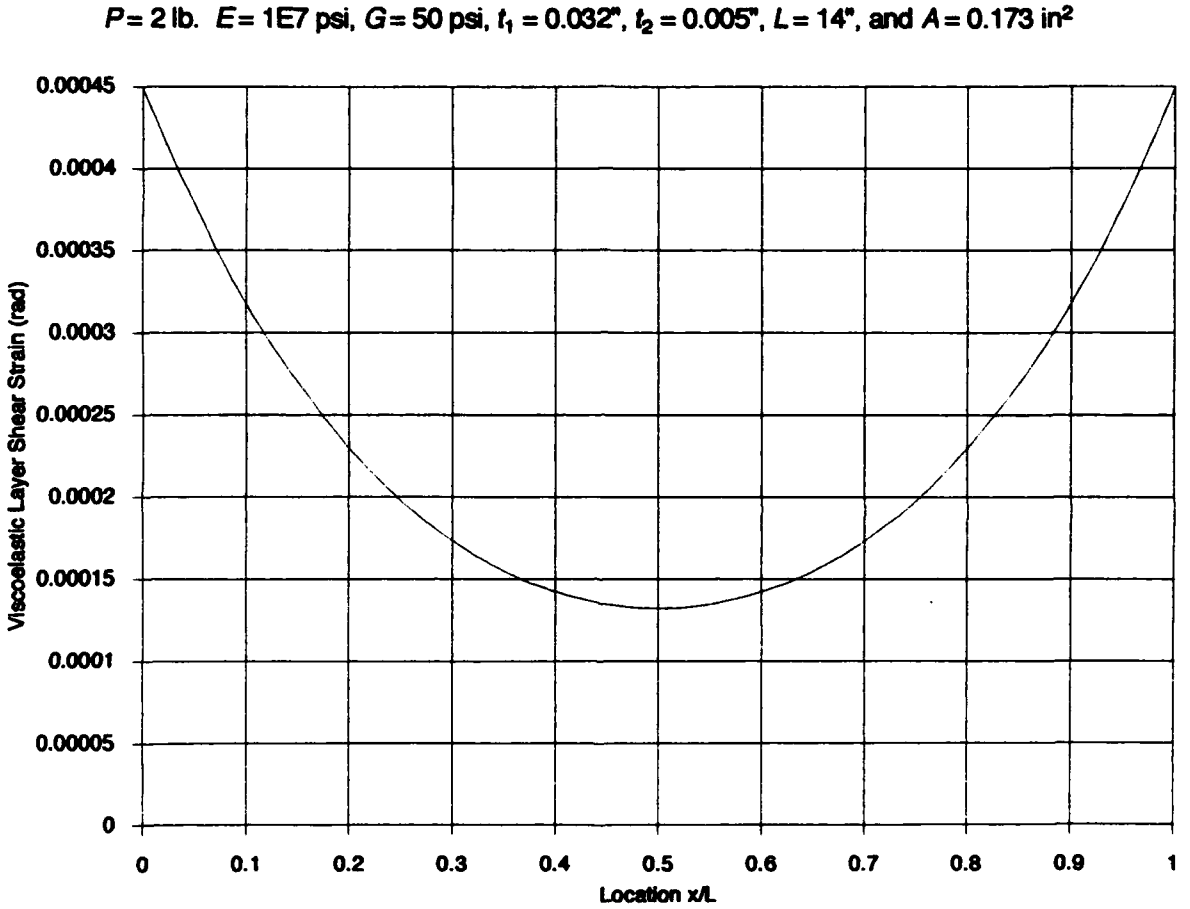

Figure 5.6 Shear Strain of Viscoelastic Layer due to Axial Loading

A quick substitution into equations (5.9) verifies that these expressions are indeed solutions. Equations (5.31-2) represent the midpoints of the constraining layers for all time (assuming a static analysis is appropriate). From (5.3), we know the shear strain is the quotient of u_3 - u_1 and t_2. This value is the *average* shear strain through the thickness. Intuitively, this concept is contradictory since we know that, at either end, one of the constraining layers has maximum stress while the other has zero stress. This is

considered to be a local end effect that dies out a very short distance into the beam according to St. Venant's principle. Loosely speaking, the shear distribution through the thickness will self-equilibrate.

Effect of Lever Geometry on Bending Analysis

The determination of the lever lengths h and s is complicated by the presence of an asymmetric bending phenomenon between the tensile and compressive halves of a vibration cycle. Gere and Timoshenko [19: 567-8] discussed the effect of eccentric loading on the displacement of a homogeneous beam-column. Their development for the compressive half of the cycle is presented here.

Consider an eccentrically loaded beam-column like the one in figure 5.7.

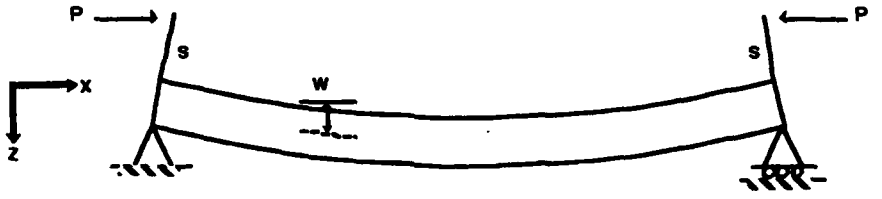

Figure 5.7 Eccentrically Loaded Beam-Column

Assume the distance s remains constant in the z-direction and that the levers are rigid. The moment at any location x along the beam is

$$M = P(s + w) \tag{5.34}$$

From strength of materials theory,

$$\begin{aligned} EIw'' &= -M = -P(s + w) \\ w'' + \frac{P}{EI}w &= \frac{-P}{EI}s \end{aligned} \tag{5.35}$$

with boundary conditions $w(0) = w(L) = 0$. If we let

$$k^2 = \frac{P}{EI} \tag{5.36}$$

the homogeneous solution to (5.35) is

$$w(x)_h = A\ \cos kx + B\ \sin kx \tag{5.37}$$

To find the particular solution, assume $w_p = Cs + D$, whose derivatives are

$$w_p' = C \quad \text{and} \quad w_p'' = 0 \tag{5.38}$$

Substitution of this form into the differential equation yields the algebraic expression

$$\frac{P}{EI}(Cs + D) = -\frac{P}{EI}s \quad \Rightarrow \quad C = -1\ ,\ D = 0 \tag{5.39}$$

Therefore,

$$w_p = -s \tag{5.40}$$

Using the boundary conditions to find the constants,

$$w(0) = A - s = 0 \quad \Rightarrow \quad A = s \tag{5.41}$$

$$w(L) = s\ \cos kL + B\ \sin kL - s = 0$$

$$\Rightarrow \quad B = s\left(\frac{1-\cos kL}{\sin kL}\right) = s\ \tan\frac{kL}{2} \tag{5.42}$$

The expression for $w(x)$ is then

$$w(x) = s\left(\tan\frac{kL}{2}\sin kx + \cos kx - 1\right) \tag{5.43}$$

The maximum deflection occurs at $x = L/2$, where

$$w\left(\frac{L}{2}\right) = s\left(\sec\frac{kL}{2} - 1\right) \tag{5.44}$$

If P was uncontrolled and allowed to grow without bound, $w(x)$ would grow to infinity as $kL/2$ approaches $\pi/2$. Fortunately, the distance over which P acts is controlled by the limited deflections of the truss. Therefore, we need not be concerned about exceeding the

yield stress of the constraining layers at $x = L/2$ and about the effect of this highly nonlinear phenomenon on the assumed linear analysis. Therefore, in choosing h and s, the check must be made that $kL/2$ is not close to $\pi/2$.

Consider the other half of the cycle, where P is *pulling* the lever tips apart. The moment M becomes $M = P(s-w)$ since the beam is deflecting *toward* the load center. The differential equation then becomes

$$w'' - \frac{P}{EI} w = -P(s - w) \tag{5.45}$$

The solution to this equation is

$$w(x) = s\left(\tanh\frac{kL}{2}\sinh kx - \cosh kx + 1\right) \tag{5.46}$$

The maximum displacement, at $x = L/2$, is given by

$$w\left(\frac{L}{2}\right) = s\left(1 - \operatorname{sech}\left(\frac{kL}{2}\right)\right) \tag{5.47}$$

The value of 1-sech $kL/2$ approaches 1 as k gets large. This phenomenon is a problem because stresses will grow high at the corners formed by the short lever and the sandwich beam. Figure 5.8 illustrates the difference between the secant and hyperbolic secant functions as their arguments become large. For comparison, the strength of materials solution is included. This solution, based on a (1 - cos θ) relationship, which is what a linear finite element solver uses. Conveniently, over a significant range of values of $kL/2$, the ordinate of the strength of materials solution is close to the midpoint between the two other functions. This fact essentially allows us to greatly simplify the analysis to a symmetric loading throughout the vibration cycle if we are willing to accept a small error. Since the strain energy is proportional to the square of the curvature (which is proportional to the moment), this error will be squared, which could produce significant error at extreme deflections in the cycle. If the value of $kL/2$ is monitored throughout the design, we can safely neglect the effects of an asymmetric bending cycle.

The equations of the curves in this illustration are the following:

$$w(L/2) \text{ For Tension} = s(\sec(kL/2)-1) \tag{5.48}$$

$$\text{Compression} = s(1\text{-sech}(kL/2)) \tag{5.49}$$

$$\text{Circular Curvature} = s(1\text{-cos}(kL/2)) \tag{5.50}$$

$s = 1$ for all curves

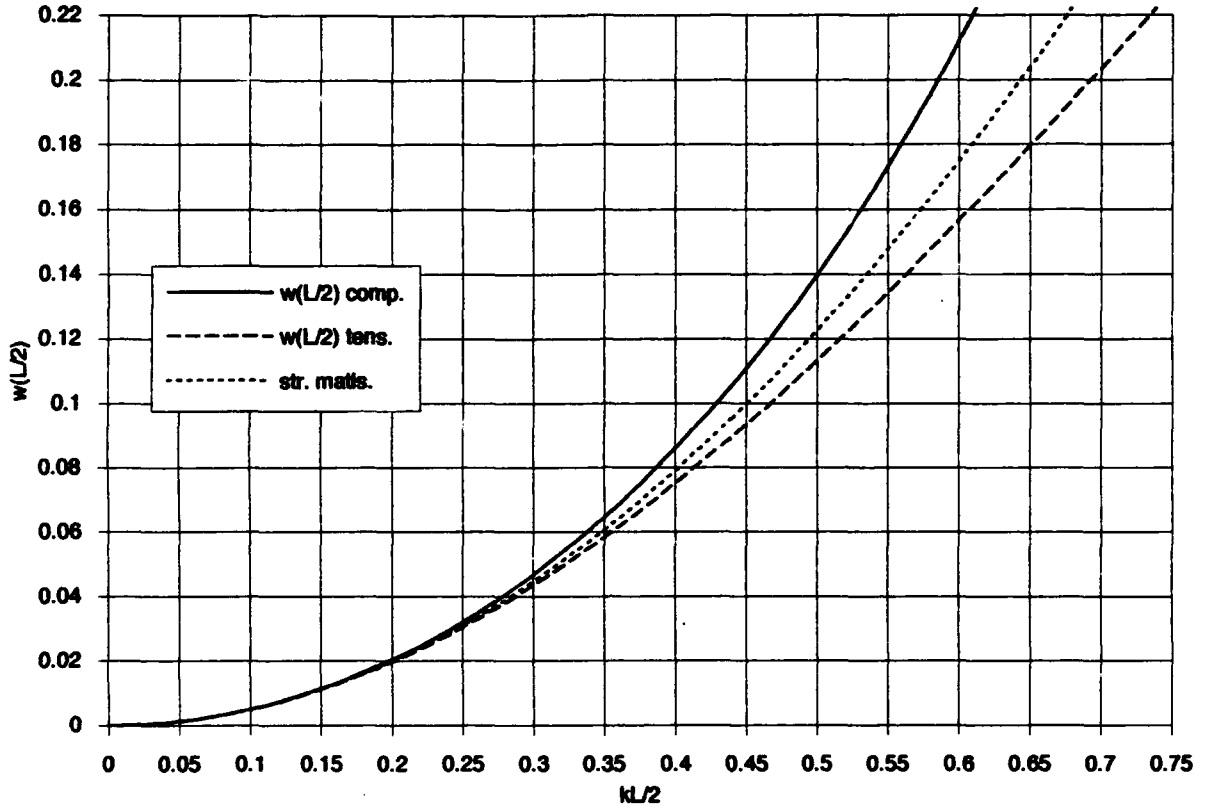

Figure 5.8 Maximum Tensile and Compressive Cycle Displacements [$w(L/2)$]

The Differential Equation of Transverse Displacement for a Three-Layer Sandwich Beam

Mead and Markus [8] used DiTaranto's derivation of the equation of longitudinal displacement of a three-layer sandwich beam [7] as a basis for developing the equation of *transverse* displacement. They converted the longitudinal variable ζ to the transverse variable w and arrived at a sixth-order differential equation similar to DiTaranto's. Their development is given in Appendix D, but the missing steps from their analysis are rigorously developed. The resulting equation, for no external forces applied in the interior, is

$$\frac{\partial^6 w}{\partial x^6} - g(1+Y)\frac{\partial^4 w}{\partial x^4} + \frac{(\rho t)}{D}\left(\frac{\partial^4 w}{\partial x^2 \partial t^2} - g\frac{\partial^2 w}{\partial t^2}\right) = 0 \tag{5.51}$$

For this equation,

$$g = \frac{2G}{Et_1 t_2}\ ,\quad Y = \frac{(Et_1)(t_1+t_2)^2}{2D}\ ,\ \text{and}\ D = \frac{Et_1^{\,3}}{6(1-\nu^2)} \tag{5.52}$$

Boundary Conditions for the Sandwich Beam

Since the equation of motion is of order six, we need six boundary conditions to find $w(x,t)$. Four boundary conditions (two displacement and two force) come from the transversely vibrating composite beam. The other two (displacement) boundary conditions come from the restraint of longitudinal motion of the constraining layers. The displacement boundary conditions are all homogeneous, but the forced boundary conditions are nonzero and time-dependent. Solutions to problems of this type are not generally obtainable by using the classical method of separating the spatial and temporal variables. Therefore, in order to solve this equation, we must convert the nonhomogeneous boundary conditions to homogeneous boundary conditions through a transformation of variables. The effect of this transformation is that the homogeneous equation of motion becomes nonhomogeneous. The resulting forced vibration problem can then be solved by modal expansion. Mindlin and Goodman [20] developed a procedure for solving these types of problems by using what they call "elementary mathematical techniques" as opposed to integral transform methods that use the Laplace and Fourier transforms.

Their solution method involves the construction of a comparison function that effectively homogenizes the time-dependent boundary conditions. Then, modal analysis is employed to find the forced response solution to the nonhomogeneous equation of motion.

Mead and Markus [8] discussed the possibility of entirely real solutions to the sixth-order differential equation. They reported that if a beam is simply supported at its ends and the faceplate displacements are unrestrained at both ends, then

$$w_i = A_i \sin \lambda_i x \tag{5.53}$$

is a possible solution.

Mead and Markus [8] developed expressions for a number of different boundary conditions. For this analysis it is assumed that the rotary inertia of the small levers is zero. This is clearly unacceptable at high frequencies, but at low frequencies the associated error will be small. In addition, axial loading will be neglected as it has already been accounted for. Assume the changes in the lever angles cause a negligible transverse displacement. This assumption gives two displacement boundary conditions:

$$[W_n]_{x=0} = [W_n]_{x=L} = 0 \tag{5.54}$$

Two more boundary conditions come from the free edges of the plates:

$$\left.\frac{\partial u_1}{\partial x}\right|_{x=L} = \left.\frac{\partial u_3}{\partial x}\right|_{x=0} = 0$$

Symmetry gives

$$\frac{\partial u_3}{\partial x} = -\frac{\partial u_1}{\partial x} \quad \Rightarrow \quad -\left.\frac{\partial u_1}{\partial x}\right|_{x=0} = 0 \tag{5.55}$$

We can equate these boundary conditions in u to boundary conditions in w by using equation (D.23) (found in Appendix D).

$$\left.\frac{\partial u_1}{\partial x}\right|_{x=L} = \frac{D}{gEt_1t_2\left(1+t_1/t_2\right)}\left[\frac{\partial^4 w}{\partial x^4} + gY\frac{\partial^2 w}{\partial x^2} - \frac{(\rho t)}{D}\frac{\partial^2 w}{\partial t^2}\right]_{x=L} = 0 \tag{5.56}$$

and

$$\left.\frac{\partial u_3}{\partial x}\right|_{x=0} = \frac{-D}{gEt_1t_2\left(1+t_1/t_2\right)}\left[\frac{\partial^4 w}{\partial x^4} + gY\frac{\partial^2 w}{\partial x^2} - \frac{(\rho t)}{D}\frac{\partial^2 w}{\partial t^2}\right]_{x=0} = 0 \tag{5.57}$$

To find the moment boundary condition, consider the summation of moments M_i of each individual layer.

$$M_1 = D_1\frac{\partial^2 w}{\partial x^2} \quad \text{and} \quad M_3 = D_3\frac{\partial^2 w}{\partial x^2} \tag{5.58}$$

M_2 results from the forces P_1 and P_3 which are opposed and offset by distance $t_2(1+t_1/t_2)$.

$$
\begin{aligned}
M_2 &= P_1\left(\frac{1}{2}\left(t_2\left(1+\frac{t_1}{t_2}\right)\right)\right) - P_3\left(\frac{1}{2}\left(t_2\left(1+\frac{t_1}{t_2}\right)\right)\right) \\
&= P_1\left(t_2\left(1+\frac{t_1}{t_2}\right)\right) \\
&= Et_1\frac{\partial u_1}{\partial x}\left(t_2\left(1+\frac{t_1}{t_2}\right)\right) \\
&= Et_1t_2\left(1+\frac{t_1}{t_2}\right)\frac{D}{gEt_1t_2\left(1+t_1/t_2\right)}\left[-\frac{\partial^4 w}{\partial x^4}+gY\frac{\partial^2 w}{\partial x^2}-\frac{(\rho t)}{D}\frac{\partial^2 w}{\partial t^2}\right] \\
&= \frac{D}{g}\left[-\frac{\partial^4 w}{\partial x^4}+gY\frac{\partial^2 w}{\partial x^2}-\frac{(\rho t)}{D}\frac{\partial^2 w}{\partial t^2}\right]
\end{aligned}
\tag{5.59}
$$

Summing M_i gives the moment as

$$
M = \frac{D}{g}\left[-\frac{\partial^4 w}{\partial x^4}+g(1+Y)\frac{\partial^2 w}{\partial x^2}-\frac{(\rho t)}{D}\frac{\partial^2 w}{\partial t^2}\right] \tag{5.60}
$$

The boundary conditions are then

$$
M(0) = -M_b \sin\omega_T t \quad \text{and} \quad M(L) = M_b \sin\omega_T t \tag{5.61}
$$

where M_b is the maximum external moment imposed by the vibrating truss at the ends for any given cycle. One important simplifying assumption is that the moments prescribed at each end are equal in magnitude and opposite in sense for all time.

Mindlin and Goodman used a convenient operator notation that is suitable here. Define the boundary condition operators B_i to be

$$
B_1 = B_4 = 1 \tag{5.62}
$$

$$
B_2 = -B_5 = \frac{D}{g}\left[-\frac{\partial^4}{\partial x^4}+g(1+Y)\frac{\partial^2}{\partial x^2}+\frac{(\rho t)}{D}\omega^2\right] \tag{5.63}
$$

where

$$-\omega^2 = \frac{\partial^2}{\partial t^2},$$

and

$$B_3 = -B_6 = \frac{D}{gEt_1t_2\left(1+{}^{t_1}\!/_{t_2}\right)}\left[-\frac{\partial^4}{\partial x^4} + gY\frac{\partial^2}{\partial x^2} + \frac{(\rho t)}{D}\omega^2\right] \tag{5.64}$$

The boundary conditions can be expressed in summation notation as

$$B_i[w(0,t)] = f_i(t) \quad , \quad i = 1,\ 2,\ 3$$
$$B_i[w(L,t)] = f_i(t) \quad , \quad i = 4,\ 5,\ 6$$

In unabridged form,

$$B_1[w(0,t)] = 0 \qquad B_4[w(L,t)] = 0$$
$$B_2[w(0,t)] = -M_b \sin\omega_T t \qquad B_5[w(L,t)] = M_b \sin\omega_T t$$
$$B_3[w(0,t)] = 0 \qquad B_6[w(L,t)] = 0 \tag{5.65}$$

where ω_T = the frequency of vibration of the external force. Zero initial conditions are assumed.

Solution of the Differential Equation

Since the boundary conditions are non-homogeneous, we will transform the variable w into v and force the boundary conditions in v to be homogeneous. To do this transformation, we assume a solution of the form

$$w(x,t) = v(x,t) + \sum_i g_i(x) f_i(t) \tag{5.66}$$

We must also transform the boundary conditions into v. Substituting (5.66) into (5.65),

$$B_1[w(0,t)] = B_1[v(0,t)] + \sum_{j=1}^{6} f_j(t) B_1\left[g_j(x)\right]$$

$$B_2[w(0,t)] = B_2[v(0,t)] + \sum_{j=1}^{6} f_j(t) B_2\left[g_j(x)\right]$$

$$
\begin{aligned}
B_3[w(0,t)] &= B_3[v(0,t)] + \sum_{j=1}^{6} f_j(t) B_3\left[g_j(x)\right] \\
B_4[w(L,t)] &= B_4[v(L,t)] + \sum_{j=1}^{6} f_j(t) B_4\left[g_j(x)\right] \\
B_5[w(L,t)] &= B_5[v(L,t)] + \sum_{j=1}^{6} f_j(t) B_5\left[g_j(x)\right] \\
B_6[w(L,t)] &= B_6[v(L,t)] + \sum_{j=1}^{6} f_j(t) B_6\left[g_j(x)\right]
\end{aligned}
\tag{5.67}
$$

We know from (5.65) that $f_2 = -f_5 = -M_b \sin \omega_T t$ and $f_1 = f_3 = f_4 = f_6 = 0$. Since the purpose of the variable transformation is to homogenize the boundary conditions in v, we must choose $g_j(x)$ so that $B_i[v(x,t)] = 0$. Therefore, we rearrange (5.67) to get

$$
\begin{aligned}
B_1[v(0,t)] &= B_1[w(0,t)] - \left\{ f_2(t) B_1\left[g_2(0)\right] + f_5(t) B_1\left[g_5(0)\right] \right\} = 0 \\
B_2[v(0,t)] &= B_2[w(0,t)] - \left\{ f_2(t) B_2\left[g_2(0)\right] + f_5(t) B_2\left[g_5(0)\right] \right\} = 0 \\
B_3[v(0,t)] &= B_3[w(0,t)] - \left\{ f_2(t) B_3\left[g_2(0)\right] + f_5(t) B_3\left[g_5(0)\right] \right\} = 0 \\
B_4[v(L,t)] &= B_4[w(L,t)] - \left\{ f_2(t) B_4\left[g_2(L)\right] + f_5(t) B_4\left[g_5(L)\right] \right\} = 0 \\
B_5[v(L,t)] &= B_5[w(L,t)] - \left\{ f_2(t) B_5\left[g_2(L)\right] + f_5(t) B_5\left[g_5(L)\right] \right\} = 0 \\
B_6[v(L,t)] &= B_6[w(L,t)] - \left\{ f_2(t) B_6\left[g_2(L)\right] + f_5(t) B_6\left[g_5(L)\right] \right\} = 0
\end{aligned}
\tag{5.68}
$$

In order to satisfy these relationships,

$$
\begin{aligned}
B_i\left[g_j(0)\right] &= \delta_{ij} \ , \quad i = 1,\ 2,\ 3 \\
B_i\left[g_j(L)\right] &= \delta_{ij} \ , \quad i = 4,\ 5,\ 6
\end{aligned}
\tag{5.69}
$$

The initial conditions expressed in v are

$$
\begin{aligned}
v(x,0) &= 0 - \sum_{i=1}^{6} f_i(0) g_i(x) = 0 \\
\dot{v}(x,0) &= 0 - \sum_{i=1}^{6} \dot{f}_i(0) g_i(x) = \omega_T M_b \left(g_2(x) - g_5(x) \right)
\end{aligned}
\tag{5.70}
$$

since

$$
\omega_T M_b \cos \omega_T(0) = \omega_T M_b
$$

$g_2(x)$ and $g_5(x)$ must be determined. We assume a polynomial form of g_i, and since at least one of the operators is of order zero, let

$$g_2(x) = a_2 + b_2x + c_2x^2 + d_2x^3 + e_2x^4 + k_2x^5 \tag{5.71}$$

To solve for g_2, we use each operator to construct an algebraic equation that is either equal to zero or unity according to (5.69).

$$B_1[g_2(0)] = 0 \Rightarrow a_2 = 0 \tag{5.72}$$

$$B_2[g_2(0)] = 1 \Rightarrow \frac{D}{g}\left[-\frac{\partial^4}{\partial x^4} + g(1+Y)\frac{\partial^2}{\partial x^2} + \frac{(\rho t)}{D}\omega^2\right][g_2(0)] = 1 \tag{5.73}$$

$$\frac{-24D}{g}e_2 + 2D(1+Y)c_2 = 1$$

$$B_3[g_2(0)] = 0 \Rightarrow -24e_2 + 2gYc_2 = 0 \tag{5.74}$$

e_2 and c_2 are now determined as

$$c_2 = \frac{1}{2D}, \quad e_2 = \frac{gY}{24D} \tag{5.75}$$

Next, we solve the boundary conditions at L by considering e_2 and c_2 to be constants.

$B_4[g_2(L)] = 0$

$$Lb_2 + L^3d_2 + L^5k_2 = -L^2c_2 - L^4e_2 \tag{5.76}$$

$B_5[g_2(L)] = 0$

$$\left[\frac{-(\rho t)}{D}\omega^2 L\right]b_2 + \left[-6g(1+Y)L - \frac{(\rho t)}{D}\omega^2 L^3\right]d_2 + \left[120L - 20g(1+Y)L^3 - \frac{(\rho t)}{D}\omega^2 L^5\right]k_2$$
$$= \left[2g(1+Y) + \frac{(\rho t)}{D}\omega^2 L^2\right]c_2 + \left[\frac{(\rho t)}{D}\omega^2 L^4 + 12g(1+Y)L^2 - 24\right]e_2 \tag{5.77}$$

$B_6[g_2(L)] = 0$

$$\left[\frac{-(\rho t)}{D}\omega^2 L\right]b_2 + \left[-6gYL - \frac{(\rho t)}{D}\omega^2 L^3\right]d_2 + \left[120L - 20gYL^3 - \frac{(\rho t)}{D}\omega^2 L^5\right]k_2$$
$$= \left[2gY + \frac{(\rho t)}{D}\omega^2 L^2\right]c_2 + \left[\frac{(\rho t)}{D}\omega^2 L^4 + 12gYL^2 - 24\right]e_2 \tag{5.78}$$

Solving (5.76-78) simultaneously,

$$b_2 = \frac{gYL^3 - 15L}{45D}\ ,\ d_2 = -\frac{gYL^2 + 3}{18DL}\ ,\ \text{and}\ \ k_2 = -\frac{gY}{120DL} \tag{5.79}$$

Therefore,

$$g_2(x) = a_2 + \frac{gYL^3 - 15L}{45D}x + \frac{1}{2D}x^2 - \frac{gYL^2 + 3}{18DL}x^3 + \frac{gY}{24D}x^4 - \frac{gY}{120DL}x^5 \tag{5.80}$$

Inserting (5.80) back into the g_2 boundary conditions will verify that they are indeed satisfied. It remains to find $g_5(x)$. We again assume the polynomial form

$$g_5(x) = a_2 + b_5x + c_5x^2 + d_5x^3 + e_5x^4 + k_5x^5 \tag{5.81}$$

$$\begin{aligned} B_1[g_5(0)] = 0 \ &\Rightarrow \quad a_5 = 0 \\ B_2[g_5(0)] = 0 \ &\Rightarrow \quad -24e_5 + 2g(1+Y)c_5 = 0 \\ B_3[g_5(0)] = 0 \ &\Rightarrow \quad -24e_5 + 2gYc_5 = 0 \end{aligned} \tag{5.82}$$

Clearly, $c_5 = e_5 = 0$. The boundary conditions at L are the following:

$$B_4[g_5(L)] = 0$$
$$Lb_5 + L^3d_5 + L^5k_5 = 0 \tag{5.83}$$

$$B_5[g_5(L)] = 1$$
$$\left[\frac{-(\rho t)}{D}\omega^2 L\right]b_5 + \left[-6g(1+Y)L - \frac{(\rho t)}{D}\omega^2 L^3\right]d_5 + \left[120L - 20g(1+Y)L^3 - \frac{(\rho t)}{D}\omega^2 L^5\right]k_5 = \frac{g}{D} \tag{5.84}$$

$$B_6[g_5(L)] = 0$$
$$\left[\frac{-(\rho t)}{D}\omega^2 L\right]b_5 + \left[-6gYL - \frac{(\rho t)}{D}\omega^2 L^3\right]d_5 + \left[120L - 20gYL^3 - \frac{(\rho t)}{D}\omega^2 L^5\right]k_5 = 0 \tag{5.85}$$

Solving (5.83-85) simultaneously,

$$b_5 = \frac{60L - 7gYL^3}{360D}\ ,\quad d_5 = \frac{gYL^2 - 6}{36DL}\ ,\quad \text{and}\quad k_5 = -\frac{gY}{120DL} \tag{5.86}$$

Therefore,

$$g_5(x) = \frac{60L - 7gYL^3}{360D}x + \frac{gYL^2 - 6}{36DL}x^3 - \frac{gY}{120DL}x^5 \tag{5.87}$$

This function also satisfies the boundary conditions. At this point, g_2 and g_5 will homogenize the boundary conditions.

The next step is to solve the nonhomogeneous equation of motion in v with the boundary and initial conditions expressed in v. Meirovitch's text [21: 303-5] contains an excellent summary of the following solution to the nonhomogeneous differential equation. We shall express the differential equation in his operator notation as

$$L[v(x,t)] + M(x)\frac{\partial^2}{\partial t^2}v(x,t) = F(x,t) - \sum_{i=1}^{6}\left[f_i(t)L[g_i(x)] + \ddot{f}_i(t)M(x)g_i(x)\right] \tag{5.88}$$

where

$$L = \frac{\partial^6}{\partial x^6} - g(1+Y)\frac{\partial^4}{\partial x^4}$$

$$M = \frac{(\rho t)}{D}\left(\frac{\partial^2}{\partial x^2} - g\right)$$

$$f_i(t) = \begin{cases} -M_b \sin\omega_T t\ , & i = 2 \\ M_b \sin\omega_T t\ , & i = 5 \\ 0 & \text{otherwise} \end{cases}$$

First, the homogeneous eigenvalue problem in v is solved. Now that the boundary conditions are homogeneous, we can separate the spatial and temporal variables by assuming a solution of the form

$$v(x,t) = \sum_{n=1}^{\infty} X_n(x)T_n(t) \tag{5.89}$$

The eigenvalue problem becomes

$$L[v(x)] - \omega^2 M[v(x)] = 0 \tag{5.90}$$

Since we are prescribing a moment at the ends, assume the mode shapes

$$v_n(x) = V_n \sin\frac{n\pi x}{L} \tag{5.91}$$

Let us pause and consider the validity of this assumption. If we investigate the dynamic motion of the fundamental mode, it is, in fact, asymmetric. Imagine pressing down on the center of the left sandwich beam depicted in Figure 5.8. This half of the vibration cycle resembles very much a beam simply supported at its tips. However, if we pull up in the middle, this deformation is better described by a fixed-fixed beam. In fact, it will be even *stiffer* than a fixed-fixed beam because as deformation causes the levers to move inward, the corners will begin rotating opposite the motion of the beam center. Clearly, by assuming this mode shape, we are describing only part of the cycle partly accurately. If we are concerned with determining the worst-case displacement scenario, equation (5.91) is probably the most conservative full-cycle mode shape to assume. However, depending on the geometry, damping factors may or may not be adversely affected by the limited displacements in the stiffer half-cycle. If the dynamic part of the solution becomes the dominant term (as in frequencies near sandwich beam resonances), then a more accurate investigation need be made with regard to what mode shapes to assume.

Figure 5.9 Deformed Geometry of Beams Pinned at Supports
(corner right angles maintained)

If we assume (5.91), then

$$\frac{\partial^6}{\partial x^6}\sin\frac{n\pi x}{L} = -\left(\frac{n\pi}{L}\right)^6 \sin\frac{n\pi x}{L}$$

$$\frac{\partial^4}{\partial x^4}\sin\frac{n\pi x}{L} = \left(\frac{n\pi}{L}\right)^4 \sin\frac{n\pi x}{L}$$

$$\frac{\partial^2}{\partial x^2}\sin\frac{n\pi x}{L} = -\left(\frac{n\pi}{L}\right)^2 \sin\frac{n\pi x}{L} \tag{5.92}$$

Substitution of these derivatives into (5.51) yields

$$-\left(\frac{n\pi}{L}\right)^6 \sin\frac{n\pi x}{L} - g(1+Y)\left(\frac{n\pi}{L}\right)^4 \sin\frac{n\pi x}{L} - \omega^2\left[\frac{D}{\rho t}\left(-\left(\frac{n\pi}{L}\right)^2 \sin\frac{n\pi x}{L} - g\sin\frac{n\pi x}{L}\right)\right] = 0 \tag{5.93}$$

$$\omega_n^{\,2} = \frac{D}{\rho t}\left(\frac{n\pi}{L}\right)^4 \left[\frac{1+g(1+Y)\left(\frac{L}{n\pi}\right)^2}{1+g\left(\frac{L}{n\pi}\right)^2}\right] \tag{5.94}$$

This expression for ω_n^2 is the same result obtained by Torvik [17].

Now we must normalize the coefficients V_n with respect to $M(x)$ of the eigenfunctions $v_n(x)$. This step turns out to be necessary in order for the units of the "dynamic" part of the solution to match the units of the "$f_i(t)g_i(x)$" part of the solution. Since $M(x)$ is a differential operator,

$$\int_0^L v_m M[v_n]\,dx = \delta_{mn} \tag{5.95}$$

where

$$v_m = V_m \sin\frac{m\pi x}{L} \quad \text{and} \quad v_n = V_n \sin\frac{n\pi x}{L}$$

$$\int_0^L V_m \sin\frac{m\pi x}{L}\left[V_n\frac{(\rho t)}{D}\left(-\left(\frac{n\pi}{L}\right)^2 \sin\frac{n\pi x}{L} - g\sin\frac{n\pi x}{L}\right)\right]dx = 1 \tag{5.96}$$

For $m \neq n$, the value of the integral is zero. For $m = n$,

$$V_n^{\,2} = \frac{-2D}{(\rho t)\left[\left(\frac{n\pi}{L}\right)^2 + g\right]L} \tag{5.97}$$

We assumed a solution of the form

$$v(x,t) = \sum_{n=1}^{\infty} v_n(x) T_n(t) \tag{5.89}$$

When this form is substituted into the non-homogeneous equation of motion, we have

$$\sum_{n=1}^{\infty}\left[T_n(t)L[v_n(x)] + \ddot{T}_n(t)M[v_n(x)]\right] = -\sum_{i=1}^{6}\left[f_i(t)L[g_i(x)] + \ddot{f}_i(t)M[v_n(x)]\right] \tag{5.98}$$

Since v_n and ω_n satisfy the eigenvalue problem (5.90), we can rewrite this expression as

$$\sum_{n=1}^{\infty}\left[\ddot{T}_n(t) + \omega_n^2 T_n(t)\right]M[v_n(x)] = -\sum_{i=1}^{6}\left[f_i(t)L[g_i(x)] + \ddot{f}_i(t)M[v_n(x)]\right] \tag{5.99}$$

This infinite set of coupled equations can be uncoupled by using orthogonality. We multiply each side by $v_m(x)$ and integrate from 0 to L. We now introduce the orthogonalized spatial coefficients

$$G_{n_i} = \int_0^L v_n(x)M[g_i(x)]\,dx \quad \text{and} \quad G_{n_i}^* = \int_0^L v_n(x)L[g_i(x)]\,dx \tag{5.100}$$

This step gives the uncoupled equations

$$\ddot{T}_n(t) + \omega_n^2 T_n(t) = N_n(t) \tag{5.101}$$

where

$$N_n(t) = \sum_{i=1}^{6}\left[G_n^* f_i(t) + G_{n_i}\ddot{f}_i(t)\right]$$

The non-zero terms $G_{n_2}, G_{n_5}, G_{n_2}^*$, and $G_{n_5}^*$ are

$$G_{n_2} = V_n \frac{(\rho t)}{D}\left\{(-1)^n\left[-2c_2\left(\frac{L}{n\pi}\right)-(6d_2-gb_2)L\left(\frac{L}{n\pi}\right)+(12e_2-gc_2)\left[2\left(\frac{L}{n\pi}\right)^3-L^2\left(\frac{L}{n\pi}\right)\right]\right.\right.$$
$$+(20k_2-gd_2)\left[6L\left(\frac{L}{n\pi}\right)^3-L^3\left(\frac{L}{n\pi}\right)\right]+ge_2\left[L^4\left(\frac{L}{n\pi}\right)+24\left(\frac{L}{n\pi}\right)^5-12L^2\left(\frac{L}{n\pi}\right)^3\right]$$
$$\left.\left.+gk_2\left[L^5\left(\frac{L}{n\pi}\right)+120L\left(\frac{L}{n\pi}\right)^5-20L^3\left(\frac{L}{n\pi}\right)^3\right]\right]+2c_2\left(\frac{L}{n\pi}\right)-2(12e_2-gc_2)\left(\frac{L}{n\pi}\right)^3$$
$$\left.-24ge_2\left(\frac{L}{n\pi}\right)^5\right\} \tag{5.102}$$

$$G_{n_5} = V_n \frac{(\rho t)}{D}(-1)^n\left[(6d_5-gb_5)\left(-L\left(\frac{L}{n\pi}\right)\right)+(20k_5-gd_5)\left(6L\left(\frac{L}{n\pi}\right)^3-L^3\left(\frac{L}{n\pi}\right)\right)\right.$$
$$\left.+gk_5\left(L^5\left(\frac{L}{n\pi}\right)+120L\left(\frac{L}{n\pi}\right)^5-20L^3\left(\frac{L}{n\pi}\right)^3\right)\right] \tag{5.103}$$

$$G^*_{n_2} = -V_n g(1+Y)\left[(-1)^n\left(-24e_2\left(\frac{L}{n\pi}\right)-120k_2L\left(\frac{L}{n\pi}\right)\right)+24e_2\left(\frac{L}{n\pi}\right)\right] \tag{5.104}$$

$$G^*_{n_5} = 120(-1)^n V_n g(1+Y)L\left(\frac{L}{n\pi}\right) \tag{5.105}$$

The length of these terms is a result of integrating the product of a sine function and a fifth-order polynomial (several integrations by parts are needed).

$N_n(t)$ can then be expanded as

$$N_n(t) = -\left(G^*_{n_2} f_2(t) + G_{n_2}\ddot{f}_2(t) + G^*_{n_5} f_5(t) + G_{n_5}\ddot{f}_5(t)\right) \tag{5.106}$$

For zero initial conditions, the temporal solution is

$$T_n(t) = \frac{1}{\omega_{SB_n}}\int_0^t N_n(\tau)\sin\omega_{SB_n}(t-\tau)\,d\tau \tag{5.107}$$

We can now write the solution for $v(x,t)$ as

$$v(x,t) = \sum_{n=1}^{\infty} v_n(x) T_n(t)$$
$$= \sum_{n=1}^{\infty} V_n \sin\frac{n\pi x}{L} \frac{1}{\omega_{SB_n}} \int_0^t N_n(\tau) \sin\omega_{SB_n}(t-\tau)\, d\tau \tag{5.108}$$

Transforming back to w using equation (5.66), the solution is

$$w(x,t) = \sum_{n=1}^{\infty} V_n \sin\frac{n\pi x}{L} \frac{1}{\omega_{SB_n}} \int_0^t N_n(\tau) \sin\omega_{SB_n}(t-\tau)\, d\tau$$
$$+M_b \sin\omega_T t \left[\frac{60L - 7gYL^3}{360D} x + \frac{gYL^2 - 6}{36DL} x^3 - \frac{gY}{120DL} x^5\right] \tag{5.109}$$
$$-M_b \sin\omega_T t \left[\frac{gYL^3 - 15L}{45D} x + \frac{1}{2D} x^2 - \frac{gYL^2 + 3}{18DL} x^3 + \frac{gY}{24D} x^4 - \frac{gY}{120DL} x^5\right]$$

This is the relative displacement of the sandwich beam with respect to a translating, rotating truss. This is an approximate solution because the polynomials are merely comparison functions and because the mode shape assumption made on the first term is approximate. A cursory look at this solution indicates that the "forcing" term will be equal to zero for all of the boundary conditions since

$$\sin\frac{n\pi x}{L}\bigg|_{x=0} = \sin\frac{n\pi x}{L}\bigg|_{x=L} = 0 \tag{5.110}$$

Since $g_i(x)$ were prescribed to satisfy the boundary conditions in v, they will automatically satisfy the boundary conditions in w. Additionally, an inspection of the comparison functions indicates that the unit is indeed a displacement. Strictly speaking, the unit is in^2, but the moment is divided by the width since this is a per unit width analysis. Finally, the suspicious lack of an "M/EI-looking" term is explained by the presence of D in each denominator. Assuming the end moments are equal, the comparison function reduces to

$$M_b \sin\omega_T t \left[\frac{12L - gYL^3}{24D} x - \frac{1}{2D} x^2 + \frac{gYL}{12D} x^3 - \frac{gY}{24D} x^4\right]$$

The following graph shows the comparison function versus a sine wave (normalized with respect to each other).

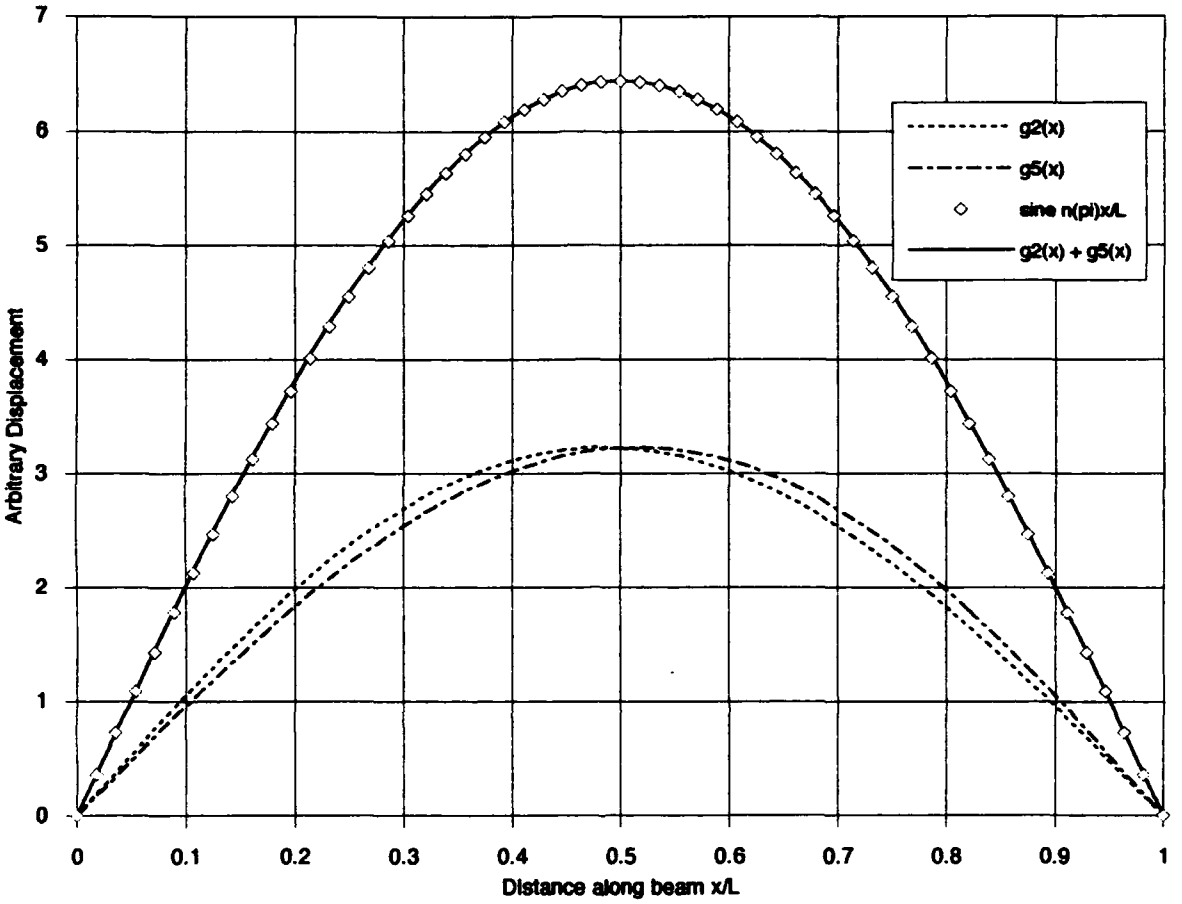

Figure 5.10 Displacement of the Comparison Function Terms as a Function of $^{x}/_{L}$ Normalized to a Sine Curve

An investigation of the convolution integral term gives

$$\frac{1}{\omega_{SB}}\int_0^t \sin\omega_T\tau \, \sin\omega_{SB}(t-\tau)\, d\tau = \frac{1}{\omega_{SB}}\left(\frac{\omega_T \sin\omega_{SB}t}{\omega_T{}^2 - \omega_{SB}{}^2} - \frac{\omega_{SB}\sin\omega_T t}{\omega_T{}^2 - \omega_{SB}{}^2}\right) \qquad (5.111)$$

The evaluation of the convolution integral reveals that the resonance phenomenon is accounted for. The $\omega_T{}^2$-$\omega_{SB}{}^2$ term in the denominator suggests that the amplitude of vibration grows without bound as ω_T approaches ω_{SB}. This will not be the case since the sandwich beam is damped. However, an investigation of ω_{SB} is warranted for likely configurations. The natural frequencies are calculated from the equation

$$f_n = \frac{1}{2\pi}\beta^2\sqrt{\frac{EI}{\rho AL^4}} \tag{5.112}$$

where β for a simply supported beam in mode 1 = π. With a fundamental truss frequency on the order of unity and a sandwich beam fundamental frequency on the order of 35 Hz, the forcing term is likely to be small for this configuration *in mode 1 vibration.* For other configurations or, even for higher modes of this configuration, this term will certainly be significant.

The forcing term, evaluated for mode 1 vibration ($n = 1$) is

$$\begin{aligned}
&V_n \sin\frac{n\pi x}{L}\frac{1}{\omega_{SB_n}}\int_0^t N_n(\tau)\sin\omega_{SB_n}(t-\tau)\,d\tau \\
&= \frac{2M_b}{L\left[\left(\pi/L\right)^2+g\right]}\sin\frac{\pi x}{L}\left\{\omega_T^{\,2}\left[gL\left(\frac{L}{\pi}\right)\left(\frac{gYL^3-12L}{24D}\right)+\left[\left(\frac{L}{\pi}\right)\left(gL^2+4\right)+4g\left(\frac{L}{\pi}\right)^3\right]\frac{1}{2D}\right.\right. \\
&-\left[\left(6L-gL^3\right)\left(\frac{L}{\pi}\right)+6gL\left(\frac{L}{\pi}\right)^3\right]\frac{gYL}{12D}+\left[\left(12L^2-gL^4\right)\left(\frac{L}{\pi}\right)+\left(12gL^2-48\right)\left(\frac{L}{\pi}\right)^3\right. \\
&\left.\left.\left.-48g\left(\frac{L}{\pi}\right)^5\right]\left(\frac{gY}{24D}\right)\right]+(1+Y)\left[\frac{2g^2Y}{D}\left(\frac{L}{\pi}\right)\right]\right\}\frac{1}{\omega_{SB}}\left(\frac{\omega_T\sin\omega_{SB}t}{\omega_T^{\,2}-\omega_{SB}^{\,2}}-\frac{\omega_{SB}\sin\omega_T t}{\omega_T^{\,2}-\omega_{SB}^{\,2}}\right)
\end{aligned} \tag{5.113}$$

Now that we know the behavior of the sandwich beams for the improved treatment under sinusoidal loading, we must determine the distribution of strain energy so that the modal loss factors of the system can be determined.

Calculation of Strain Energy

In order to obtain the loss factor η, the energy dissipated per cycle D_S must be found. The quantity D_S per unit width per unit length is

$$D_s = \pi G'' t_2 |\gamma|^2 \tag{5.114}$$

Appendix E contains the development of D_S. To find D_S, γ must first be determined.

Earlier in this chapter, we assumed the total shear strain to be the superposition of shear strain due to axial loading and shear strain due to bending. Using equation (5.33), the shear strain due to the axial load P is

$$\gamma_s = \frac{u_1 - u_3}{t_2} = \frac{P}{\sqrt{g}AEt_2}\left[\frac{-\tanh\frac{\sqrt{g}L}{2}\sinh\sqrt{g}x + \cosh\sqrt{g}x}{-\tanh\frac{\sqrt{g}L}{2}\sinh\sqrt{g}L + \cosh\sqrt{g}L}\right]\sin\omega_T t \qquad (5.115)$$

We can obtain γ_b from the development of the sixth-order differential equation of motion for transverse displacement (Appendix D). The equation for the shear strain due to bending is

$$\gamma_b = (1 + t_1/t_2)\frac{\partial w}{\partial x} + \frac{u_1 - u_3}{t_2} \qquad (5.116)$$

We also know that

$$Et_1\left(\frac{\partial^2 u_1}{\partial x^2} - \frac{\partial^2 u_3}{\partial x^2}\right) - 2G\left(\frac{u_1 - u_3}{t_2}\right) = 2G(1 + t_1/t_2)\frac{\partial w}{\partial x} \qquad (5.117)$$

In addition, we determined the quantities $\partial u_1/dx$ and $\partial u_3/dx$. Since we know the first derivatives of u_i, their second derivatives can be determined. We can rearrange (5.117) to isolate the part that equals γ_b. The other side of the equation, which is in terms of known quantities, must also equal γ_b.

$$\frac{Et_1}{2G}\left(\frac{\partial^2 u_1}{\partial x^2} - \frac{\partial^2 u_3}{\partial x^2}\right) = (1 + t_1/t_2)\frac{\partial w}{\partial x} + \frac{u_1 - u_3}{t_2} = \gamma_b \qquad (5.118)$$

After differentiating $\partial u_1/dx$ and $\partial u_3/dx$, γ_b is found to be

$$\gamma_b = \frac{Et_1}{2G}\left(\frac{2D}{gEt_1t_2(1+t_1/t_2)}\right)\left\{\sum_{n=1}^{\infty} C_n \cos\frac{n\pi x}{L}\left[\frac{\rho t}{D}\frac{n\pi}{L}\frac{M_b}{\omega_{SB_n}} \times \right.\right.$$
$$\left[\frac{-\omega_{SB_n}^2\,\omega_T \sin\omega_{SB_n}t + \omega_T^2\,\omega_{SB_n}\sin\omega_T t}{\omega_T^2 - \omega_{SB_n}^2}\right]$$
$$\left.+\left[\left(\left(\frac{n\pi}{L}\right)^5 - gY\left(\frac{n\pi}{L}\right)^3\right)\frac{M_b}{\omega_{SB_n}}\left[\frac{\omega_T\sin\omega_{SB_n}t - \omega_{SB_n}\sin\omega_T t}{\omega_T^2 - \omega_{SB_n}^2}\right]\right]\right] \qquad (5.119)$$
$$\left.+M_b\sin\omega_T t\left[-gY(6a_3+24a_4x) - \frac{\rho t}{D}\omega_T^2\left(a_1+2a_2x+3a_3x^2+4a_4x^3\right)\right]\right\}$$

where

$$C_n = \left\{\omega_T^2\left[gL\left(\frac{L}{\pi}\right)\left(\frac{gYL^3-12L}{24D}\right)+\left[\left(\frac{L}{\pi}\right)(gL^2+4)+4g\left(\frac{L}{\pi}\right)^3\right]\frac{1}{2D}\right.\right.$$
$$-\left[\left(6L-gL^3\right)\left(\frac{L}{\pi}\right)+6gL\left(\frac{L}{\pi}\right)^3\right]\frac{gYL}{12D}+\left[\left(12L^2-gL^4\right)\left(\frac{L}{\pi}\right)+\left(12gL^2-48\right)\left(\frac{L}{\pi}\right)^3\right.$$
$$\left.\left.-48g\left(\frac{L}{\pi}\right)^5\right]\left(\frac{gY}{24D}\right)\right]+(1+Y)\left[\frac{2g^2Y}{D}\left(\frac{L}{\pi}\right)\right]\Bigg\}$$

$$a_1 = \frac{12L - gYL^3}{24D}$$
$$a_2 = -\frac{1}{2D}$$
$$a_3 = \frac{gYL}{12D}$$
$$a_4 = -\frac{gY}{24D}$$

Appendix F contains the unabridged development of γ_b. The total shear strain is then

$$\gamma = \gamma_s - \gamma_b \qquad (5.120)$$

There are six separate terms in x:

$$\sinh\sqrt{g}\,x\ ,\ \sinh\sqrt{g}\,x\ ,\ \cos(\pi x/L)\ ,\ x\ ,\ x^2,\ \text{and}\ x^3$$

To square and integrate this complex quantity over the length would involve many separate integrals. Therefore, a numerical technique is in order. Before this, however, some simplification can be done.

An investigation of the expression for γ indicates that part of the shear strain is dependent on $\sin\omega_{SB}t$. Since the amplitude of vibration of the truss is transient, the entire solution is, in fact, transient. However, due to the inherently high damping of the sandwich beam component,the terms having a factor of $\sin\omega_{SB}t$ will become small much sooner than the terms dependent on $\sin\omega_T t$. The $\sin\omega_{SB}t$ terms represent the transient response of a sandwich beam due to an initial impulse excitation. Once the sandwich beam's individual response is damped, these terms will be a small contributor to system response. In effect, after the initial damping of the sandwich beam occurs, we will have, loosely speaking, a quasi-static vibration condition that will be perpetuated by the truss. Therefore, if we eliminate the $\sin\omega_{SB}t$ -dependent terms, the resulting loss factor will be conservative. The effect on the solution will be as follows: if the initial amplitude is unity, the total system will damp relatively quickly over the first few periods of ω_{SB} and then settle to the slower decay of the $\sin\omega_T t$ terms. By eliminating the $\sin\omega_{SB}t$ terms, we will begin decaying at the rate of the $\sin\omega_T t$ terms. Therefore, the amplitude of response will be higher for all time t than if those terms were included. Remember, the goal of the project is to make the $\sin\omega_T t$ rate of decay greater than the rate of decay *for the conventional treatment.* The following figure shows decaying oscillation envelopes that illustrate this concept.

The equations for this illustration are

$$\begin{aligned} \text{improved} &= e^{-.5t} \\ \text{sb} &= 0.4e^{-2.5t} \\ \text{sum} &= e^{-.5t} + 0.4e^{-2.5t} \\ \text{conv.} &= .6e^{-.25t} \end{aligned} \qquad (5.121)$$

To reiterate, this simplification is only reasonable because $\omega_{SB} \gg \omega_T$.

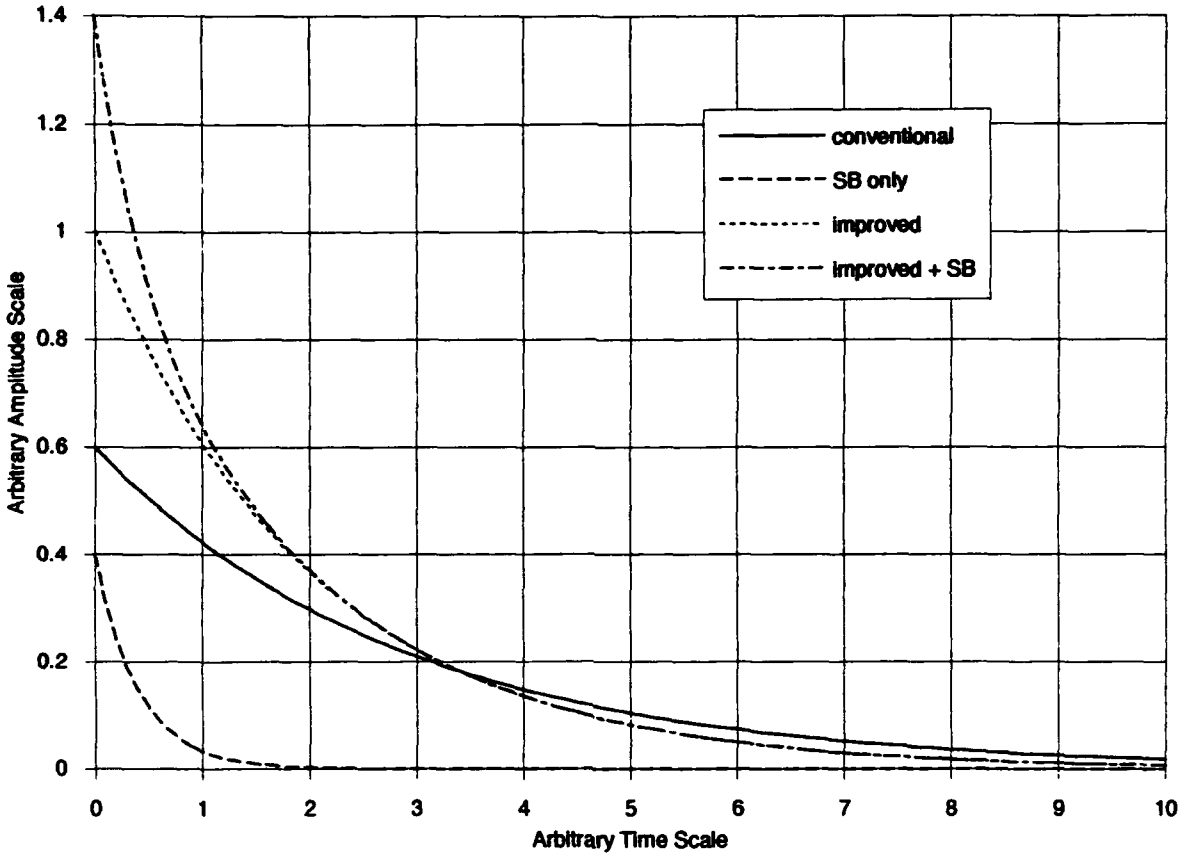

Figure 5.11 Illustration of Effects of Neglecting Highly Damped Terms

Extracting the $\sin\omega_{SB}t$ - dependent terms from γ_b and setting $n = 1$ leaves

$$\gamma_b = \frac{Et_1}{2G}\left(\frac{2D}{gEt_1t_2(1+t_1/t_2)}\right)M_b \sin\omega_T t\left\{C\cos\frac{\pi x}{L}\left[\frac{\rho t}{D}\frac{\pi}{L}\left(\frac{\omega_T^2}{\omega_T^2-\omega_{SB}^2}\right)\right.\right.$$
$$\left.+\left(\left(\frac{\pi}{L}\right)^5 - gY\left(\frac{\pi}{L}\right)^3\right)\left(\frac{1}{\omega_T^2-\omega_{SB}^2}\right)\right] \qquad (5.122)$$
$$\left.-gY(6a_3+24a_4x)-\frac{(\rho t)}{D}\omega_T^2\left(a_1+2a_2x+3a_3x^2+4a_4x^3\right)\right\}$$

The expression for γ_S is unchanged since the analysis was assumed to be quasi-static.

Calculation of The Mode 1 Loss Factor

The expression for the loss factor of the system is

$$\eta = \frac{D}{2\pi U} = \frac{D_{ve1} + D_{ve2}}{2\pi\left(U_{truss} + U_{levers} + U_{ve1} + U_{ve2} + U_{SB1} + U_{SB2}\right)} \tag{5.123}$$

In order to calculate η, the unknown quantities M_b and P needed to be determined because they impact the viscoelastic strain energy and damping energy terms. The finite element analysis program I-DEAS™ (a product of Structural Dynamics Research Corporation) was used to construct a truss model. This model was the same one used to determine the undamped natural frequencies and mode shapes. M_b and P are dependent on the geometry and the loading, so a parametric study was conducted to determine the dimensions h (long lever length), s (short lever length), t (thickness t_1), and the cross-section of the levers. The goal of the study was to minimize the percentage of total system strain energy located in the truss elements. The study was basically an iterative process whereby different configurations of h, s, t, and the cross-section were input to I-DEAS. The loading was assumed to be a linearly increasing distributed load from zero at the clamped end of the truss to a maximum at the tip, as the following diagram illustrates.

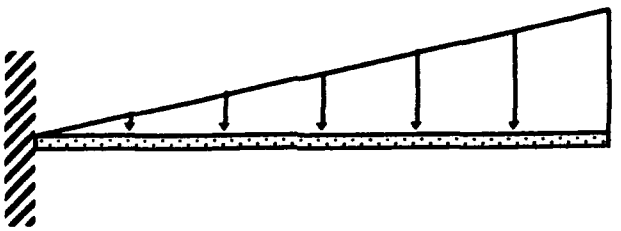

Figure 5.12 Depiction of Finite Element Static Load

Interestingly, this load gives almost the identical mode shape of mode 1. This load was applied by way of point loads on the nodes of the finite element model.

The static solution from I-DEAS is almost exactly equal to the strength of materials solution for a similar loading. The finite element program output data consisted of displacements, strain energies, and element forces. The total elastic strain energy

solution for the undamped truss was 0.92 lb. in. from I-DEAS, while the strength of materials solution was

$$U = \int_0^L \frac{M(x)^2}{2EI}\,dx \quad = \quad 0.84 \text{ lb. in. for } M = \frac{q_o}{6}\left(2L^2 - 3Lx + \frac{1}{L}x^3\right) \qquad (5.124)$$

where q_o for this calculation was backed out by using the I-DEAS moment of 35.135 lb. in. This result was considered to be close enough to verify the finite element model. The element forces data was then assumed to be close enough to use in the theoretical expressions for D_s, U_s, and η_s. Appendix G briefly describes the procedure for determining the dimensions of the damping device. As a result of the parametric study in Appendix G, the chosen configuration reduced the total elastic strain energy in the system from 0.92 lb. in. to 0.63 lb. in. (based on the finite element output data).

During the parametric study, it was discovered that a wide sandwich beam placed in the root truss bay has the effect of transferring a large portion of the strain energy in the bay down to subsequent bays. Therefore, a two-bay configuration was considered. The penalty for adding a second sandwich beam is the weight of an extra set of levers. This added weight reduced the total allowable width of the sandwich beams. A few preliminary estimate configurations indicated that, not only did the total percentage of the strain energy in the sandwich beams increase, but the total elastic strain energy was significantly *decreased.* Reducing the total elastic strain energy is desirable because the value of the denominator in η decreases.

The winning configuration, constrained by the readily available materials and construction capabilities of the resources on Wright-Patterson Air Force Base, is the following:

long lever length $h = 7$ in.
short lever length $s = 1.25$ in.
sandwich plate thickness $t_1 = 0.032$ in.
cross – section $= 0.75$ in. $\times$ 0.080 in.
wide sandwich beam width $b_1 = 5.4$ in.
slim sandwich beam width $b_1 = 5.4$ in.

Figures 6.2-9 show the damping device.

The thickness of the viscoelastic layer, t_2, was the only parameter left to be determined. t_2 is a key parameter in the expression of damping energy, which is

$$\begin{aligned} D_s &= \int_{Volume} \pi G'' |\gamma|^2 dV \\ &= \pi G'' b t_2 \int_0^L |\gamma|^2 dx \end{aligned} \tag{5.125}$$

Once the configuration was set, a curve of t_2 vs. integrated shear strain could be constructed. One big problem with this method is that G^* is a complex quantity, which makes calculation cumbersome. Therefore, Matlab™, a commercial matrix manipulation computer program designed to handle complex algebra, was employed for the purpose of iterating through a number of thicknesses t_2. A numerical iterative function file was constructed, and results were analyzed. This program comprises Appendix H.

The resulting values of energy dissipation for nominal thicknesses were several times higher than the elastic strain energy in the truss. Because the viscoelastic material is so compliant, it is conceivable that this amount of dissipation is possible, but large deflections must occur before these strains can be realized. It seems that, for a given thickness, assuming the truss deflection is unaffected by the sandwich beam thickness, doubling the beam displacement will roughly quadruple the energy dissipation. There seems to be no significant penalty for trying to get the largest elastic displacements the material will allow.

During the iteration process, it was discovered that a single term dominates the expression for γ (for configurations of interest). The term is

$$-\frac{Et_1}{2G}\left(\frac{2D}{gEt_1t_2\left(1+t_1/t_2\right)}\right)gY\left(6a_3+24a_4x\right)$$

where

$$a_3 = \frac{gYL}{12D},\quad a_4 = \frac{-gY}{24D},\quad \text{and } M_b = \frac{(\text{lever tip load } P)(\text{short lever length } s)}{\text{sandwich beam width } b}$$

This term is found in the comparison function part of γ. The term is linear and antisymmetric about the center. If we examine the $x = 0$ end of the sandwich beam, only the "$6a_3$" part of this term is present. For the given load magnitude (P = 2.42 lb. for a 4" tip displacement), the shear strain reaches a minimum value of about 1.05 radians at t_2 =

0.015" and then increases with increasing t_2. The figure below illustrates the behavior of the term with changing t_2.

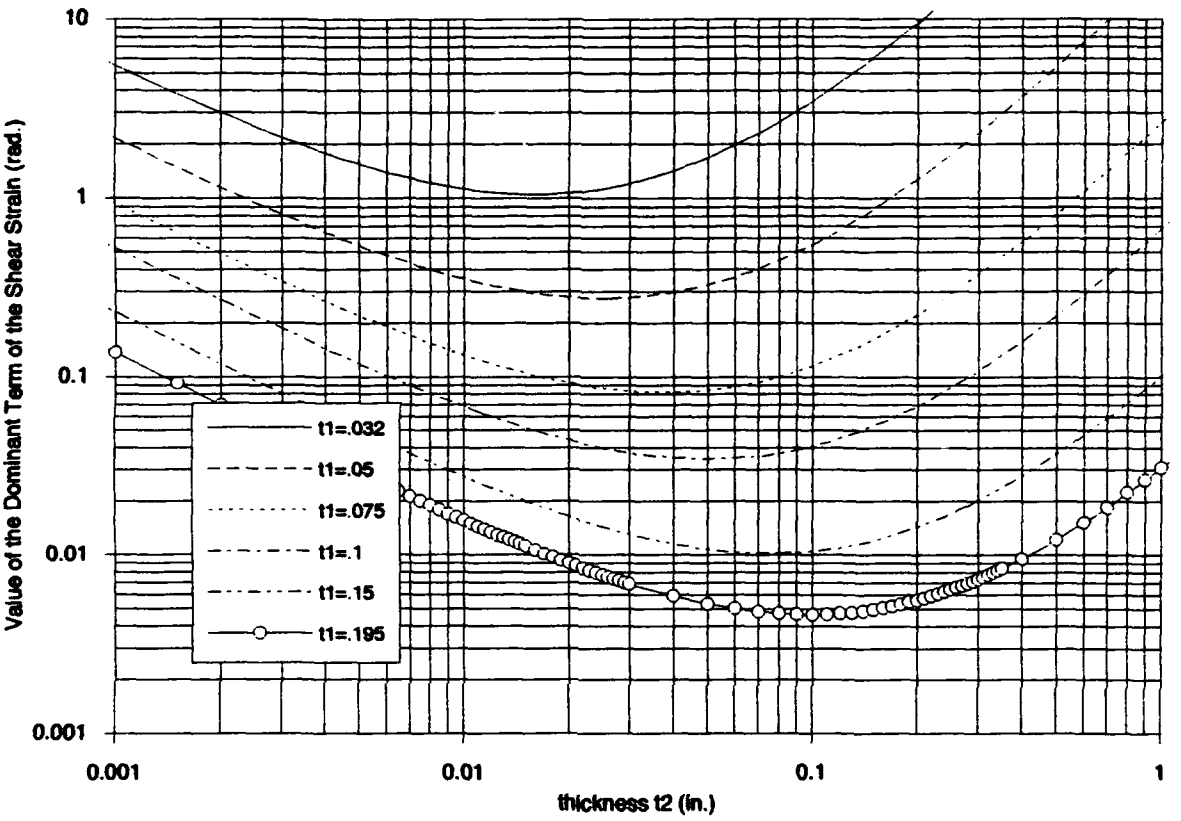

Figure 5.13 Damping Trend of Dominant Term With Varying Thicknesses t_2

Intuitively, this supposed behavior beyond $t_2 = 0.015$" must be in error. Cottle [22] discovered the theoretical phenomenon of increasing damping out past the region where damping begins to decrease, as did the author while investigating Torvik's five-layer beam analysis. According to the equation for energy dissipated per cycle D_s, an increase in volume of viscoelastic material causes a proportional increase in damping, but viscoelastic layer thickness has an inverse *squared* relationship with damping energy. It was presumed that this theoretical increase in shear strain with increasing thickness could be the result of the breakdown of one or more of the assumptions of the analysis. It appears this phenomenon generally becomes significant as the viscoelastic material occupies a significant percentage of the beam cross-sectional area. Torvik's more general analysis (Appendix B) does not make the simplification of $t_1 = t_3$, so the shear strain term remains

$$\gamma_b = \left(1 + \frac{t_1 + t_3}{2t_2}\right)\frac{\partial w}{\partial x} + \left(\frac{u_1 - u_3}{t_2}\right) \quad \text{rather than} \quad \gamma_{SB} = \left(1 + t_1/t_2\right)\frac{\partial w}{\partial x} + \left(\frac{u_1 - u_3}{t_2}\right)$$

When t_1 » (t_2 and t_3) , this effect will not be significant until t_2 gets really large because t_1 dominates the coefficient of $\partial w/\partial x$.

The assumption whose breakdown would probably have the greatest impact is the one that says the viscoelastic layer does not resist direct strains. Clearly, as t_2 becomes large (on the order of 10t), the bending stiffness becomes significant with respect to $E_1 t_1^3$, especially for higher frequencies where the elastic shear modulus G_2 is high.

Since a close scrutiny of the algebra did not result in finding a math error, it was decided to test a *number* of different viscoelastic thicknesses. Even if the magnitude of the experimental results was not in line with the theory, it was hoped that a trend could be observed from the testing of three thicknesses.

According to the Matlab numerical integration file, the expected values for the mode 1 loss factors for various thicknesses were the following:

t_2	D_1 (lb.in.)	D_2 (lb.in.)	U_T+U_{SB}	U_{ve1}	U_{ve2}	η
.005"	18.23	6.72	0.65	4.84	1.78	0.55
.015"	25.56	9.42	0.65	6.78	2.5	0.56
.030"	67.21	24.83	0.65	17.83	6.59	0.58

Table 5.1 Theoretical Damping Values for Improved Treatment

VI. Experiment and Results

The two parts of this project - theoretical development that led to the design of the damping device, and laboratory testing - were closely intertwined during all phases of this effort. For example, the design of the conventional damping treatment could not proceed without the resonant frequency data obtained from impacting the truss. Much has already been said with regard to the apparatus of this study. Chapter 3 contains a detailed drawing of the truss, and Appendix G describes the dimensions of the components of the improved damping device. In addition, the method of obtaining modal frequencies and damping ratios is well known, and a detailed overview of the testing procedure is not necessary (Appendix A describes how the truss frequencies and loss factors were obtained). Consequently, most of the laboratory work is included in this section of the report. First, the improved damping device will be described in detail. Then a brief explanation of the procedure for how the data was collected will follow. Finally, the reduced data (modal frequencies and loss factors) will be presented. Appendix I contains the tabulated raw data.

Apparatus

The electronic equipment used for collecting data was a typical setup for modal analysis. The schematic diagram below includes the most important components.

Both the force transducer and the accelerometer were calibrated for consistency over the operating ranges of force and acceleration, but determining calibration constants was not necessary since the output data was a transfer function in the frequency domain. The calibration constants would merely shift the entire curve up or down; it would not affect the shape.

The conventional damping treatment consists of 16 aluminum strips measuring 1.00" x 18.0" x 0.032." The damping material, 0.005" thick 3M ISD-112, came in the form of a large roll and was applied to one side of each aluminum strip. The strips cover both sides of each longitudinal truss member. The strips on the tip end of the truss had to be trimmed to about 16."

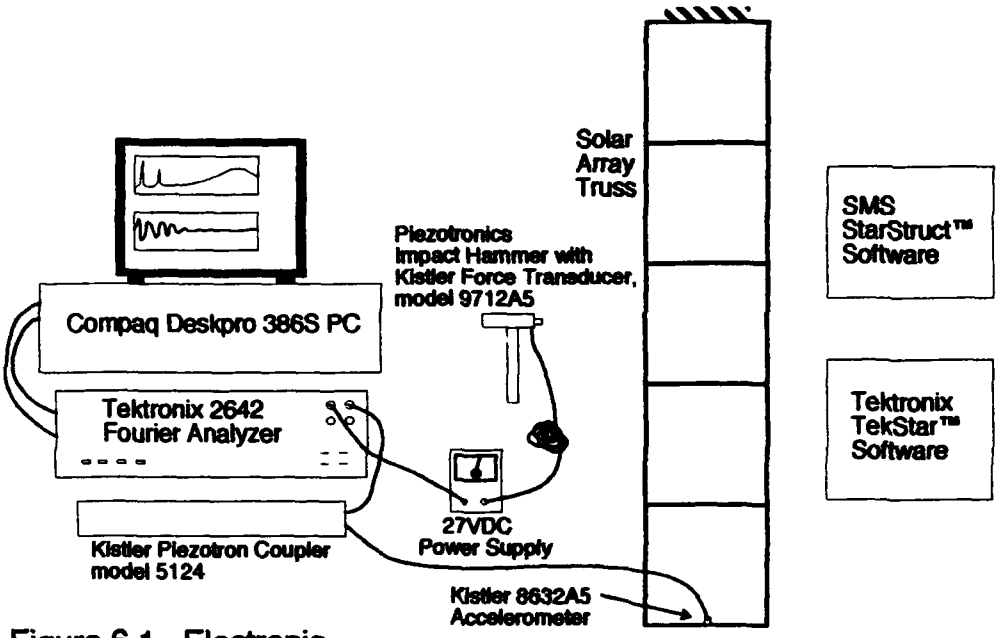

Figure 6.1. Electronic Equipment Setup

The components of the improved damping device are illustrated in the diagrams below. The sandwich plates overlap by about 12.5".

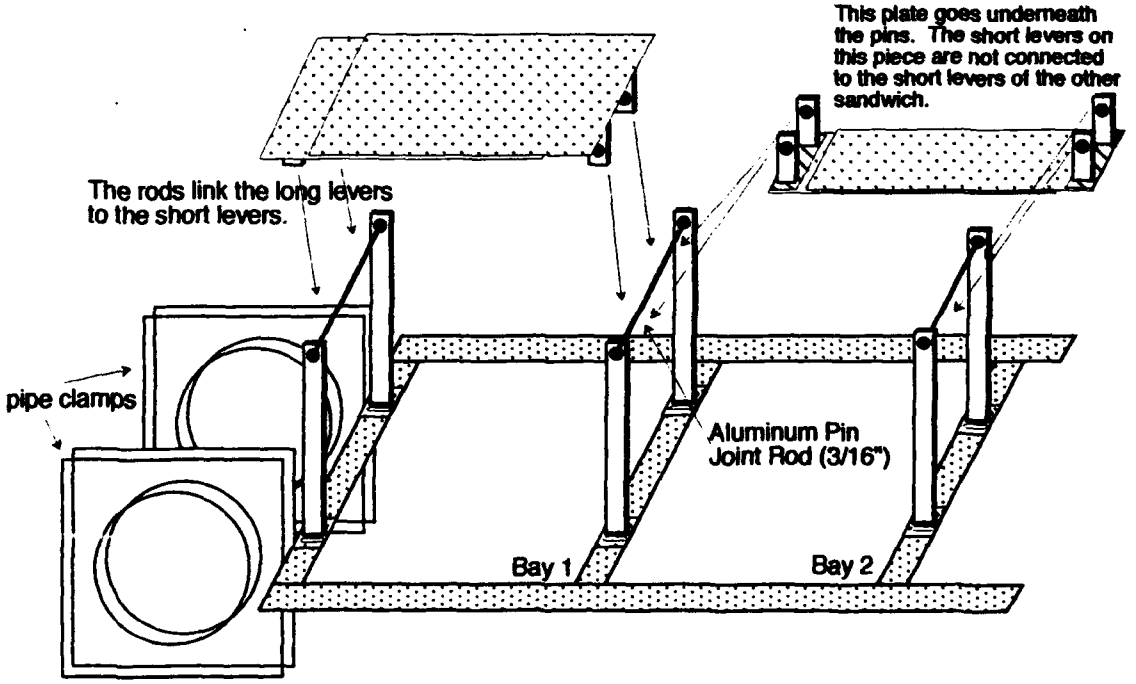

Figure 6.2 Close-up View of Truss Damping Device

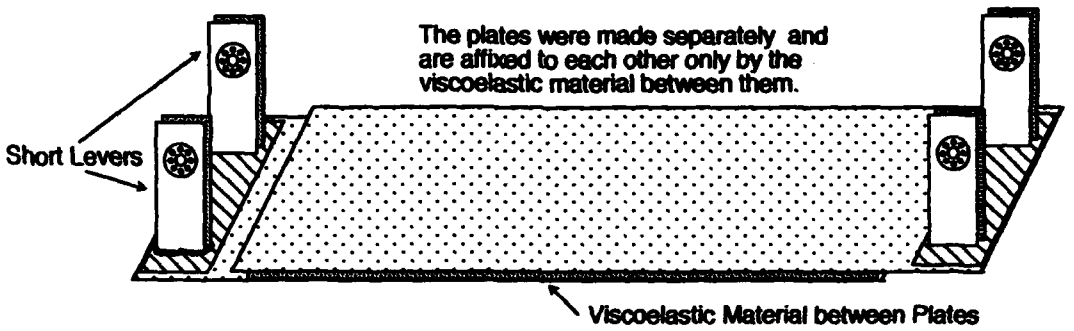

Figure 6.3 Closeup View of 2.3" Sandwich Beam

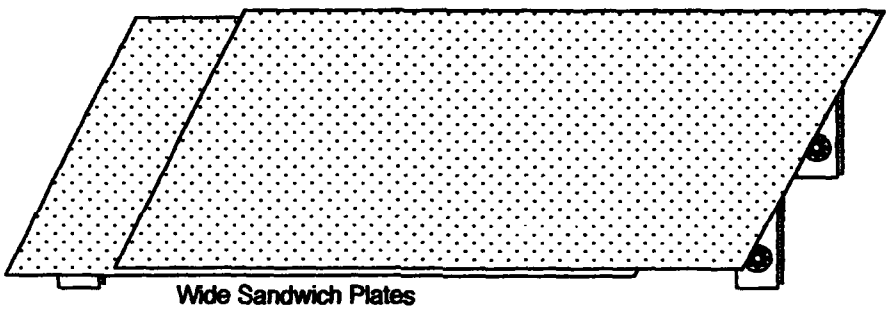

Figure 6.4 Top View of 5.4" Sandwich Plates

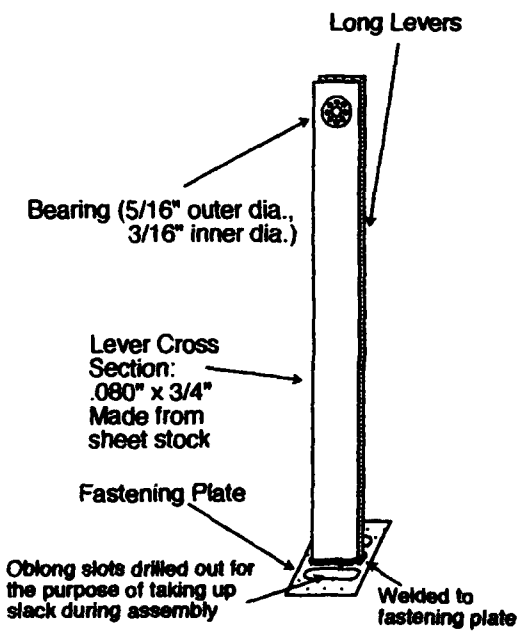

Figure 6.5 Detail of Long Lever and Truss Fastening Plate

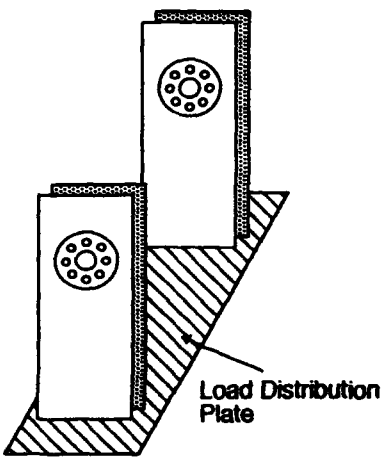

Figure 6.6 Load Distribution Plate for Short Lever - SB Plate Interface

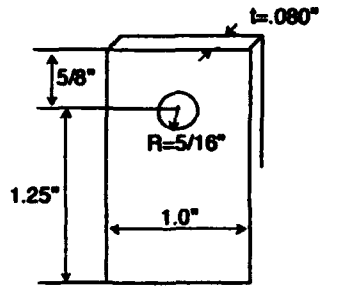

Figure 6.7 Short Lever
(not to scale)

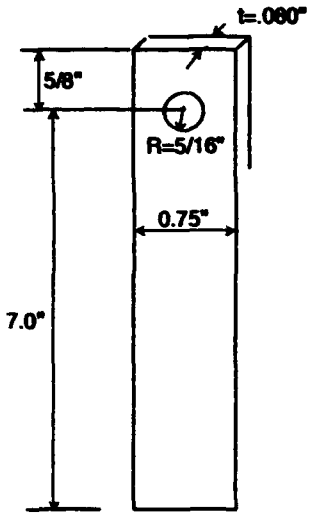

Figure 6.8 Long Lever
(not to scale)

The fabrication of the sandwich plates required a slight modification from the original design. The design called for a *welded* connection between the load distribution plates and the sandwich plates. Because the materials are so thin (0.032"), warping of the sandwich plate would surely have resulted from welding. Consequently, the short lever/distribution plate component had to be riveted to the sandwich plate. Figure 6.9 below shows the rivet patterns for the 2.3" and 5.4" plates.

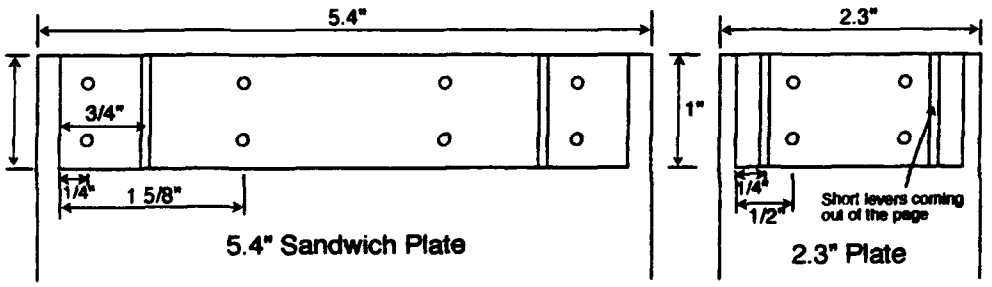

Figure 6.9 Distribution Plate Rivet Patterns with Dimensions

The rivets are $^1/_{32}$" countersunk solid rivets. They formed an excellent connection between the sandwich plates and levers.

Some problems arose from the welds being slightly out of square. Once the individual parts were fabricated, they were assembled with tape for the purpose of mapping out the drill holes for connection to the truss. Once the holes were drilled, only assembly remained before testing began.

One of the built-in "fudge factors" of the design was the oblong hole pattern in the fastening plates. The slack that existed was very helpful during the actual bolting of the device to the truss. Everything was set up easily, leaving only the machine screws on the bottom to tighten. The device was able to be secured tightly to the truss while the rods rotated with a minimum amount of friction.

Applying the viscoelastic material to the aluminum required patience and care because it is so sticky. In the application of the damping material, air bubbles became trapped at the interface (this problem is very difficult to avoid, especially for wide areas such as the large sandwich beam). Most of the bubbles were removed by pricking them repeatedly with a pin. It was virtually impossible to remove all of the air. However, a good bond was achieved, one that was free of delamination at even the most highly stressed regions. One of the most reliable indications of debonding is the presence of an audible "crack" or "pop" upon deformation of the beam. The beams did not make this sound even when strained far beyond the limits of the testing.

Experimental Procedure

The logical sequence for the experiment was to obtain all data on the improved treatment before proceeding to test the conventional treatment. As stated in Chapter 5, three viscoelastic thicknesses were chosen for testing because the theoretical values of t_2 were suspect. The three thicknesses and the reasons for their choice are listed below.

t_2 = 0.005" fell in the theoretical range where the shear strain is largely dependent on the term $(1 + t_1/t_2)$.

t_2 = 0.015" was the theoretical minimum for the dominant term in the expression for shear strain (discussed earlier).

t_2 =0.030" is in the theoretical range where the shear strain term $(t_1 + t_2)^2$ starts becoming significant. Recall Figure 5.13 for reference.

The basic procedure for testing all configurations (including the conventional treatment) was as follows:

1.) Set up the Tektronix TekStar software.
2.) Apply the accelerometer to the structure at a point of interest.
3.) Impact the structure with the hammer.

4.) Record the transfer function of accelerance/force over a given frequency band (for all of the tests, the frequency band was either 0-20 Hz or 0-50 Hz). This ratio is actually the ratio of output power spectral density over input power spectral density.

5.) Repeat step 4 for the desired number of trials.

6.) Input data to the SMS-StarStruct software.

7.) Use the polynomial curve fit feature to record resonant frequencies and damping ratios.

8.) Repeat steps 2-7 for different accelerometer and force locations.

For each viscoelastic thickness, this procedure was repeated over twenty times, each time using a different accelerometer/impact location combination. The locations were chosen based on the positions of the nodes and antinodes of the various modes of interest.

For the low modes, collecting repeatable transfer function data was difficult when a sharp impact was used. Because the power spectral density of a sharp impact is relatively uniform over the entire frequency range of interest, the low modes simply did not receive enough input power to cause large deflections. For this reason, an alternative impact method was developed for achieving good low mode data. If the hammer tip was barely in contact with the structure at the beginning of an impact and accelerated rapidly, the sharpness of the impulse was reduced because the impact occurred over a longer time period (about 100-120 msec for a "slow" impact as compared with 15-20 msec for a sharp impact). The resulting power spectrum was a more-or-less flat curve out to about 10 Hz, at which point it rolled off by several orders of magnitude out to 20 Hz. Despite this rolloff, the slower impact gave smooth, consistent transfer function curves in the low frequency range (0-20 Hz) that, in turn, gave accurate curve fits.

Results

The results from the testing make up five sets of data, which are the following:

Set 1 - Undamped Modal Frequency and Loss Factor Data

Set 2 - Improved Treatment Frequency and Damping Data, $t_2 = 0.005"$

Set 3 - Improved Treatment Frequency and Damping Data, $t_2 = 0.015"$

Set 4 - Improved Treatment Frequency and Damping Data, $t_2 = 0.030"$

Set 5 - Conventional Treatment Frequency and Damping Data, $t_2 = 0.005"$

The reduced data is presented here for convenience. The raw data, which is presented in the form it was actually taken, appears in Appendix I. The only difference is that the modal damping ratios were converted to loss factors by multiplying by two.

Some of the information in the tables is abbreviated. The following is an explanation of what everything means:

Test - a number of impacts whose frequency response functions are averaged into a single frequency response function.

Response and *Excitation* - the location of the accelerometer and impact, respectively, on the truss. Zero is defined at the root of the truss, while unity is at the truss tip. The majority of the response locations were on the cross members, placed at intervals of 0.2L down the truss. The "R" or "L" indicate placement on the right or left side of the truss. If no "R" or "L" is present, the accelerometer is positioned in the center of the cross member. The presence of a "Y" indicates that the accelerometer's active axis is in the plane of the truss. If no "Y" is present, the active axis is orthogonal to the truss plane. A negative sign indicates that the truss was impacted on the back side. This was only done when something was in the way. Finally, the SB denotes placement on the sandwich beam device itself. BSB1Y, for example, denotes "bottom of large sandwich beam, active axis in the y-direction." MSB1 denotes "middle of sandwich beam 1, active axis in the z-direction." .6R denotes "located 60% of the way down the truss on the right side, active axis in the z-direction."

f_i - frequency of mode i

$\%_i$ - damping ratio of mode i, expressed in percent (this number is the result of the polynomial curve fit)

Details - the best way to describe this is to use an example. "1K, 5, slow, 0-20" means "1024 instantaneous time samples per impact, five slow impacts, frequency band 0-20 Hz."

The blank spaces in the tables mean that no peak was present or that the frequency band did not include that particular mode.

Note that the loss factor scale is different for each graph.

Trial	f1	η Bend 1	f2	η Bend 2	f3	η Tors. 1	f4	η Bend 3	f5	η Tors. 2	f6	η Bend 4
1	1.045	0.00651	5.97	0.00291			16.45	0.00176				
2	1.055	0.00705	5.97	0.00241			16.45	0.00179				
3	1.048	0.00731	5.98	0.00332			16.45	0.00155				
4	1.051	0.0116	5.937	0.00252			16.42	0.00168				
5	1.051	0.01127	5.937	0.00254			16.42	0.00171				
6	1.046	0.00502	5.95	0.00253			16.467	0.00156				
7	1.047	0.00855	5.952	0.00316			16.467	0.00168			31.682	0.00095
8	1.045	0.00609	5.951	0.00326			16.439	0.00158			31.734	0.00111
9	1.047	0.00854	5.954	0.00331	7.4	0.00151	16.443	0.00159	21.681	0.00419	31.738	0.00106
10	1.045	0.01412	5.933	0.00346	7.362	0.00218	16.442	0.00168	21.872	0.00563	31.675	0.0009
11	1.052	0.01403	5.94	0.00257	7.369	0.00136	16.442	0.00151			31.675	0.00088

Table 6.1 Data Set 1 - Damping Tests, Undamped Truss

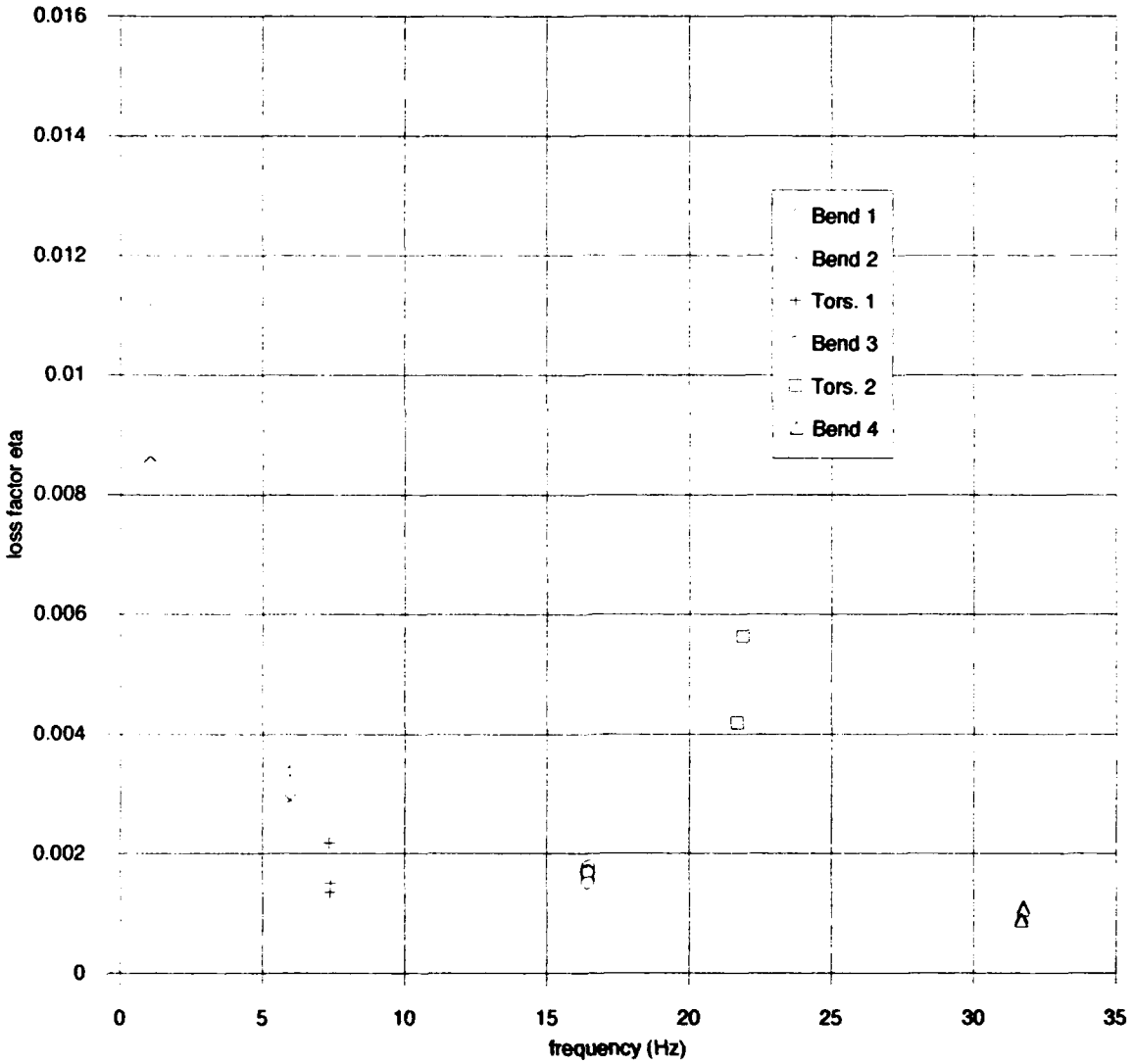

Figure 6.10 Loss Factors, Undamped Truss

Test	Resp	Excit	f1	η Bend 1	f2	η Bend 2	f3	η Tors. 1	f4	η Bend 3	f5	η Tors. 2	f6	η Bend 4	details
1	1R	0.8	1.247	0.0276	5.72	0.0143	7.623	0.0154	14.77	0.0285			27.303	0.0375	4K,4,sharp 0-50
2	1R	1	1.251	0.039	5.798	0.0199	7.477	0.005	14.405	0.0352					2K,3,slow,0-20
3	1R	1	1.252	0.039	5.799	0.0199	7.482	0.0039	14.407	0.0032					2K,3,sharp,0-20
4	1R	0.6	1.28	0.0543	5.795	0.0183	7.472	0.005	14.497	0.047					2K,3,sharp,0-20
5	1R	0.4	1.296	0.0464	5.796	0.016	7.481	0.0041	14.56	0.0478					2K,5,sharp,0-20
6	1R	-0.2			5.797	0.0184	7.443	0.0021	14.612	0.0427			26.155	0.0247	4K,4,sharp,0-50
7	1R	SB1M	1.3	0.0583	5.802	0.0184	7.563	0.0023	14.588	0.0476	20.825	0.0133	26.123	0.0262	4K,4,sharp,0-50
8	1R	.4R	1.238	0.0445	5.8	0.0178	7.483	0.0041	14.515	0.0365	20.528	0.0195	26.691	0.0368	4K,4,sharp,0-50
9	1R	.6R	1.258	0.0406	5.796	0.0174	7.486	0.004	14.401	0.0281	20.265	0.0134	25.947	0.0121	4K,4,sharp,0-50
10	1	6R			5.662	0.0122	7.594	0.0037	14.413	0.0314			26.193	0.0173	4K,4,sharp,0-50
11	1	0.6	1.24	0.0436	5.801	0.018			14.399	0.032			26.117	0.0308	4K,4,sharp,0-50
12	1	0.4	1.275	0.0402	5.807	0.0187			14.407	0.028			26.145	0.0333	4K,4,sharp,0-50
13	1	0.6	1.25	0.0426	5.799	0.0194			14.383	0.0298					4K,3,slow,0-20
14	1	0.4	1.251	0.0453	5.8	0.0195			14.411	0.033					4K,3,slow,0-20
15	1	0.2	1.257	0.0464	5.799	0.0194	7.574	0.0032	14.397	0.026					4K,3,slow,0-20
16	1	0.8	1.254	0.0384	5.807	0.0173			14.402	0.0295					2K,3,slow,0-20
17	1	0.8	1.253	0.0402	5.813	0.0177			14.398	0.0295			26.093	0.0261	2K,3,slow,0-50
18	1	1	1.257	0.0378	5.807	0.017			14.396	0.0297					2K,3,slow,0-20
19	1	1	1.254	0.0391	5.807	0.0174			14.413	0.0311			26.393	0.0054	2K,3,sharp,0-50
20	1	1			5.811	0.0148			14.362	0.0248			26.124	0.029	2K,3,sharp,0-50
21	1	0.6	1.261	0.0378	5.81	0.0171			14.426	0.0266			26.108	0.0274	2K,3,sharp,0-50
22	1	0.6	1.259	0.0358	5.809	0.0168			14.431	0.0237					2K,3,slow,0-20
23	1	-0.4	1.26	0.037	5.811	0.0171			14.373	0.022					2K,3,slow,0-20
24	1	-0.4			5.829	0.0164			14.415	0.026			26.142	0.0241	4K,3,sharp,0-50
25	0.8	0.8							14.439	0.0248			26.123	0.0304	4K,3,sharp,0-50
26	0.8	0.8	1.258	0.0337					14.445	0.0285					2K,3,slow,0-20
27	0.6	0.6			5.823	0.0172			14.494	0.0314					2K,3,slow,0-20
28	0.6	0.6			5.827	0.0186			14.458	0.036			26.284	0.0287	4K,3,sharp,0-50
29	0.4	0.4			5.83	0.0174			14.479	0.0299			26.145	0.0269	4K,3,sharp,0-50
30	1R	1R	1.258	0.0373	5.806	0.0171	7.493	0.0054	14.436	0.0369					2K,3,slow,0-20
31	1R	1R		0	5.81	0.0174	7.5	0.0046	14.472	0.034			26.269	0.0277	4K,3,sharp,0-50
32	1R	6R	1.249	0.042	5.82	0.0128	7.497	0.0044	14.384	0.0262			26.606	0.0087	4K,3,sharp,0-50
33	1R	6R	1.261	0.039	5.812	0.0176	7.491	0.005	14.422	0.0256					2K,3,slow,0-20
34	1R	BSB1Y					7.504	0.0043							2K,3,slow,0-20
35	1R	BSB1Y					7.506	0.0043					26.314	0.0237	4K,3,sharp,0-50
36	BSB1Y	.6R					7.527	0.0047					26.455	0.0108	4K,3,sharp,0-50
37	BSB1Y	.6R	1.261	0.0303			7.523	0.0054							2K,3,slow,0-20
38	BSB1Y	BSB1Y					7.53	0.0043							2K,3,slow,0-20
39	BSB1Y	BSB1Y													

Table 6.2 Data Set 2 - Damping Tests, Improved Treatment, t2 = 0.005"

Test	Resp	Excit	f1	η Bend 1	f2	η Bend 2	f3	η Tors. 1	f4	η Bend 3	f5	η Tors. 2	f6	η Bend 4	details
1	1	0.6	1.219	0.0304	5.719	0.0228			14.174	0.0516					1K,5,slow,0-20
2	1	0.8	1.219	0.0344	5.741	0.0205			14.185	0.0484			25.77	0.0687	1K,5,slow,0-50
3	1	0.4	1.22	0.0322	5.718	0.023			14.177	0.0446			26.05	0.0543	2K,5,slow,0-50
4	1	SB1M	1.222	0.0331	5.718	0.0223			14.16	0.0496			25.981	0.064	2K,5,slow,0-50
5	1	0.6	1.22	0.0305	5.718	0.0222			14.183	0.0484			25.816	0.0573	2K,5,sharp,0-50
6	1	SB1M	1.222	0.0326	5.719	0.0223			14.179	0.0502			25.924	0.0562	2K,5,sharp,0-50
7	1	0.2	1.216	0.0269	5.716	0.0219			14.176	0.049			26.041	0.0647	2K,5,sharp,0-50
8	2R	6R			5.755	0.0203	7.543	0.0032	14.201	0.041	22.08	0.0046	25.617	0.0491	2K,5,sharp,0-50
9	2R	1R			5.74	0.0229	7.502	0.0036	14.192	0.031					2K,5,sharp,0-20
10	2R	1R			5.748	0.0241	7.504	0.004	14.172	0.0323			25.901	0.0135	2K,5,sharp,0-50
11	2R	1			5.748	0.0225	7.477	0.0014	14.215	0.0501			25.852	0.0545	2K,5,sharp,0-50
12	MSB1	0.8	1.228	0.032	5.772	0.0152			14.215	0.0501					2K,5,slow,0-50
13	MSB1	1	1.227	0.0311	5.751	0.0228			14.23	0.0503					2K,5,slow,0-50
14	MSB1	1	1.22	0.0268	5.748	0.0228			14.275	0.0515			25.982	0.0665	2K,5,sharp,0-50
15	0.2	1			5.746	0.022			14.234	0.048			26.038	0.0614	2K,5,sharp,0-50
16	6RY	1RY		IN PLANE BENDING - f = 21.556, eta = .0037											2K,5,sharp,0-50
17	6R	4R			5.791	0.0146	7.505	0.004	14.132	0.0542	20.278	0.0059	25.968	0.0135	2K,5,sharp,0-50
18	6R	4R	1.206	0.0323	5.773	0.0199	7.499	0.0036	14.107	0.0514	20.294	0.0055	25.971	0.0133	2K,5,sharp,0-50
19	6R	2R			5.762	0.0177	7.501	0.0035	14.159	0.0506	20.317	0.0053	26.02	0.0085	2K,5,sharp,0-50
20	1R	6R			5.838	0.0223	7.513	0.0033	14.229	0.0415	20.187	0.0057	25.953	0.0105	2K,5,sharp,0-50
21	1R	4R	1.186	0.0727	5.754	0.0249	7.489	0.0033	14.215	0.0302	20.247	0.0089	25.939	0.0095	2K,5,sharp,0-50
22	1R	1L			5.778	0.0251	7.486	0.0036	14.264	0.0278	20.235	0.0082	25.925	0.0085	2K,5,sharp,0-50
23	1R	1L	1.221	0.0367	5.732	0.0241	7.475	0.0041	14.255	0.0316	20.137	0.0053	25.93	0.0096	2K,5,slow,0-50
24	1R	4R	1.221	0.035	5.743	0.0231	7.482	0.0036	14.251	0.0501	20.262	0.0229	25.906	0.0121	2K,5,slow,0-50

Table 6.3 Data Set 3 - Damping Tests, Improved Treatment, t2 = 0.015"

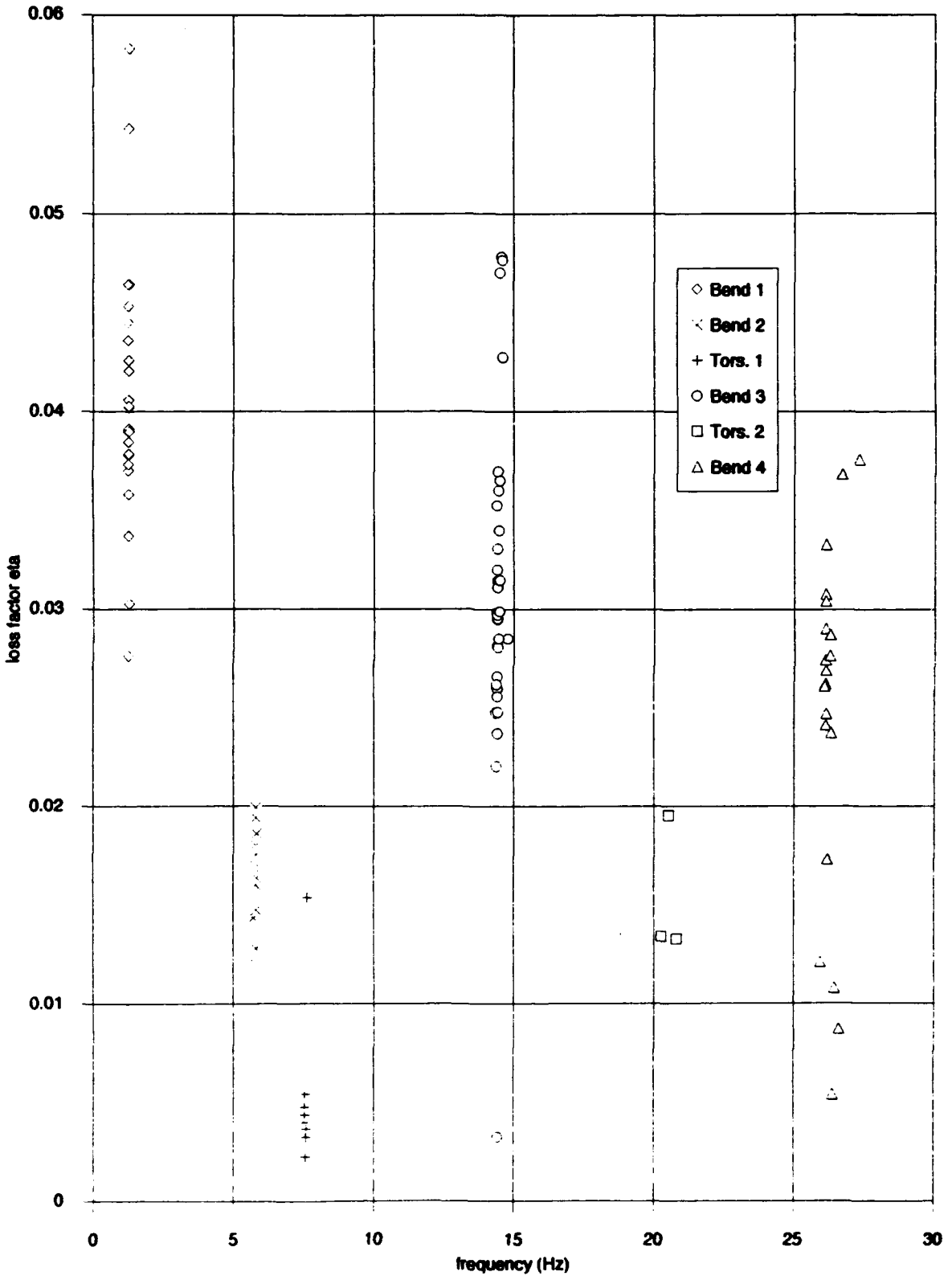

Figure 6.11 Loss Factors, Improved Treatment, $t_2 = 0.005"$

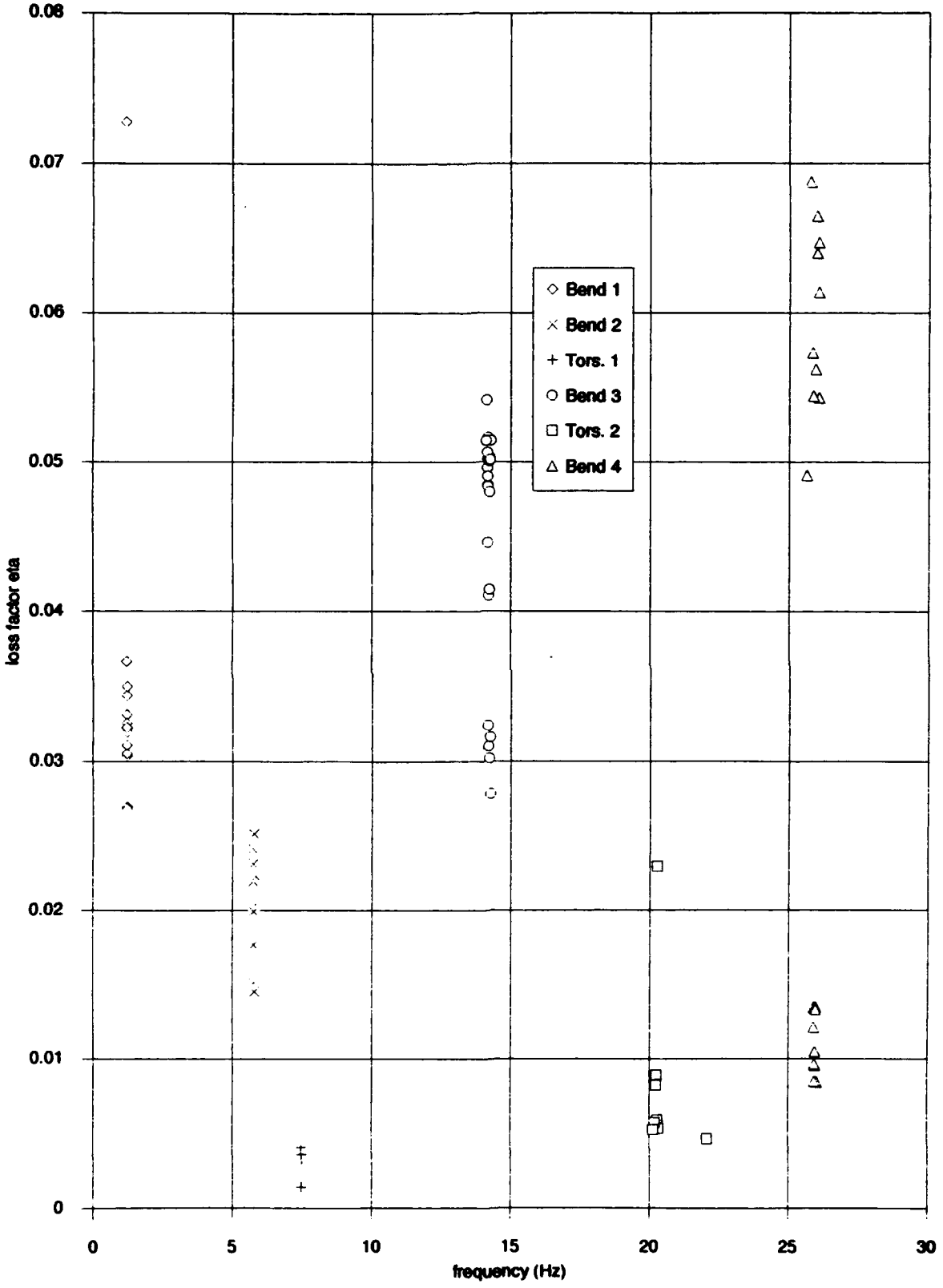

Figure 6.12 Loss Factors, Improved Treatment, t_2 = 0.015"

Test	Resp.	Excit.	f1	η Bend 1	f2	η Bend 2	f3	η Tors. 1	f4	η Bend 3	f5	η Tors. 2	f6	η Bend 4	details
1	1	0.8	1.235	0.037	5.741	0.022			14.154	0.054					2K,3,slow,0-20
2	1	0.8	1.242	0.022	5.779	0.018			14.103	0.051			25.983	0.061	4K,3,sharp,0-50
3	1	1	1.178	0.02	5.737	0.019			14.236	0.05			26.393	0.055	4K,3,sharp,0-50
4	1	1	1.236	0.035	5.731	0.025			14.176	0.06					2K,3,slow,0-20
5	1	1	1.236	0.038	5.729	0.024			14.217	0.058			26.638	0.016	4K,3,sharp,0-50
6	1	0.6	1.238	0.034	5.733	0.024			14.109	0.057					2K,3,slow,0-20
7	1	0.6	1.246	0.028	5.729	0.034			14.209	0.053					2K,3,slow,0-20
8	1	-0.4	1.251	0.022	5.72	0.022			14.179	0.051			25.944	0.057	4K,3,sharp,0-50
9	1	-0.4	1.239	0.034	5.732	0.023			14.074	0.043					2K,3,slow,0-20
10	0.8	0.8	1.245	0.042					14.105	0.061					2K,3,slow,0-20
11	0.8	0.8							14.199	0.067			26.033	0.04	4K,3,sharp,0-50
12	0.6	0.6							14.028	0.041					2K,3,slow,0-20
13	0.6	0.6	1.239	0.03	5.744	0.023			14.27	0.035					2K,3,slow,0-20
14	0.4	0.4			5.748	0.03			14.306	0.048			25.813	0.058	4K,3,sharp,0-50
15	1R	1R	1.239	0.029	5.742	0.024			14.313	0.047			25.977	0.019	4K,3,sharp,0-50
16	1R	1R	1.241	0.034	5.727	0.018	7.47	0.004	14.093	0.061	20.534	0.01	25.431	0.007	4K,3,sharp,0-50
17	1R	.6R	1.237	0.038	5.272	0.021	7.474	0.004	14.029	0.006					2K,3,slow,0-20
18	1R	.6R	1.246	0.037	5.747	0.017	7.477	0.004	14.309	0.044	20.427	0.007	25.357	0.011	4K,3,sharp,0-50
19	1R	BSB1Y			5.739	0.021	7.48	0.004	13.644	0.015	20.392	0.007	25.308	0.014	4K,3,sharp,0-50
20	1R	BSB1Y			5.721	0.024	7.475	0.004	13.61	0.014					2K,3,slow,0-20
21	BSB1Y	.6R					7.504	0.003	13.498	0.015					2K,3,slow,0-20
22	BSB1Y	.6R					7.505	0.004	13.51	0.014			25.164	0.017	4K,3,sharp,0-50
23	1R	BSB2Y			5.728	0.022	7.478	0.004	13.555	0.028	20.526	0.003	25.205	0.016	4K,3,sharp,0-50
24	1R	BSB2Y	1.254	0.033	5.727	0.023	7.477	0.004	13.685	0.014					2K,3,slow,0-20

Table 6.4 Data Set 4 - Damping Tests, Improved Treatment, t2 = 0.030"

Test	Resp.	Excit.	f1	η Bend 1	f2	η Bend 2	f3	η Tors. 1	f4	η Bend 3	f5	η Tors. 2	f6	η Bend 4	details
1	1	1	1.053	0.095	6.318	0.133			18.061	0.162					1K,3,slow,0-20
2	1	1			6.317	0.119			17.912	0.132			33.905	0.151	2K,3,sharp,0-50
3	1	1	1.051	0.093	6.352	0.137			19.239	0.084					1K,3,slow,0-20
4	1	1	1.05	0.098	6.345	0.137			18.467	0.166					1K,3,slow,0-20
5	1	1			6.375	0.124			17.927	0.139			34.082	0.15	2K,3,sharp,0-50
6	1	1			6.331	0.134			17.971	0.139			34.101	0.148	2K,3,sharp,0-50
7	1	0.8	1.056	0.09					17.97	0.114					1K,3,slow,0-20
8	1	0.6	1.073	0.065	6.339	0.129			17.887	0.145					2K,3,sharp,0-50
9	1	0.4			6.367	0.137			17.958	0.137			34.01	0.152	2K,3,sharp,0-50
10	1	0.2			6.377	0.13			17.968	0.14			33.989	0.147	2K,3,sharp,0-50
11	0.8	0.4	1.064	0.082					17.776	0.133					1K,3,slow,0-20
12	0.6	1	0.862	0.091	6.368	0.134			17.958	0.144			33.968	0.147	2K,3,sharp,0-50
13	0.4	0.2			6.318	0.126			17.966	0.141			33.794	0.15	2K,3,sharp,0-50
14	0.8	0.2							17.964	0.142			33.983	0.147	2K,3,sharp,0-50
15	1R	1R	1.052	0.083			6.544	0.02							1K,3,slow,0-20
16	1R	1R	1.053	0.087			6.545	0.02							1K,3,slow,0-20
17	1R	.77R	1.081	0.105			6.54	0.012	17.994	0.115	20.127	0.035	35.262	0.05	2K,3,sharp,0-50
18	1R	.77R	1.083	0.087			6.553	0.013	18.043	0.122	20.142	0.03	35.205	0.104	2K,3,sharp,0-50
19	1R	.5R	1.074	0.096			6.553	0.013	18.193	0.131	20.192	0.032	35.13	0.097	2K,3,sharp,0-50
20	1R	.52R	1.075	0.103			6.545	0.009			20.108	0.034			2K,3,sharp,0-50
21	1R	.52R	1.089	0.099			6.542	0.01			20.108	0.035	34.933	0.03	2K,3,sharp,0-50
22	.7R	1R	1.056	0.052			6.549	0.012	17.994	0.121	19.954	0.042	35.407	0.063	2K,3,sharp,0-50
23	.5R	1R					6.55	0.011			20.053	0.038	35.099	0.023	2K,3,sharp,0-50
24	1Y	1RY		IN PLANE BENDING - f = 20.394 Hz, eta = .1534											2K,3,sharp,0-50
25	1Y	1RY		IN PLANE BENDING - f = 20.390 Hz, eta = .1475											2K,3,sharp,0-50

Table 6.5 Data Set 5 - Damping Tests, Conventional Treatment, t2 = 0.005"

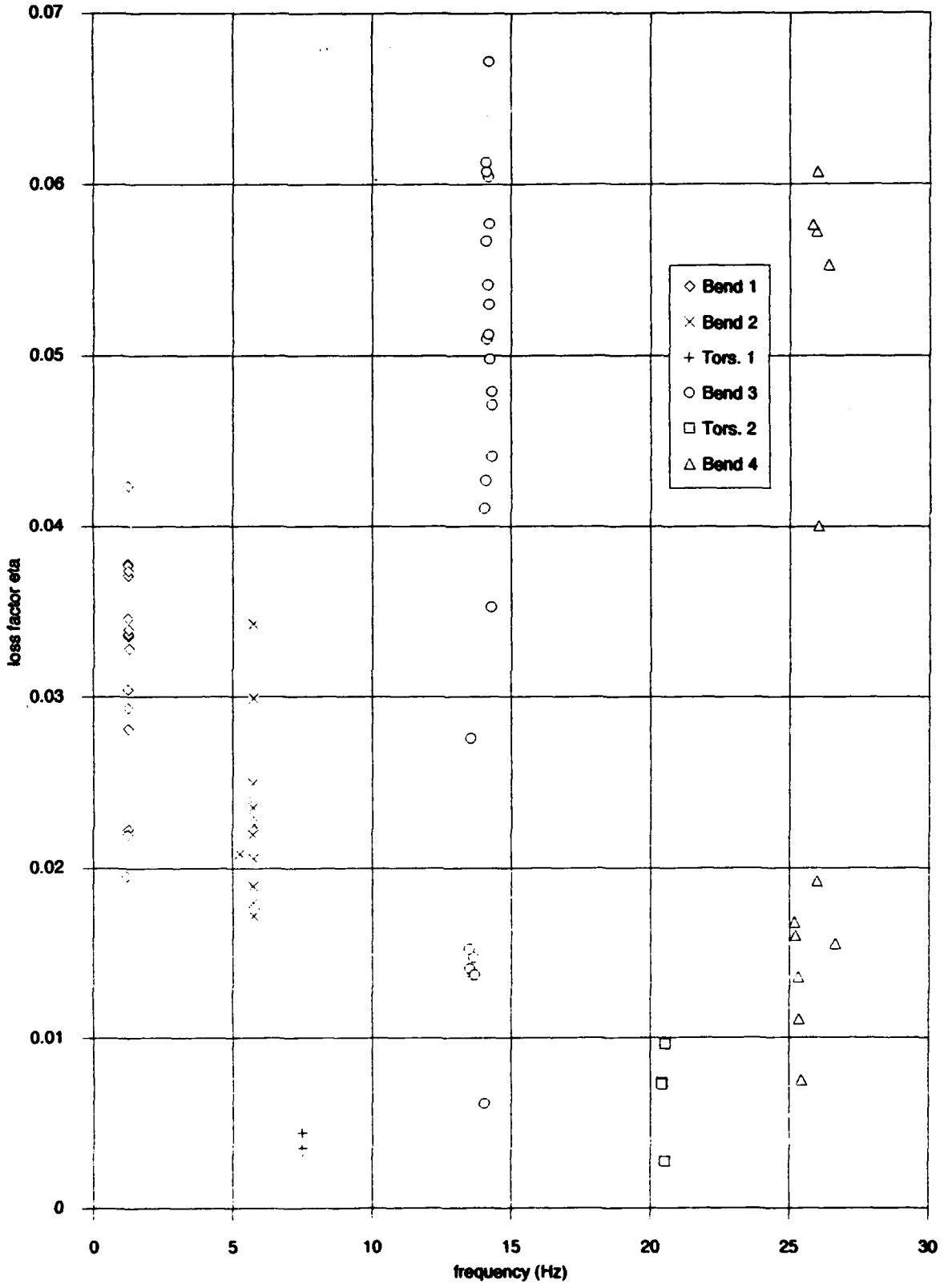

Figure 6.13 Loss Factors, Improved Treatment, t_2 = 0.030"

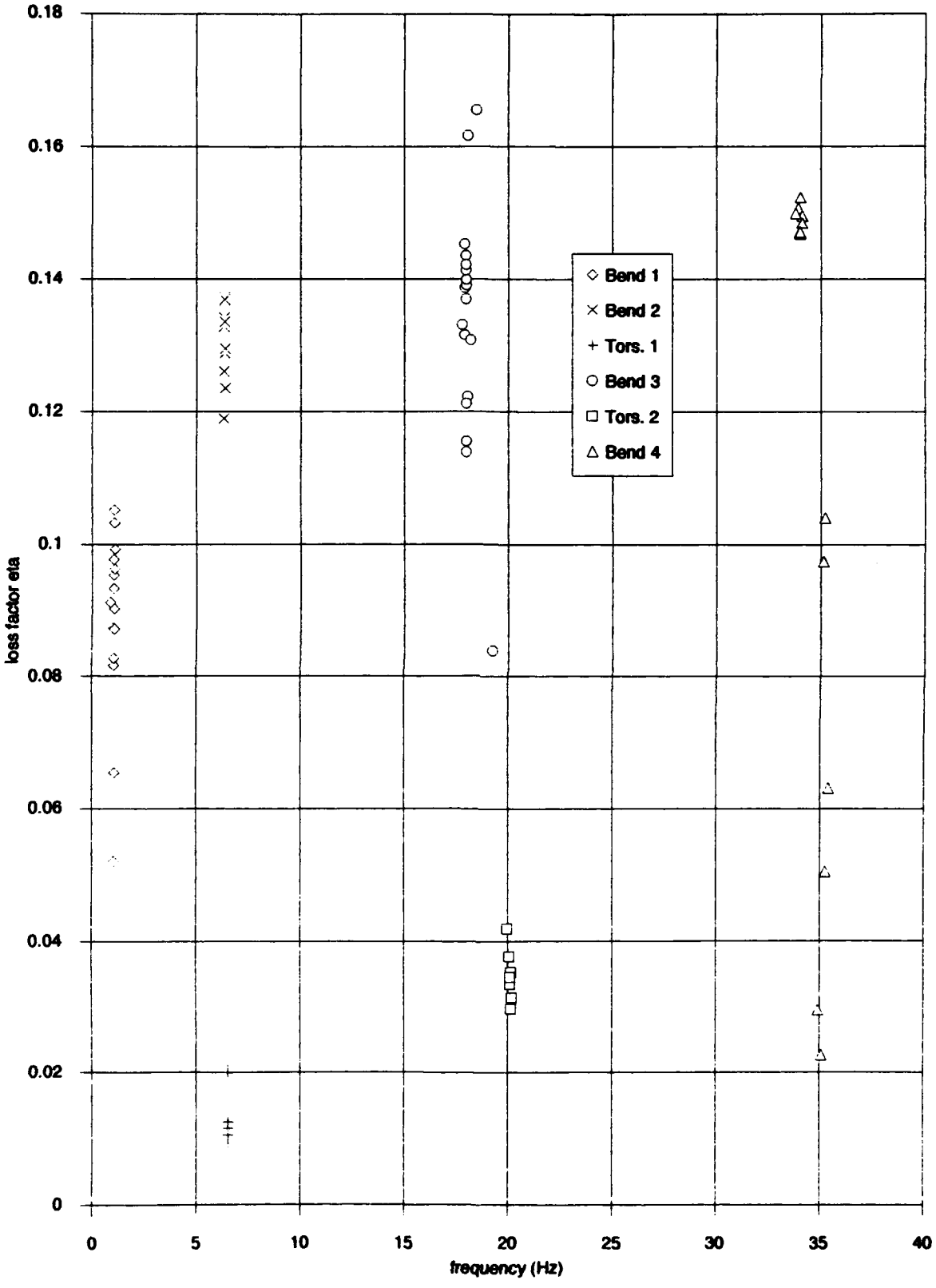

Figure 6.14 Loss Factors, Conventional Treatment, $t_2 = 0.005"$

Observations of Results

Collecting the loss factor data for the improved treatment was difficult because the addition of the damping device brought quite a number of new system modes into the frequency band from 0-50 Hz. The data is very consistent with regard to frequency, but there is a wide scatter of loss factor values for most of the modes of interest. The most prominent new modes introduced to the system were the following:

- fundamental sandwich beam bending modes (above 30 Hz)
- fundamental "rocking" modes of the entire sandwich beam device (this motion was in a plane parallel to the truss plane, with sandwich beam 1 resonating at about 14 Hz and sandwich beam 2 resonating at about 27 Hz)
- in-plane rotational mode of the entire sandwich beam device, where the axis of rotation (orthogonal to the truss plane) occurred at the middle set of levers

Some of the impact locations excited these modes more than the modes of interest, and some of the loss factor data points are grouped at two or more distinct values η. It is believed that, for some data points, the curve fitter found these modes instead of the modes of interest. For example, the fourth bending mode of the truss (at about 27 Hz) was believed to be one of the more highly damped modes, yet the scatter of points ranges from low to high. For all of the improved treatment graphs (Figures 6.11-13), the frequency of 27 Hz has two distinct groupings. A look at the data sets indicates that the low damping values were recorded during impacts that excited torsion. Intuitively, the rocking back and forth of the damping device should produce negligible damping. Therefore, it was concluded that the lowly damped groupings are attributable to the resonance of sandwich beam 2. For a similar example, consider the scatter of the third truss bending mode and the relatively tight grouping of a few points well below the rest of the mode 3 data. They too are the result of torsion-inducing impacts, but are attributable to the rocking of sandwich beam 1.

Other than these two examples, the data is relatively good. An exception to this conclusion is that the mode 1 data is highly scattered with regard to loss factor. This scatter is caused by a number of factors. First, the frequency band was from 0-20 Hz for most of the mode 1 data points. Noting Table 6.4, two of the three lowest values of η_1 were procured from tests with bandwidth 0-*50* Hz. 1 Hz is on the low edge of this band, and the frequency response function was exceptionally "ragged" in this region (a condition which made for an unreliable curve fit). Second, the accelerometer specification for the lower frequency limit is 0.5 Hz, but the output begins to roll off

somewhere between 0.5 Hz and 1 Hz. The effect of this rolloff is probably a decrease in the signal-to-noise ratio (which causes a random distribution of damping values), but it was considered to be small because the slow impact technique provided ample power in the low frequency region to obtain a strong output voltage.

It is important to mention here that the data points should not be averaged into a single value. For any given mode, each data point represents the damping value recorded for a *particular* combination of accelerometer location and impact location. If the accelerometer or impact location is near a node, the output voltage will be small, and the corresponding curve fit will yield a less reliable damping value than if the output signal were higher. In order to be impartial, as many data points were recorded as could be reasonably obtained for any given frequency response function. Curve fitting all possible data served the dual function of helping discern sensitivities in the testing procedure. Finally, even though the truss was relatively massive compared to the accelerometer, the sway of large truss deflections caused the accelerometer cable to influence the output. Appendix C addresses this particular problem. It should be emphasized that this particular problem, although annoying, did *not* significantly affect the data.

The data from the conventional treatment (Figure 6.14) was very good for all modes except the "fourth bending" mode. It was reputed that the two distinct groupings are actually two modes. The undamped truss data showed the fourth bending mode at 32 Hz, while the third torsion mode was determined to be about 40 Hz. The effect of adding the conventional treatment caused the fourth bending mode to shift up to about 34 Hz due to a stiffening of the long members in out-of-plane bending. Conversely, because the conventional treatment was applied at the furthest distance possible from the axis of torsion, the added mass caused the third torsion mode to shift *down* to about 35 Hz.

Conclusions Based on the Experimental Results

It is clear from viewing the loss factor graphs that the damping device did *not* achieve the levels of modal damping that the theory predicted. The predicted damping values were believed to be too high before any of the data was collected, but they were listed at the end of Chapter 5 as calculated. It is obvious from reviewing Table 5.1 that the energies in the viscoelastic layer predicted by the Matlab program completely dominate the finite element prediction of truss strain energy. Based on the expected relative deflections of the pin joint rod axes, it was difficult to believe that such a small volume of material could possess such a large fraction of the total strain energy.

There were a number of suspected reasons why the Matlab computer program gave such high vales of strain and damping energy. Test results for $t_2 = 0.015$" gave damping ratios that were much lower than expected. It was initially presumed that the high theoretical values for strain energy were the result of an incorrectly determined moment M_b. The moment, taken from the finite element static solution described in Chapter 5, was supposedly too high because of the load P on the short lever tips. The only way to verify this suspicion was to conduct a small test to determine the *actual* force/displacement relationship between the lever rods.

A test apparatus was set up to determine the behavior of the sandwich beams in both tension *and* compression. While the beams were gradually loaded with calibrated weights, the deflection of the rod axis was recorded with the aid of a traveling microscope. The microscope is a precision instrument which uses an eddy current sensor to determine the displacement. The machine gives results to within 0.00005".

With the $t_2 = 0.005$" sandwich beams fastened to the truss, a number of readings were taken for various tip deflections. The truss was loaded by a point load at the center of the second cross member from the bottom (.8L) to obtain the desired tip deflections. Figure 6.15 shows the rod axis displacements. This data gave known displacements of the lever tips for a known truss tip displacement. The 1 and 2 denote different trials.

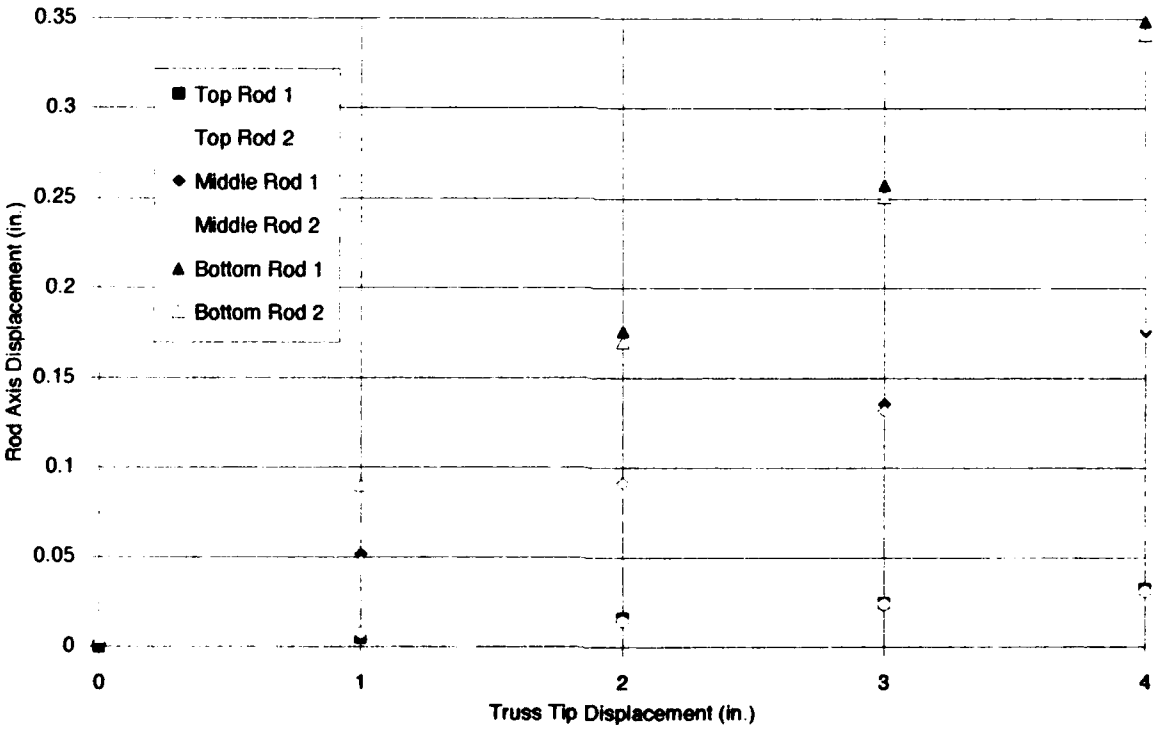

Figure 6.15 Tip Displacement vs. Lever Rod Axis Vertical Displacement

After collecting this data, the sandwich beams were removed from the truss. Then they were loaded in tension and compression with a known load in order to obtain the force/displacement relationship between the lever tips. Figures 6.16-6.19 (next page) show graphically the results of these tests. From these graphs, it is apparent that, indeed, the sandwich beams behave quite differently in tension than compression. The theory also predicts a divergence of the cycle halves as discussed in Chapter 5 (see Figure 5.8 for the theoretical curves).

The real information to deduce from analyzing the force/displacement relationship is noting *at what load* the divergence between cycle halves becomes significant. It seems that the appropriate level of caution was taken in determining the geometric parameters h, s, t, and the cross-section.

The next step was to use a best guess linear approximation of all the data for a given configuration. Both tension and compression data was taken into account for this guess. The resulting slope is the effective spring constant k_{eff} between the rods.

Once the spring constant was determined, finding the actual load P between the rods for a given truss tip displacement was a simple matter of multiplying k_{eff} by the actual rod displacement. The results of this "mini-study" are tabulated here for a four-inch truss tip displacement. The value of the rod axis displacement Δ is based on the actual relative rod displacements for the $t_2 = 0.005$" configuration. It was believed the actual displacements of the $t_2 = 0.030$" configuration would be very close. This belief is based on the fact that *none* of the configurations stiffened up the truss significantly more than any other.

	t_2 = .005"	Δ(in)	P	t_2 = .030"	Δ(in)	P
SB 1	k ≈ 14 lb/in	.145"	2 lb.	k ≈ 12 lb/in	.145"	1.7 lb.
SB 2	k ≈ 5.3 lb/in	.17"	.9 lb.	k ≈ 4.7 lb/in	.17"	.8 lb.

Table 6.6 Sandwich Beam Force/Displacement Experimental Data

After the actual force/displacement relationships were found, a modified finite element analysis was conducted using this data. The sandwich beam and short lever components in each bay were replaced by a single member whose "effective" stiffnesses was backed out by using the relation

$$F = k_{eff}\, x \text{ where } k_{eff} = \frac{AE_{eff}}{L} \tag{6.1}$$

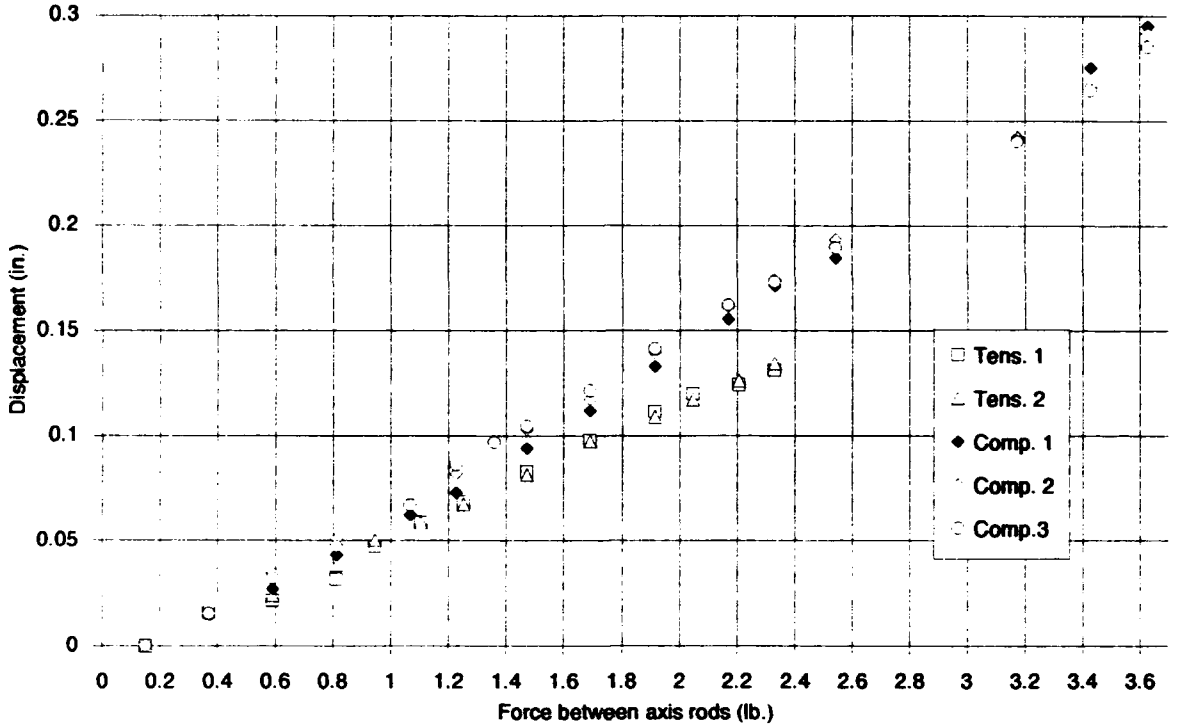

Figure 6.16 Force-Displacement Relationship - Sandwich Beam **1**, $t_2 = 0.005$"

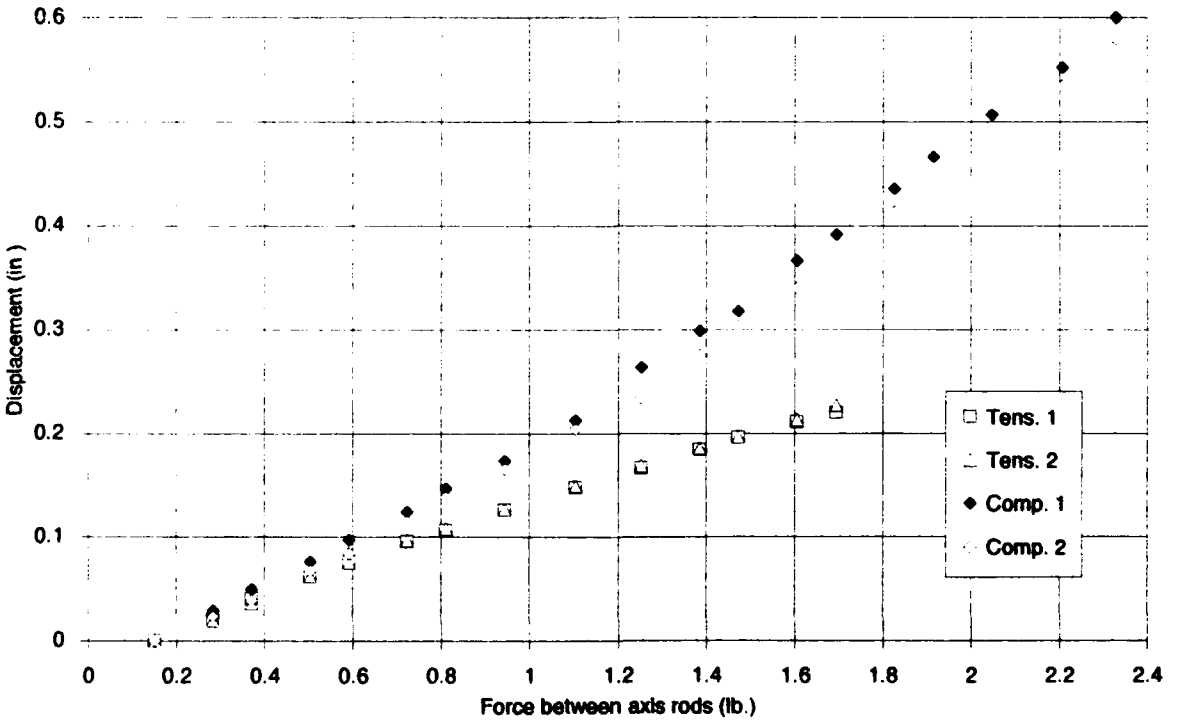

Figure 6.17 Force-Displacement Relationship - Sandwich Beam **2**, $t_2 = 0.005$"

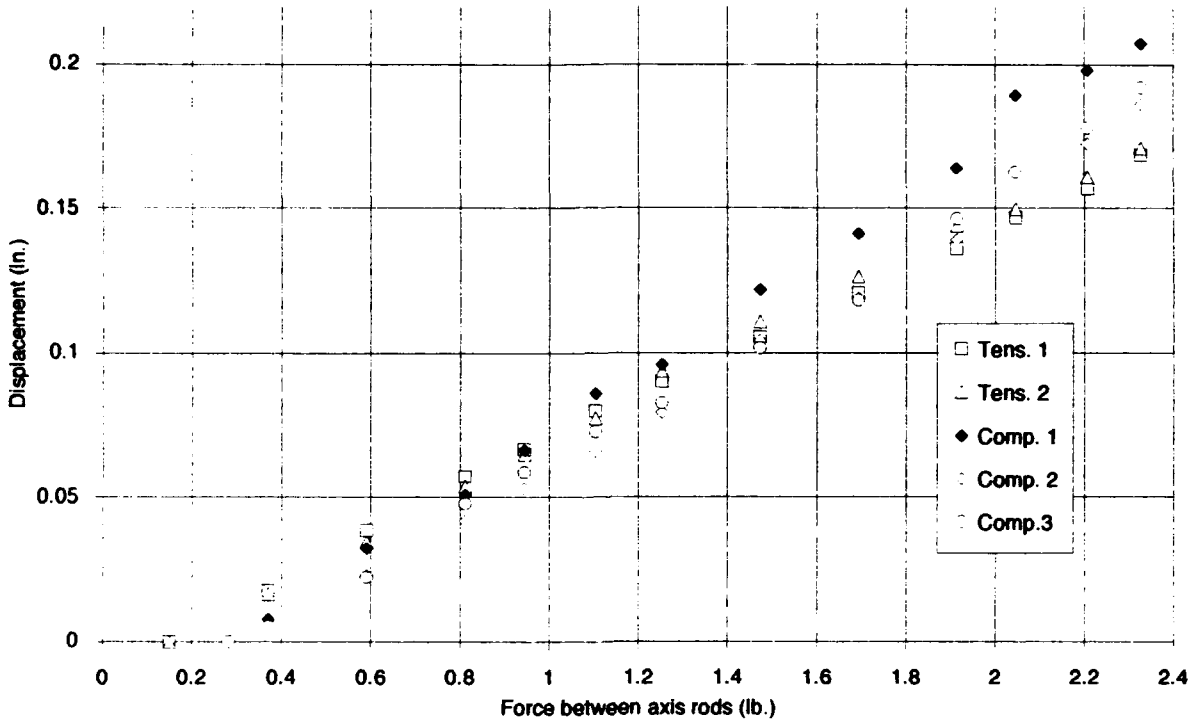

Figure 6.18 Force-Displacement Relationship - Sandwich Beam **1**, $t_2 = 0.030"$

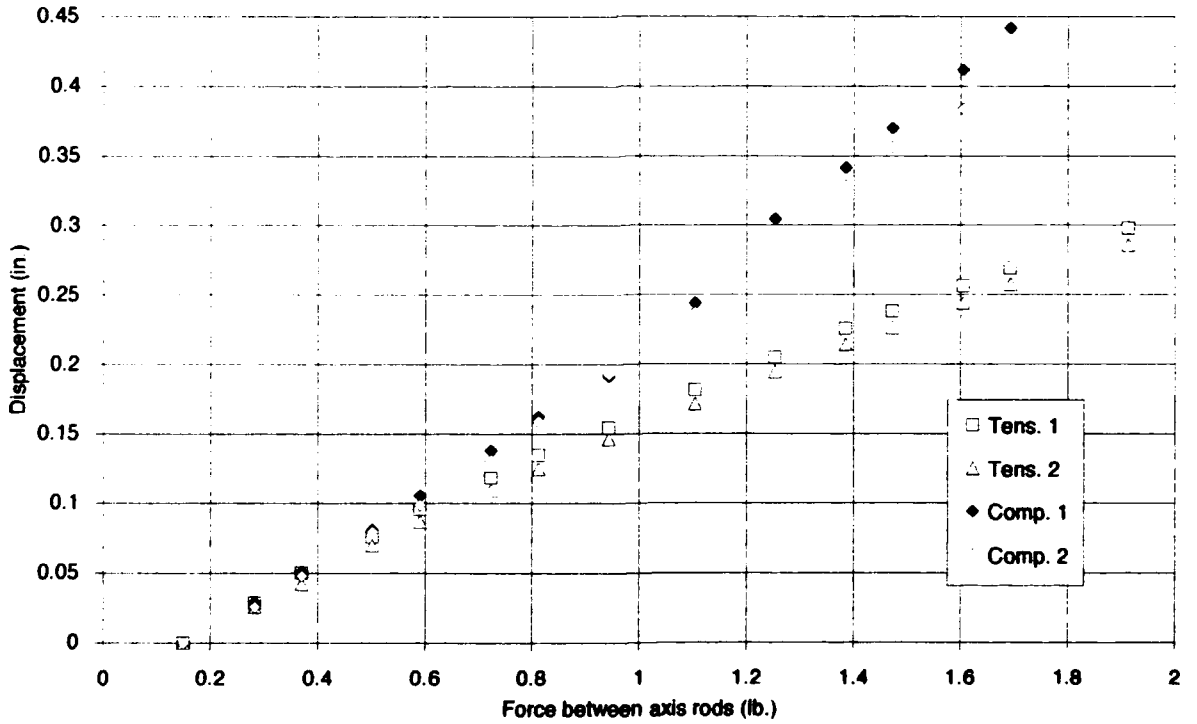

Figure 6.19 Force-Displacement Relationship - Sandwich Beam **2**, $t_2 = 0.030"$

Table 6.7 shows the tabulated results of two static models, one for each t_2. The dynamic analyses were not useful for displacements because the maximum displacement (in this case the truss tip elements) is default set to one meter. However, the distribution of strain energy in the dynamic analyses is almost identical to the static load results (±0.5%). In addition, the percentage of total strain energy contained in the replacement member configuration is close to the sum of the strain energy in the sandwich beam and short lever elements of the "accurate" models.

configuration	Δ(in)	P
SB 1, t_2 = 0.005"	.124"	1.71 lb.
SB 2, t_2 = 0.005"	.120"	.579 lb.
SB 1, t_2 = 0.030"	.131"	1.51 lb.
SB 2, t_2 = 0.030"	.122"	.520 lb.

Table 6.7 Modified Finite Element Model Results

Based on this data, it was concluded that the moment obtained by the finite element analysis is *not* the source of the high theoretical shear strains.

Another possible reason for the discrepancy between theory and experiment is the assumption that the flexural rigidity D is independent of t_2. Clearly, when viscoelastic material bonds two sandwich plates together, the effective stiffness of the composite structure is stiffer in bending than two sandwich plates with nothing between them to resist the shear forces.

To investigate this phenomenon, another small test was conducted. Two sandwich beams, whose outer plates each measured 18" x 1.00" x 0.032", were fabricated in order to relate the change in stiffness with changes in the viscoelastic thickness. The two viscoelastic thicknesses tested were 0.005" and 0.015". Each beam was cantilevered (both plates clamped) and impacted several times to determine the fundamental frequency. Since the fundamental frequencies were close to one another, it was assumed that the shear modulus of the viscoelastic was constant. With an experimentally determined value of f_o, the effective moment of inertia of the composite beam can be found by using the frequency equation

$$f = \frac{1}{2\pi}\beta^2\sqrt{\frac{EI_{eff}}{\rho AL^4}} \tag{6.2}$$

where β = 1.875 for a cantilever beam vibrating in its fundamental mode and E is the elastic modulus for aluminum. We can back out I_{eff} as

$$I_{eff} = \left(2\pi f \beta^2\right)^2 \frac{L^4}{E} \rho A$$
$$= \left(2\pi f \beta^2\right)^2 \frac{L^4}{E} \left(\rho_{Al} A_{Al} + \rho_{ve} A_{ve}\right) \tag{6.3}$$

This expression was used to calculate the effective stiffnesses displayed below.

freq. (Hz)	undamped η	undamped Iz (in^4)	freq. (Hz)	η for t_2 = 0.005"	Iz for t_2 = 0.005" (in^4)	freq. (Hz)	η for t_2 = 0.015"	Iz for t_2 = 0.015" (in^4)
4.148	0.01216	5.97E-06	6.8	0.219	1.65465E-05	6.652	0.3016	1.68E-05
4.147	0.01282	5.97E-06	6.91	0.215	1.70862E-05	6.605	0.3096	1.66E-05
			6.82	0.211	1.6644E-05	6.604	0.3072	1.66E-05
			6.97	0.192	1.73842E-05	6.685	0.315	1.7E-05
			6.82	0.215	1.6644E-05	6.76	0.3136	1.73E-05
			6.89	0.229	1.69874E-05			
			6.82	0.222	1.6644E-05			
			6.89	0.221	1.69874E-05			

Table 6.8 Frequencies, Loss Factors and Effective Moments of Inertia of Test Beams

For both viscoelastic thicknesses, the effective area moment of inertia is roughly tripled. This observation raised the question of what would happen if these values of I were used in the Matlab program in place of the flexural rigidity D. This is a straight substitution because the test beams have unit width and the same thickness as the sandwich plates. Interestingly, this simple change reduced the strain energy to what can be considered a reasonable magnitude. Table 6.9 lists these results.

t_2	D_1 (lb.in.)	D_2 (lb.in.)	U_T+U_{SB}	U_{ve1}	U_{ve2}	η
.005"	0.225	0.0832	0.65	0.0597	0.0221	0.067
.015"	0.316	0.117	0.65	0.0837	0.0309	0.0901
.030"	0.831	0.307	0.65	0.22	0.0814	0.1904

Table 6.9 Loss Factor Calculations Using Tripled Flexural Rigidity D and Old FE Model Data

Notice that the strain energy value in the previous results is from the "accurate" FE model. In addition, the old FE loads (2.42 lb. and 0.96 lb. for sandwich beams 1 and 2, respectively) were used in the Matlab program. When the modified FE strain energy

calculation (0.78 lb. in. for the replacement member model) and the experimentally determined loads P are used, the results become the following:

t_2	P_1(lb.)	D_1 (lb.in.)	P_2(lb.)	D_2 (lb.in.)	U_T+U_{SB}	U_{ve1}	U_{ve2}	η
.005"	1.7	.111	.8	.0577	.766	.0295	.0153	.033
.015"	1.82	.1785	.84	.0893	.776	.0473	.0237	.050
.030"	2.0	.568	.9	.270	.778	.1505	.0715	.132

Table 6.10 Loss Factor Calculations Using Tripled Flexural Rigidity D, Modified FE Model Data, and Experimentally Determined Loads P

It should be mentioned that the loads P from the FE model (Table 6.7) are lower than the experimentally determined values used here. The effect of this discrepancy is that the tabulated value of elastic strain energy $U_T + U_{SB}$ would be lower for the given loads P, giving a still lower loss factor. In any case, Tables 6.9 and 6.10 illustrate the sensitivity of the results to the assumed flexural rigidity D.

The development of the sixth-order equation of motion (Appendix D) shows how the extension of the constraining layers are converted from expressions in terms of u to expressions in terms of w. It is difficult to find the real effect of D on these terms because the derivation's intermediate steps convert the u-derivative terms into expressions that have no physical meaning. When the u-derivative term (Equation D.23) is substituted into Equation (D.22), a D shows up in the denominator of the coefficient. Therefore, even though the flexural rigidity D is a number based on bending phenomena, this quantity affects the value of extensional terms.

The experimental data from the *conventional* treatment agrees very well with the theory. The expected results at the end of Chapter 4 list only the first two modes. In fact, the loss factors for the first *four* bending modes are close to the theoretical curves. Table 6.11 compares the theory with the results of the experiment.

Mode Number	Theoretical Prediction of η	Experimental Result of η
1	$\eta \approx 0.105$	$\eta \approx 0.09$
2	$\eta \approx 0.14$	$\eta \approx 0.13$
3	$\eta \approx 0.145$	$\eta \approx 0.14$
4	$\eta \approx 0.135$	$\eta \approx 0.15$

Table 6.11 Comparison of Theoretical vs. Experimental Damping Values, Conventional Treatment

It should be noted that the theoretical values are only a rough estimate based on Figure 6.14. Considering the number of simplifying assumptions that were made regarding this analysis, these results are about as close as one can expect.

VII. Recommendations for Further Research

The organization and nature of this thesis project leaves many "loose ends" that can be individually investigated. Several of the conclusions based on the experimental results from the previous chapter are really questions because the author ran out of time. For a thesis, the presentation of the results is rather unorthodox. However, for a scientific research endeavor, the issues that were addressed were a natural consequence of the disparity between the theory and the experimental results. Truthfully, some of the problem issues are unanswered.

Some of the assumptions made in the analysis are suspect and warrant further investigation. The assumed shape of the sandwich beam in its fundamental bending mode was a sine wave. This problem has already been addressed in Chapter 5. Another possible source for error is in the assumed boundary conditions. As Cottle [22: 18] observed, a three-layer sandwich beam actually has *eight* boundary conditions, two of which go to zero because the *difference* of the extensional displacements u_i is considered instead of their absolute values. However, in the sandwich beam given in this study, there is some question as to *which* two boundary conditions go away. As discussed in Chapter 5, the assumed extensional boundary conditions were zero strain at the ends. Actually, only one of the sandwich plates has zero longitudinal strain at either end. What about the boundary condition on the other plate (the plate that must transfer the moment to the three-layer interior)? Recall that the problem was divided into two parts; the direct shear static case and the total (static plus dynamic) bending case. It seems that if the tension in the sandwich plate is considered in one part, it ought to be disregarded in the other part so as not to contribute to the solution twice.

Perhaps the most neglected area of this project was the procedure for finding the dimensions of the damping device. It was believed that this part of the project was relatively simple, and not much time was spent on it in consequence. This was a serious error in judgment because optimizing the "non-damping" parts would have allowed considerably more damping material to be applied. However, choosing smaller dimensions for these parts might have invalidated the theory because of the asymmetric bending phenomena. Clearly, this is a more difficult problem than a cursory look would indicate. Using the finite elements turned out to be a convenient way of finding strain energy distributions and iterating through several candidate configurations. However, the

method for eliminating parameters was not at all an optimal technique. Much work needs to be done on this problem alone.

One positive observation from the "improved" treatment is that a measurable amount of damping was achieved despite the relatively small area of coverage (with respect to the conventional treatment). The area of viscoelastic coverage of the sandwich beams is about 96 $in.^2$ as compared with 280 $in.^2$ for the conventional treatment. This difference is significant and probably has a lot to do with the disparity in modal loss factors between treatments. For some existing structures, it may not be possible to cover as much area as the conventional treatment does.

Another area of this study that was not treated with appropriate diligence is the transfer of strain energy with structural additions like the damping device. Perhaps the reason for this is that the idea for what the damping device would look like was decided early in the project, long before this problem was discovered. This type of premature decision-making is not a very sound design philosophy. In retrospect, it appears that forcing the strain energy into a desired region by *adding stiffness* is just as important as designing the actual damping device. The idea of using added stiffness in certain regions as part of the damping treatment is certainly one that could produce fruitful results. For this particular project, consider what would happen if the second sandwich beam and levers were eliminated and all of their weight was used to stiffen up the four truss bays furthest from the built-in end. This concept can be best described as designing in a structural "weak link" where the vast majority of the total strain energy resides (of course, the weak section would still have to be fail-safe. This would be an excellent study.

A design technique that was not considered was the partial coverage concept presented in Nokes and Nelson's 1968 paper [23]. To be absolutely fair, this idea should have been employed in a competing configuration. Certainly, this option could be used in concert with other ideas like Plunkett and Lee's segmenting technique.

For this thesis, all the joints were modeled and constructed as ideal connections. Any design that would actually be used would most likely involve damped joints as well as damped beams. One possible study might be to compare the effect of adding damping in the joints as well as in the main part of a damping addition.

Finally, it is unfortunate that the dynamic terms in this project's analysis were insignificant compared to the quasi-static terms. It is possible to conceive a structure where the dynamic response of the sandwich beam is a major factor. Verifying the

dynamic part of a time-dependent boundary condition solution with an experiment is a problem worth studying.

VIII. Conclusion

Experimental results show that *the sandwich beam damping device did not exceed the conventional damping treatment for any modes of truss vibration.* Modal loss factors for the conventional treatment were approximately three times higher than the sandwich beam device. The conventional treatment was well-designed and well-constructed, and the experimental results verify that Plunkett and Lee's segmented constraining layer analysis is accurate.

This project turned out to have complexities (both theoretical and experimental) that were not anticipated at the outset. Even though the sandwich beam damping device *appears* simple, it is not. A number of separate analyses are required to describe the oscillatory motion of the device.

The expression for the displacement of the three-layer sandwich beam is quite complicated, and is only an approximate solution since part of the solution is a comparison function that satisfies the boundary conditions but not the differential equation. The accuracy of the solution is further reduced by the assumption of simple mode shapes that made finding a solution in series form possible. Despite its complexity, expressions were obtained for the shear strain of the viscoelastic layer, which is a function of the derivatives of the displacement w. For the given sandwich beam configuration, a single term dominated the expression for shear strain. This term caused problems in interpreting the results of a computer program that performed numerical integration. The program gave relatively high values of viscoelastic strain energy and damping energy. Although this problem was not solved, two possible reasons for the high values were investigated by conducting small-scale experiments. The result of these investigations were that the problem with the expression for shear strain was not found. One possible reason why this problem could not be solved is that Mindlin and Goodman's method for finding displacement solutions to problems with time-dependent boundary conditions is mathematically ill-suited for using information from its higher derivatives. It is apparent that the accuracy of the comparison functions (which are really truncated series solutions of sinusoids) degrades considerably as more and more derivatives are taken.

Appendix A - *Characterization of the Test Article and Finite Element Model*

The purpose of characterizing the undamped response of the test article was threefold; the system natural frequencies, mode types, and undamped modal loss factors had to be found. These three sets of data comprise the adequate characterization of the test article.

The finite element model described in Chapter 2 was used as a comparison. Some modes are close in frequency, and the model helped spot frequency regions of high modal density.

Several trials were needed for the purpose of distinguishing mode types. For example, if the accelerometer is placed on one of the tip corners, the transfer function will register both out-of-plane bending and torsional modes. The two were distinguished from one another simply by performing other trials where the accelerometer was placed on the longitudinal axis (in the center of a cross member). Additional trials were conducted for determining the in-plane bending modes by flipping the active direction of the accelerometer and impacting the truss both in and out of the plane. The results are tabulated below for the first nine modes. The modal loss factors were determined only for the first six modes. The curve fitter in the SMS StarStruct™ software package was employed for this purpose. Its output was in percent damping, and the tabulated results shown as η are double the value of percent damping.

Mode	Freq. (Hz)	Mode Type	modal η	FE predicted frequency	Percent Difference (1-FE/exp.)*100
1	1.05	Bending 1	0.008	0.955	9
2	6	Bending 2	0.003	5.94	1
3	7.4	Torsion 1	0.002	7.98	-7.3
4	16.5	Bending 3	0.0015	16.5	0
5	22	In-plane 1	0.0015	24.2	-10
6	22.5	Torsion 2	0.0005	23.2	-3.1
7	31.9	Bending 4	0.001	31.7	0.6
8	37.6	Torsion 3		41.3	-9.8
9	50	Bending 5		49.3	1.4

Table A.1 Comparison of Finite Element Model and Experimental Modal Frequencies

The modal loss factors are averaged over three trials where the force was applied gradually over about 100 ms. The maximum truss tip deflection was about four inches.

Appendix B - *Analysis of a Five Layer Sandwich Beam Using the Variational Calculus*

The following is taken from Torvik's paper [17]. Some of the steps omitted in his paper are included for clarity, and a few simplifications are made in the application of this development to the 2D truss structure.

Consider the following slice dx of a layered beam.

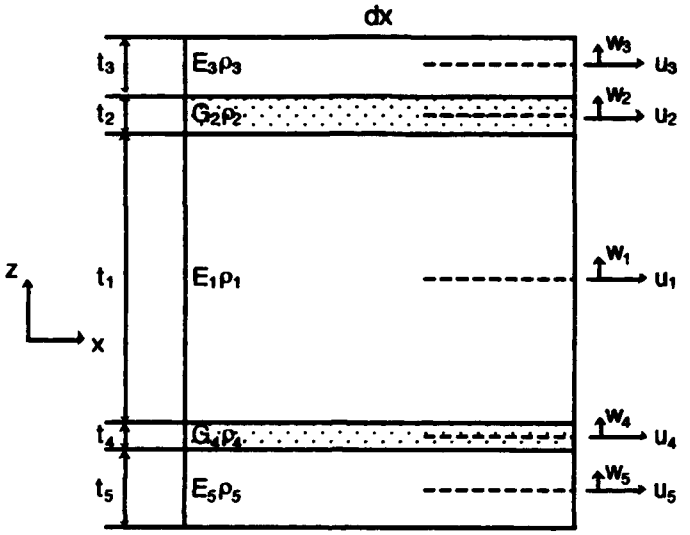

Figure B.1 Differential Slice *dx* of a Layered Beam

For this development, assume that the thicknesses remain constant so that $w(x,t)$ is the same for all layers. Assume the shear layers do not carry any bending or axial load (because $G_i \ll E_i$). Finally, the beam is assumed to be of unit width.

Hamilton's principle will be used to formulate the equations of motion and the boundary conditions.

The elastic strain energy due to bending is

$$U_b = \sum \frac{E_i t_i^3}{12(1-\nu^2)} \int_0^L \frac{1}{2}\left(\frac{\partial^2 w}{\partial x^2}\right)^2 dx$$
$$= \left(D_1 + D_3 + D_5\right) \int_0^L \frac{1}{2}\left(\frac{\partial^2 w}{\partial x^2}\right)^2 dx \qquad \text{(B.1)}$$

where

$$D_i = \frac{E_i t_i^3}{12(1-\nu^2)}$$

E = Young's Modulus

ν = poisson's ratio

w = the transverse displacement of the cross - section

t_i = the thickness of layer i

In unabridged form,

$$\begin{aligned} U_t &= \sum E_i t_i \int_0^L \frac{1}{2}\left(\frac{\partial u}{\partial x}\right)^2 dx \\ &= E_1 t_1 \int_0^L \frac{1}{2}\left(\frac{\partial u_1}{\partial x}\right)^2 dx + E_3 t_3 \int_0^L \frac{1}{2}\left(\frac{\partial u_3}{\partial x}\right)^2 dx + E_5 t_5 \int_0^L \frac{1}{2}\left(\frac{\partial u_5}{\partial x}\right)^2 dx \end{aligned} \tag{B.2}$$

The strain energy in the viscoelastic layers due to shear is

$$\begin{aligned} U_s &= G_4 t_4 \int_0^L \frac{1}{2}\left(\frac{u_1 - u_5}{t_4} + \left(1 + \frac{t_1 + t_5}{2t_4}\right)\frac{\partial w}{\partial x}\right)^2 dx \\ &+ G_2 t_2 \int_0^L \frac{1}{2}\left(\frac{u_1 - u_3}{t_4} + \left(1 + \frac{t_1 + t_3}{2t_2}\right)\frac{\partial w}{\partial x}\right)^2 dx \end{aligned} \tag{B.3}$$

The kinetic energy of a slice dx of the composite structure is

$$T = \left(\rho_1 t_1 + \rho_2 t_2 + \rho_3 t_3 + \rho_4 t_4 + \rho_5 t_5\right)\int_0^L \frac{1}{2}\left(\frac{\partial w}{\partial t}\right)^2 dx \tag{B.4}$$

Since we are using this analysis to study the 2D truss, we must deal with the cross members. We will assume they act as rigid bodies (having zero strain energy for all time). For the frequency range of interest, this is a good assumption. Therefore, $U_{xm} = 0$. However, they do possess kinetic energy equal to

$$T_{x-m} = \frac{1}{2}\rho_1 A_1 L_x \left(\frac{\partial w}{\partial t}\right)^2\Bigg|_{x=14.03} + \frac{1}{2}\rho_1 A_1 L_x \left(\frac{\partial w}{\partial t}\right)^2\Bigg|_{x=28.1} + \frac{1}{2}\rho_1 A_1 L_x \left(\frac{\partial w}{\partial t}\right)^2\Bigg|_{x=42.16} + \frac{1}{2}\rho_1 A_1 L_x \left(\frac{\partial w}{\partial t}\right)^2\Bigg|_{x=56.25} + \frac{1}{2}\rho_1 A_1 L_x \left(\frac{\partial w}{\partial t}\right)^2\Bigg|_{x=70.25} \tag{B.5}$$

where L_x = the length of each cross - member (13.0 in.).

These discrete masses on a continuous structure will prevent us from being able to assume an orthogonal modal expansion, but we can simplify to orthogonalize them at the expense of some accuracy. To do this, a modified mass density ρ' was used. Since the cross-members possess roughly half of the truss's mass, the modified mass density ρ' is

$$\rho' = 1.5\rho \tag{B.6}$$

Since the loss factor η_S will be shown to be independent of ρ', the effect on the accuracy of the solution will be minimal. A modified finite element model was constructed to compare the result of using ρ' with massless cross-members versus the "accurate" FE model. Indeed, the natural frequencies are minimally affected for the first five modes (±4% between models). Therefore, this was considered to be a safe assumption.

Hamilton's principle is the following:

$$\delta \int_{t_1}^{t_2} (L + W)\, dt = 0 \tag{B.7}$$

where

$$L = \sum T - \sum U$$

W = external work terms

If we let

$$D = D_1 + D_3 + D_5$$

$$(\rho_i t_i) = \left(\rho_1' t_1 + \rho_2 t_2 + \rho_3 t_3 + \rho_4 t_4 + \rho_5 t_5\right)$$

$$d_2 = 1 + \frac{t_1 + t_3}{2t_2}$$

$$d_4 = 1 + \frac{t_1 + t_5}{2t_4}$$

substitute ρ' for ρ, and consider only one of the long members in pure out-of-plane bending (no torsion), then

$$\delta\int_{t_1}^{t_2}\left[-\int_0^L\left(\frac{1}{2}D\left(\frac{\partial^2 w}{\partial x^2}\right)^2+\frac{1}{2}E_1t_1\left(\frac{\partial u_1}{\partial x}\right)^2+\frac{1}{2}E_3t_3\left(\frac{\partial u_3}{\partial x}\right)^2+\frac{1}{2}E_5t_5\left(\frac{\partial u_5}{\partial x}\right)^2\right.\right.$$
$$\left.+\frac{1}{2}G_2t_2\left(\frac{u_3-u_1}{t_2}+d_2\frac{\partial w}{\partial x}\right)^2+\frac{1}{2}G_4t_4\left(\frac{u_1-u_5}{t_4}+d_4\frac{\partial w}{\partial x}\right)^2\right)dx \qquad \text{(B.8)}$$
$$\left.+\int_0^L\frac{1}{2}(\rho_i t_i)\left(\frac{\partial w}{\partial t}\right)^2dx+\left(M\frac{\partial w}{\partial x}+Vw+F_1u_1+F_3u_3+F_5u_5\right)\Big|_0^L\right]dt=0$$

Taking the variations with respect to the ten dependent variables .

$$\frac{\partial^2 w}{\partial x^2},\ \frac{\partial w}{\partial x},\ w,\ \frac{\partial w}{\partial t},\ u_1,\ u_3,\ u_5,\ \frac{\partial u_1}{\partial x},\ \frac{\partial u_3}{\partial x},\ \text{and}\ \frac{\partial u_5}{\partial x},$$

$$\int_{t_1}^{t_2}\left[-\int_0^L\left(D\frac{\partial^2 w}{\partial x^2}\delta\frac{\partial^2 w}{\partial x^2}+E_1t_1\frac{\partial u_1}{\partial x}\delta\frac{\partial u_1}{\partial x}+E_3t_3\frac{\partial u_3}{\partial x}\delta\frac{\partial u_3}{\partial x}+E_5t_5\frac{\partial u_5}{\partial x}\delta\frac{\partial u_5}{\partial x}\right.\right.$$
$$+G_2t_2\left(\frac{u_3-u_1}{t_2}+d_2\frac{\partial w}{\partial x}\right)\left(\frac{1}{t_2}\delta u_3-\frac{1}{t_2}\delta u_1+d_2\delta\frac{\partial w}{\partial x}\right)$$
$$\left.+G_4t_4\left(\frac{u_1-u_5}{t_4}+d_4\frac{\partial w}{\partial x}\right)\left(\frac{1}{t_4}\delta u_1-\frac{1}{t_4}\delta u_5+d_4\delta\frac{\partial w}{\partial x}\right)\right)dx \qquad \text{(B.9)}$$
$$\left.+\int_0^L(\rho_i t_i)\frac{\partial w}{\partial t}\delta\frac{\partial w}{\partial t}dx+\left(M\delta\frac{\partial w}{\partial x}+V\delta w+F_1\delta u_1+F_3\delta u_3+F_5\delta u_5\right)\Big|_0^L\right]dt=0$$

In order to group these expressions into their respective spatial variables, we must integrate the differential variations

$$\delta\frac{\partial^2 w}{\partial x^2},\ \delta\frac{\partial w}{\partial x},\ \delta\frac{\partial w}{\partial t},\ \delta\frac{\partial u_1}{\partial x},\ \delta\frac{\partial u_3}{\partial x},\ \text{and}\ \delta\frac{\partial u_5}{\partial x}$$

by parts. Taking each term separately,

$$-\int_0^L D\frac{\partial^2 w}{\partial x^2}\delta\frac{\partial^2 w}{\partial x^2}dx = -D\frac{\partial^2 w}{\partial x^2}\delta\frac{\partial w}{\partial x}\Big|_0^L + \int_0^L D\frac{\partial^3 w}{\partial x^3}\delta\frac{\partial w}{\partial x}dx$$

$$= -D\frac{\partial^2 w}{\partial x^2}\delta\frac{\partial w}{\partial x}\Big|_0^L + D\frac{\partial^3 w}{\partial x^3}\delta w\Big|_0^L - \int_0^L D\frac{\partial^4 w}{\partial x^4}\delta w\,dx \qquad \text{(B.10)}$$

$$-\int_0^L E_1 t_1\frac{\partial u_1}{\partial x}\delta\frac{\partial u_1}{\partial x}dx = -E_1 t_1\frac{\partial u_1}{\partial x}\delta u_1\Big|_0^L + \int_0^L E_1 t_1\frac{\partial^2 u_1}{\partial x^2}\delta u_1\,dx \qquad \text{(B.11)}$$

$$-\int_0^L E_3 t_3\frac{\partial u_3}{\partial x}\delta\frac{\partial u_3}{\partial x}dx = -E_3 t_3\frac{\partial u_3}{\partial x}\delta u_3\Big|_0^L + \int_0^L E_3 t_3\frac{\partial^2 u_3}{\partial x^2}\delta u_3\,dx \qquad \text{(B.12)}$$

$$-\int_0^L E_5 t_5\frac{\partial u_5}{\partial x}\delta\frac{\partial u_5}{\partial x}dx = -E_5 t_5\frac{\partial u_5}{\partial x}\delta u_5\Big|_0^L + \int_0^L E_5 t_5\frac{\partial^2 u_5}{\partial x^2}\delta u_5\,dx \qquad \text{(B.13)}$$

$$-\int_0^L G_2 t_2\left(\frac{u_3-u_1}{t_2}+d_2\frac{\partial w}{\partial x}\right)\left(\frac{1}{t_2}\delta u_3-\frac{1}{t_2}\delta u_1+d_2\delta\frac{\partial w}{\partial x}\right)dx$$

$$= \int_0^L -G_2\left(\frac{1}{t_2}u_3\delta u_3-\frac{1}{t_2}u_1\delta u_3-\frac{1}{t_2}u_3\delta u_1+\frac{1}{t_2}u_1\delta u_1+d_2\frac{\partial w}{\partial x}\delta u_3-d_2\frac{\partial w}{\partial x}\delta u_1\right. \qquad \text{(B.14)}$$

$$\left.+d_2u_3\delta\frac{\partial w}{\partial x}-d_2u_1\delta\frac{\partial w}{\partial x}+d_2^2t_2\frac{\partial w}{\partial x}\delta\frac{\partial w}{\partial x}\right)dx$$

The last integral has itself three integrations by parts, which are

$$-\int_0^L G_2d_2u_3\delta\frac{\partial w}{\partial x}dx = -G_2d_2u_3\delta w\Big|_0^L + \int_0^L G_2d_2\frac{\partial u_3}{\partial x}\delta w\,dx$$

$$\int_0^L G_2d_2u_1\delta\frac{\partial w}{\partial x}dx = G_2d_2u_1\delta w\Big|_0^L - \int_0^L G_2d_2\frac{\partial u_1}{\partial x}\delta w\,dx \qquad \text{(B.15)}$$

$$-\int_0^L G_2d_2^2t_2\frac{\partial w}{\partial x}\delta\frac{\partial w}{\partial x}dx = -G_2d_2^2t_2\frac{\partial w}{\partial x}\delta w\Big|_0^L + \int_0^L G_2d_2^2t_2\frac{\partial^2 w}{\partial x^2}\delta w\,dx$$

The other shear term gives a similar result.

$$-\int_0^L G_4 t_4 \left(\frac{u_1 - u_5}{t_4} + d_4 \frac{\partial w}{\partial x} \right) \left(\frac{1}{t_4} \delta u_1 - \frac{1}{t_4} \delta u_5 + d_4 \delta \frac{\partial w}{\partial x} \right) dx$$

$$= \int_0^L -G_4 \left(\frac{1}{t_4} u_1 \delta u_1 - \frac{1}{t_4} u_5 \delta u_1 - \frac{1}{t_4} u_1 \delta u_5 + \frac{1}{t_4} u_5 \delta u_5 + d_4 \frac{\partial w}{\partial x} \delta u_1 - d_4 \frac{\partial w}{\partial x} \delta u_5 \right. \quad \text{(B.16)}$$

$$\left. + d_4 u_1 \delta \frac{\partial w}{\partial x} - d_4 u_5 \delta \frac{\partial w}{\partial x} + d^2 t_4 \frac{\partial w}{\partial x} \delta \frac{\partial w}{\partial x} \right) dx$$

where

$$-\int_0^L G_4 d_4 u_1 \delta \frac{\partial w}{\partial x} dx = -G_4 d_4 u_1 \delta w \Big|_0^L + \int_0^L G_4 d_4 \frac{\partial u_1}{\partial x} \delta w \, dx$$

$$\int_0^L G_4 d_4 u_5 \delta \frac{\partial w}{\partial x} dx = G_4 d_4 u_5 \delta w \Big|_0^L - \int_0^L G_4 d_4 \frac{\partial u_5}{\partial x} \delta w \, dx \quad \text{(B.17)}$$

$$-\int_0^L G_4 d_4{}^2 t_4 \frac{\partial w}{\partial x} \delta \frac{\partial w}{\partial x} dx = -G_4 d_4{}^2 t_4 \frac{\partial w}{\partial x} \delta w \Big|_0^L + \int_0^L G_4 d_4{}^2 t_4 \frac{\partial^2 w}{\partial x^2} \delta w \, dx$$

The kinetic energy term is dealt with by switching the temporal and spatial integrals, performing the integration by parts on the variation of the temporal derivative, and prescribing the variation on w at times t_1 and t_2 to be zero. There results

$$\int_0^L \left[\int_{t_1}^{t_2} (\rho_i t_i) \frac{\partial w}{\partial t} \delta \frac{\partial w}{\partial t} dt \right] dx = \int_0^L \left[(\rho_i t_i) \frac{\partial w}{\partial t} \delta w \Big|_{t_1}^{t_2} - \int_{t_1}^{t_2} (\rho_i t_i) \frac{\partial^2 w}{\partial t^2} \delta w \, dt \right] dx$$

$$= -\int_{t_1}^{t_2} \left[\int_0^L (\rho_i t_i) \frac{\partial^2 w}{\partial t^2} \delta w \, dx \right] dt \quad \text{(B.18)}$$

Substituting these integrations back into Hamilton's principle yields an integral of the form

$$\int_{t_1}^{t_2} \left[\int_0^L \left((\text{EOM for w}) \delta w + (\text{EOM for } u_1) \delta u_1 + (\text{EOM for } u_3) \delta u_3 + (\text{EOM for } u_5) \delta u_5 \right) dx \right.$$

$$\left. + (\text{the expressions that make up the boundary conditions}) \right] dt = 0 \quad \text{(B.19)}$$

The individual equations of motion are then

$$D \frac{\partial^4 w}{\partial x^4} - G_2 d_2 \left(d_2 t_2 \frac{\partial^2 w}{\partial x^2} + \frac{\partial u_3}{\partial x} - \frac{\partial u_1}{\partial x} \right) - G_4 d_4 \left(d_4 t_4 \frac{\partial^2 w}{\partial x^2} + \frac{\partial u_1}{\partial x} - \frac{\partial u_5}{\partial x} \right) + (\rho_i t_i) \frac{\partial^2 w}{\partial t^2} = 0 \quad \text{(B.20)}$$

$$E_1 t_1 \frac{\partial^2 u_1}{\partial x^2} - \frac{G_4}{t_4} u_1 + \frac{G_4}{t_4} u_5 - G_4 d_4 \frac{\partial w}{\partial x} + \frac{G_2}{t_2} u_3 - \frac{G_2}{t_2} u_1 + G_2 d_2 \frac{\partial w}{\partial x} = 0 \qquad \text{(B.21)}$$

$$E_3 t_3 \frac{\partial^2 u_3}{\partial x^2} - \frac{G_2}{t_2} u_3 + \frac{G_4}{t_4} u_1 - G_2 d_2 \frac{\partial w}{\partial x} = 0 \qquad \text{(B.22)}$$

$$E_5 t_5 \frac{\partial^2 u_5}{\partial x^2} + \frac{G_4}{t_4} u_1 - \frac{G_4}{t_4} u_5 + G_4 d_4 \frac{\partial w}{\partial x} = 0 \qquad \text{(B.23)}$$

with corresponding boundary conditions

$$\left(-D\frac{\partial^2 w}{\partial x^2} + M\right)\delta\frac{\partial w}{\partial x}\Big|_0^L = 0$$

$$\left(D\frac{\partial^3 w}{\partial x^3} - G_2 d_2\left(d_2 t_2 \frac{\partial w}{\partial x} + u_3 - u_1\right) - G_4 d_4\left(d_4 t_4 \frac{\partial w}{\partial x} + u_1 - u_5\right) + V\right)\delta w\Big|_0^L = 0$$

$$\left(-E_1 t_1 \frac{\partial u_1}{\partial x} + F_1\right)\delta u_1\Big|_0^L = 0$$

$$\left(-E_3 t_3 \frac{\partial u_3}{\partial x} + F_3\right)\delta u_3\Big|_0^L = 0 \qquad \text{(B.24)}$$

$$\left(-E_5 t_5 \frac{\partial u_5}{\partial x} + F_5\right)\delta u_5\Big|_0^L = 0$$

We can condense this set of four equations to three, but before we can do this, we multiply (B.22) by E_1t_1/E_5t_5, (B.23) by E_1t_1/E_3t_3, and (B.20) by $^1/_D$. u_1" stays the same.

$$\frac{\partial^4 w}{\partial x^4} - \frac{G_4}{Dt_4^2}\left(t_4 + \frac{t_1 + t_5}{2}\right)^2 t_4 \frac{\partial^2 w}{\partial x^2} - \frac{G_4}{Dt_4}\left(t_4 + \frac{t_1 + t_5}{2}\right)\frac{\partial u_1}{\partial x} + \frac{G_4}{Dt_4}\left(t_4 + \frac{t_1 + t_5}{2}\right)\frac{\partial u_5}{\partial x}$$

$$- \frac{G_2}{Dt_2^2}\left(t_2 + \frac{t_1 + t_3}{2}\right)^2 t_2 \frac{\partial^2 w}{\partial x^2} - \frac{G_2}{Dt_2}\left(t_2 + \frac{t_1 + t_3}{2}\right)\frac{\partial u_3}{\partial x} + \frac{G_2}{Dt_2}\left(t_2 + \frac{t_1 + t_3}{2}\right)\frac{\partial u_1}{\partial x} + \frac{(\rho_i t_i)}{D}\frac{\partial^2 w}{\partial t^2} = 0$$

(B.25)

$$E_1 t_1 \frac{\partial^2 u_1}{\partial x^2} - \frac{G_4}{t_4} u_1 + \frac{G_4}{t_4} u_5 - G_4 d_4 \frac{\partial w}{\partial x} + \frac{G_2}{t_2} u_3 - \frac{G_2}{t_2} u_1 + G_2 d_2 \frac{\partial w}{\partial x} = 0 \qquad \text{(B.26)}$$

$$E_1 t_1 \frac{\partial^2 u_3}{\partial x^2} + \frac{E_1 t_1 G_2}{E_3 t_3 t_2} u_1 - \frac{E_1 t_1 G_2}{E_3 t_3 t_2} u_3 - \frac{E_1 t_1 G_2}{E_3 t_3 t_2}\left(t_2 + \frac{t_1 + t_3}{2}\right)\frac{\partial w}{\partial x} = 0 \qquad \text{(B.27)}$$

$$E_1 t_1 \frac{\partial^2 u_5}{\partial x^2} + \frac{E_1 t_1 G_4}{E_5 t_5 t_4} u_1 - \frac{E_1 t_1 G_4}{E_5 t_5 t_4} u_5 + \frac{E_1 t_1 G_4}{E_5 t_5 t_4}\left(t_4 + \frac{t_1 + t_5}{2}\right)\frac{\partial w}{\partial x} = 0 \qquad \text{(B.28)}$$

Now subtract (B.26) from (B.28) and subtract (B27) from (B26) to obtain

$$-\left(\frac{\partial^2 u_1}{\partial x^2} - \frac{\partial^2 u_5}{\partial x^2}\right) + \left(1 + \frac{E_1 t_1}{E_5 t_5}\right)\frac{G_4}{E_1 t_1 t_4}(u_1 - u_5) + \left(1 + \frac{E_1 t_1}{E_5 t_5}\right)\frac{G_4}{E_1 t_1 t_4}\left(t_4 + \frac{t_1 + t_5}{2}\right)\frac{\partial w}{\partial x}$$
$$- \frac{G_2}{E_1 t_1 t_2}\left(t_2 + \frac{t_1 + t_3}{2}\right)\frac{\partial w}{\partial x} - \frac{G_2}{E_1 t_1 t_2}(u_3 - u_1) = 0 \qquad \text{(B.29)}$$

$$-\frac{G_4}{D t_4}\left(t_4 + \frac{t_1 + t_5}{2}\right)\left(\frac{\partial u_1}{\partial x} - \frac{\partial u_5}{\partial x}\right) + \frac{\partial^4 w}{\partial x^4} + \frac{(\rho_i t_i)}{D}\frac{\partial^2 w}{\partial t^2} - \frac{G_4}{D t_4}\left(t_4 + \frac{t_1 + t_5}{2}\right)^2 \frac{\partial^2 w}{\partial x^2}$$
$$- \frac{G_2}{D t_2}\left(t_2 + \frac{t_1 + t_3}{2}\right)^2 \frac{\partial^2 w}{\partial x^2} - \frac{G_2}{D t_2}\left(t_2 + \frac{t_1 + t_3}{2}\right)\left(\frac{\partial u_3}{\partial x} - \frac{\partial u_1}{\partial x}\right) = 0 \qquad \text{(B.30)}$$

$$-\frac{G_4}{E_1 t_1 t_4}(u_1 - u_5) - \frac{G_4}{E_1 t_1 t_4}\left(t_4 + \frac{t_1 + t_5}{2}\right)\frac{\partial w}{\partial x} + \left(1 + \frac{E_1 t_1}{E_3 t_3}\right)\frac{G_2}{E_1 t_1 t_2}\left(t_2 + \frac{t_1 + t_3}{2}\right)\frac{\partial w}{\partial x}$$
$$+ \left(\frac{\partial^2 u_1}{\partial x^2} - \frac{\partial^2 u_3}{\partial x^2}\right) + \left(1 + \frac{E_1 t_1}{E_3 t_3}\right)\frac{G_2}{E_1 t_1 t_2}(u_3 - u_1) = 0 \qquad \text{(B.31)}$$

The mode shape of the cantilevered composite beam is a combination of cos and cosh terms. However, as the mode number increases, the majority of the beam has the mode shape of a sine wave. Therefore, we assume a bending mode shape of $\sin {}^{n\pi x}/_{L}$ and will accept the error in the low modes where a larger percentage of the beam is affected by the cosh part of the displacement expression. In addition, the axial displacements of the constraining layers are assumed to have a mode shape of $\cos {}^{n\pi x}/_{L}$ Finally, assume a temporal dependence of $e^{i\omega t}$. The assumed solutions have the form

$$w = We^{i\omega t}\sin\frac{n\pi x}{L} \quad \text{and} \quad u_i = U_i e^{i\omega t}\cos\frac{n\pi x}{L} \qquad \text{(B.32)}$$

Operating on eqs.(B.29-31), the new equations become

$$\left[\left[1+\left(\frac{L}{n\pi}\right)^2\left(1+\frac{E_1t_1}{E_5t_5}\right)\frac{G_4}{E_1t_1t_4}\right](U_1-U_5)+\left[\left(\frac{L}{n\pi}\right)\left(1+\frac{E_1t_1}{E_5t_5}\right)\frac{G_4}{E_1t_1t_4}\left(t_4+\frac{t_1+t_5}{2}\right)\right.\right.$$
$$\left.\left.-\left(\frac{L}{n\pi}\right)\frac{G_2}{E_1t_1t_2}\left(t_2+\frac{t_1+t_3}{2}\right)\right]W-\left(\frac{L}{n\pi}\right)^2\frac{G_2}{E_1t_1t_2}(U_3-U_1)\right]e^{i\omega t}\cos\left(\frac{n\pi x}{L}\right)=0 \tag{B.33}$$

$$\left[\frac{G_4}{Dt_4}\left(\frac{L}{n\pi}\right)^3\left(t_4+\frac{t_1+t_5}{2}\right)(U_1-U_5)+\left[1-\left(\frac{L}{n\pi}\right)^4\frac{(\rho_it_i)}{D}\omega^2+\left(\frac{L}{n\pi}\right)^2\frac{G_4}{Dt_4}\left(t_4+\frac{t_1+t_5}{2}\right)^2\right.\right.$$
$$\left.\left.+\left(\frac{L}{n\pi}\right)^2\frac{G_2}{Dt_2}\left(t_2+\frac{t_1+t_3}{2}\right)^2\right]W+\frac{G_2}{Dt_2}\left(\frac{L}{n\pi}\right)^3\left(t_2+\frac{t_1+t_3}{2}\right)(U_3-U_1)\right]e^{i\omega t}\sin\left(\frac{n\pi x}{L}\right)=0 \tag{B.34}$$

$$\left[-\frac{G_4}{E_1t_1t_4}\left(\frac{L}{n\pi}\right)^2(U_1-U_5)-\left[\left(\frac{L}{n\pi}\right)\left(1+\frac{E_1t_1}{E_3t_3}\right)\frac{G_2}{E_1t_1t_2}\left(t_2+\frac{t_1+t_3}{2}\right)\right.\right.$$
$$\left.\left.-\left(\frac{L}{n\pi}\right)\frac{G_4}{E_1t_1t_4}\left(t_4+\frac{t_1+t_5}{2}\right)\right]W+\left[1+\left(\frac{L}{n\pi}\right)^2\left(1+\frac{E_1t_1}{E_3t_3}\right)\frac{G_2}{E_1t_1t_2}\right](U_3-U_1)\right]e^{i\omega t}\cos\left(\frac{n\pi x}{L}\right)=0 \tag{B.35}$$

At this point, we define quantities that help simplify the algebraic expressions. Define

$$\begin{aligned}
q_1&=\left(\frac{n\pi}{L}\right)\left(t_4+\frac{t_1+t_5}{2}\right) & q_5&=\frac{G_4}{E_1t_1t_4}\left(\frac{L}{n\pi}\right)^2\\
q_2&=\left(\frac{n\pi}{L}\right)\left(t_2+\frac{t_1+t_3}{2}\right) & q_6&=\frac{G_2}{E_1t_1t_2}\left(\frac{L}{n\pi}\right)^2\\
q_3&=1+\frac{E_1t_1}{E_5t_5} & q_7&=\frac{Et_1}{D}\left(\frac{L}{n\pi}\right)^2\\
q_4&=1+\frac{E_1t_1}{E_3t_3} & q_8&=\left(\frac{L}{n\pi}\right)^4\frac{(\rho_it_i)}{D}\omega^2
\end{aligned} \tag{B.36}$$

to help simplify the arithmetic. Making these substitutions and putting the amplitudes of the expressions in matrix form,

$$\begin{bmatrix}1+q_3q_5 & q_1q_3q_5-q_2q_6 & -q_6\\ q_1q_5q_7 & 1+q_7\left(q_1^2q_5+q_2^2q_6\right)-q_8 & q_2q_6q_7\\ -q_5 & q_2q_4q_6-q_1q_5 & 1+q_4q_6\end{bmatrix}\begin{Bmatrix}(U_1-U_5)\\ W\\ (U_3-U_1)\end{Bmatrix}=0 \tag{B.37}$$

Setting the determinant of this matrix equal to zero and solving for the frequency ω^2 yields the frequency equation for free vibration of the system. Since only q_8 contains ω^2 (with a constant coefficient), we need to isolate q_8. Since the design for the improved treatment has been prescribed to be symmetric and the structure and constraining layers will have the same modulus, $E_1 = E_3 = E_5 = E$, $t_5 = t_3$, $t_4 = t_2$, and $G_4^* = G_2^* = G^*$. Therefore, $q_1 = q_2$, $q_3 = q_4$, and $q_5 = q_6$. Consequently,

$$\det \begin{bmatrix} 1+q_3q_5 & q_1q_3q_5 - q_1q_5 & -q_5 \\ q_1q_5q_7 & 1+q_7\left(q_1^2q_5 + q_1^2q_5\right) - q_8 & q_1q_5q_7 \\ -q_5 & q_1q_3q_5 - q_1q_5 & 1+q_3q_5 \end{bmatrix} = 0 \tag{B.38}$$

Solving the determinant for q_8,

$$q_8 = \frac{1+q_5(q_3-1)+2q_1^2q_5q_7}{1+q_5(q_3-1)} \tag{B.39}$$

Letting

$$g = q_5(q_3-1)\left(\frac{n\pi}{L}\right)^2 = G^*\left(\frac{1}{Et_2t_3}\right)$$

and

$$Y = \frac{2q_1^2q_7}{(q_3-1)} = \frac{2Et_3\left(t_2 + \frac{t_1+t_3}{2}\right)^2}{D},$$

we now endeavor to find the system loss factor η_s. To do this, we:

- find the positive imaginary square root of q_8
- express $[q_8]^{1/2}$ as $R + iI$ and assume the response

$$e^{-It}\sin Rt$$

- compare this with the known response of a damped linear system

$$e^{-\zeta\omega_n t}\sin\omega_d t$$

- consequently,

$$\frac{I}{R} = \frac{\zeta\omega_n}{\omega_d} = \frac{\omega_n\zeta}{\omega_n\sqrt{1-\zeta^2}}.$$

Assuming the loss factor $\eta = 2\zeta$,

$$\eta_s = \frac{2\left(\frac{I}{R}\right)}{\left[1+\left(\frac{I}{R}\right)^2\right]^{1/2}}.$$

The following procedure was used to calculate I and R:

Since G^* is a complex quantity, g^* is too. Let

$$g^* = \mathrm{Re}(g^*) + \mathrm{Im}(g^*) = g_r + g_i,$$

$$X = \left(\frac{L}{n\pi}\right)^2, \quad \text{and} \quad Y = Y.$$

q_8 is rewritten as

$$q_8 = \frac{1 + g_r X + g_i X + g_r XY + g_i XY}{1 + g_r X + g_i X}$$

Rationalizing the denominator and letting $g_i = i\eta_v g_r$,

$$\mathrm{Re}(q_8) = \frac{1 + g_r X(2+Y) + g_r^2 X^2 (1+Y)(1+\eta_v^2)}{(1+g_r X)^2 + (\eta_v g_r X)^2}$$

$$\mathrm{Im}(q_8) = \frac{\eta_v g_r XY}{(1+g_r X)^2 + (\eta_v g_r X)^2}$$

where η_v is the viscoelastic material loss factor.

We then find the magnitude and angle of the complex square root of q_8.

$$\mathrm{mag}(q_8) = [\mathrm{Re}(q_8)^2 + \mathrm{Im}(q_8)^2]^{1/2}$$

$$\mathrm{angle}(q_8) = \tan^{-1}\frac{\mathrm{Im}(q_8)}{\mathrm{Re}(q_8)}$$

$$\mathrm{mag}[(q_8)^{1/2}] = \sqrt{\mathrm{mag}(q_8)}$$

$$\mathrm{angle}[(q_8)^{1/2}] = \frac{\mathrm{angle}(q_8)}{2}$$

Finally,

$$R = \mathrm{Re}[(q_8)^{1/2}] = \mathrm{mag}[(q_8)^{1/2}]\cos\left(\mathrm{angle}[(q_8)^{1/2}]\right)$$

$$I = \mathrm{Im}[(q_8)^{1/2}] = \mathrm{mag}[(q_8)^{1/2}]\sin\left(\mathrm{angle}[(q_8)^{1/2}]\right)$$

This process allowed for efficient parametric study on a computer spreadsheet.

Appendix C - *Comparison of Experimental and Theoretical Modal Loss Factors (Modes 1 and 2) for Various Constrained Layer Segment Lengths on a 6061-T6 Al 11" Beam*

Three 11" beams with cross-section 0.126" x 0.75" were fabricated for the purposes of verifying the accuracy of the 3M data and determining the repeatability of accurate data. All damping segments were prefabricated by 3M. The material properties are described below for T=70°F.*

Material	Density ρ	E	G	ν	η_v
Constraining Layer	.1 lb/in^3	10 Mpsi	3.8 Mpsi	0.33	0.03
Damping Layer, Mode 1	.04 lb/in^3	240 psi	80 psi	0.49	0.9
Damping Layer, Mode 2	.04 lb/in^3	500 psi	170 psi	0.49	0.9

Table C.1 3M ISD 112 Material Property Data

*The values of G^*,E, and η for the damping layer are courtesy of 3M. All other values were transcribed from Mantena, Gibson, and Hwang's paper [18].

Figure C1 shows the undamped beam data. Each data point consists of the curve fitted value of percent damping (multiplied by two to get η) based on a set of twenty impact trials whose frequency response functions were averaged into a single FRF.

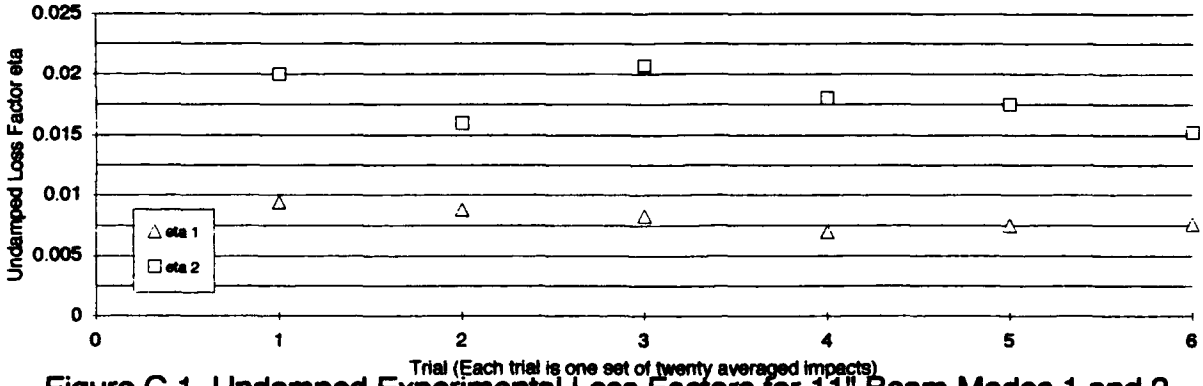

Figure C.1 Undamped Experimental Loss Factors for 11" Beam Modes 1 and 2

The corresponding data is tabulated below.

Trial	η 1	η 2
1	0.0094	0.02
2	0.0088	0.016
3	0.0083	0.0207
4	0.007	0.018
5	0.0075	0.0175
6	0.0076	0.0152

Table C.2 Undamped Modal Loss Factors

There was a significant amount of 60 Hz noise in the signal. This effect was minimized by using the maximum number of samples (4096) for each FRF and by choosing the minimum frequency bandwidth needed for testing. In addition, the accuracy of the data was sensitive to the following:

- location of the accelerometer (cleaner, more consistent data was obtained when the accelerometer was near the clamped end of the truss)
- impact location (clean, gently sloping force-time histories gave more consistent data than sharp-impulse and double-hit impacts)
- machine warmup
- battery strength in the force transducer power supply
- bandwidth chosen for the curve fit (more samples/trial and wider curve fit bandwidths gave more consistent damping percentages)
- amount of tension (or slack) in the accelerometer cable. This particular variable had the greatest influence on accuracy and repeatability. It was determined through trial-and-error that a loose cable of medium length (20") with the accelerometer placed as close to the cantilevered end as possible was the most desirable setup. Fortunately, the effect of the cable tension is small when collecting data on the truss because the truss is much more massive than the 11" beams.

The outcome of the undamped beam testing was the undamped modal loss factors for modes 1 and 2 (0.008 and 0.018, respectively). These values were then subtracted from the experimental damped modal loss factors to obtain the actual damped moal loss factors.

The following data represents the damped modal loss factors for given segment lengths of damping treatment. The treatment was applied over the entire length on both sides of the beam. Each data point is double the curve fitted value of percent damping based on the averaged FRF of ten impact trials. Remember, the value of the reduced η = exper. η - undamped η.

Length	reduced eta 1	reduced eta 2	Length	reduced eta 1	reduced eta 2
0.37	0.0072	0.011	2.5	0.0412	0.0342
0.37	0.0076	0.011	2.5	0.0408	0.038
0.37	0.0073	0.0125	2.5	0.0404	0.0384
0.75	0.0131	0.0228	3.06	0.0408	0.0384
0.75	0.0136	0.0212	3.06	0.0406	0.0308
0.75	0.0135	0.027	3.06	0.0404	0.033
0.75	0.014	0.0248	4	0.0328	0.0262
0.75	0.0148	0.0208	4	0.0332	0.023
0.75	0.0149	0.0192	4	0.0328	0.0234
0.95	0.02	0.0302	5	0.031	0.0296
0.95	0.02	0.0288	5	0.0356	0.0314
0.95	0.0204	0.031	5	0.0356	0.0308
1.2	0.0212	0.0302	6.13	0.0306	0.0296
1.2	0.0224	0.0278	6.13	0.03	0.028
1.2	0.022	0.031	6.13	0.0302	0.0286
1.55	0.0304	0.0274	8	0.0276	0.025
1.55	0.0304	0.0322	8	0.0274	0.0238
1.55	0.0298	0.0396	8	0.0278	0.0204
1.97	0.0362	0.0434	10	0.0258	0.0172
1.97	0.0362	0.0418	10	0.027	0.0134
1.97	0.0358	0.0452	10	0.0256	0.0111

Table C.3 Experimental Data, 11" Beam Experiment

Figure (4.3) is displayed again for convenience.

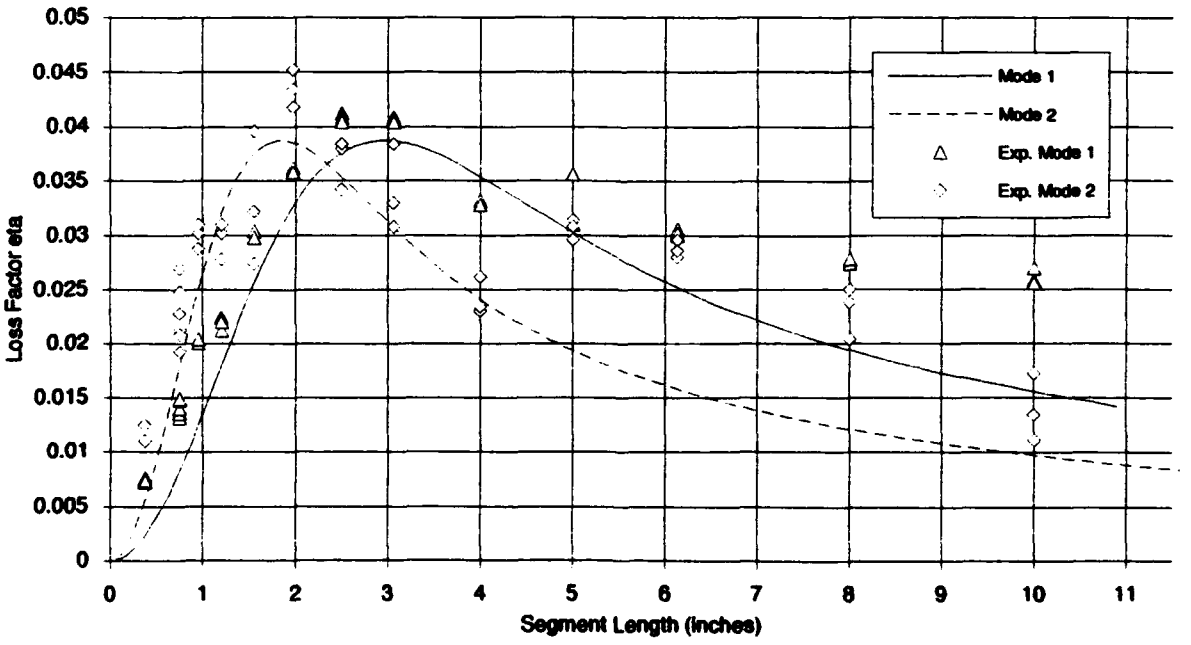

Figure 4.3 Experimental vs. Theoretical η for Various Segment Lengths

Appendix D - *Derivation of the Differential Equation of Motion of Transverse Displacement of a Three-Layer Sandwich Beam*

The following development is mostly taken from Mead and Markus' article [8]. Some steps that were omitted in the article are developed in full here.

Consider again the slice dx of a three layer sandwich beam of unit width.

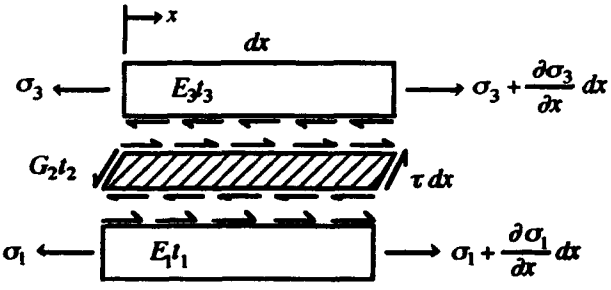

Figure D.1. Differential Slice dx of a Three-Layer Sandwich Beam

The following assumptions are made for this analysis:

- the beam is symmetric ($E_1 = E_3 = E$, $t_3 = t_1$)
- shear strains in the constraining layers are negligible
- direct strain in the viscoelastic layer is negligible
- the viscoelastic layer thickness t_2 is constant for all x and time
- the transverse displacements of each layer are equal at any location x
- the effects of shear deformation and rotary inertia are negligible

Unlike the direct shear case, the shear strain in the viscoelastic layer has *two* terms and is given by

$$\gamma = \frac{\partial u}{\partial z} + \frac{\partial w}{\partial x} \tag{D.1}$$

It is seen that

$$\begin{aligned} \frac{\partial u}{\partial z} &= \frac{t_1 + t_3}{2t_2}\frac{\partial w}{\partial x} + \frac{u_3 - u_1}{t_2} \\ &= \frac{t_1}{t_2}\frac{\partial w}{\partial x} + \frac{u_3 - u_1}{t_2} \end{aligned} \tag{D.2}$$

where u_i are the longitudinal displacements of the constraining layers. The shear strain is then

$$\gamma = \left(1 + \frac{t_1}{t_2}\right)\frac{\partial w}{\partial x} + \frac{u_3 - u_1}{t_2} \tag{D.3}$$

where γ is the average shear strain through the thickness t_2. The shear stress is equal to

$$\tau = G\gamma = G\left[\left(1 + \frac{t_1}{t_2}\right)\frac{\partial w}{\partial x} + \frac{u_3 - u_1}{t_2}\right] \tag{D.4}$$

The flexural rigidity D of the face plates is given by

$$D_i = \frac{E t_1^{\,3}}{12(1-\nu^2)} \quad \Rightarrow \quad D = \sum D_i \tag{D.5}$$

where i are the elastic layers 1 and 3.

Mead and Markus neglected poisson effects, but the addition of the $(1-\nu^2)$ term adds little complexity. Since the thicknesses of the layers are small compared to their width b, this term will remain.

The total shear force on a cross-section is the summation of the shear forces acting through the thickness of each layer. Hence, the shear force S is

$$S = S_1 + S_2 + S_3 \tag{D.6}$$

where

$$S_1 = D_1\frac{\partial^3 w}{\partial x^3} \quad \text{and} \quad S_3 = D_3\frac{\partial^3 w}{\partial x^3} \tag{D.7}$$

The quantity S_2 is given by the shear stress τ times the thickness over which it acts. Therefore,

$$S_2 = -\tau t_2\left(1 + \frac{t_1}{t_2}\right) \tag{D.8}$$

where the minus sign indicates that the positive shear force direction is the opposite as the positive shear stress direction. Making the appropriate substitutions,

$$S = D\frac{\partial^3 w}{\partial x^3} - Gt_2\left(1 + \frac{t_1}{t_2}\right)\left[\left(1 + \frac{t_1}{t_2}\right)\frac{\partial w}{\partial x} + \frac{u_3 - u_1}{t_2}\right] \tag{D.9}$$

The distributed loading internal to the boundaries is the derivative of the total shear force.

$$p = \frac{\partial S}{\partial x} \tag{D.10}$$

Since the sandwich beam will have no externally applied forces in its interior except for the inertial loading,

$$p = -(\rho t)\frac{\partial^2 w}{\partial t^2} = D\frac{\partial^4 w}{\partial x^4} - Gt_2\left(1+\frac{t_1}{t_2}\right)\left[\left(1+\frac{t_1}{t_2}\right)\frac{\partial^2 w}{\partial x^2} + \frac{1}{t_2}\left(\frac{\partial u_3}{\partial x} - \frac{\partial u_1}{\partial x}\right)\right] \tag{D.11}$$

where

$$(\rho t) = \sum_{i=1}^{3} \rho_i t_i = \text{ mass of the sandwich beam per unit length } .$$

Next, consider the axial forces P_i. Assume these forces act along the neutral surfaces of the individual constraining layers and have magnitudes

$$P_i = \sigma_i A_i = E\varepsilon_i t_i = Et_i \frac{\partial u_i}{\partial x} \tag{D.12}$$

It is noted here that, for a unit width, $A_i = t_i$, so

$$P_1 = Et_1 \frac{\partial u_1}{\partial x} \quad \text{and} \quad P_3 = Et_1 \frac{\partial u_3}{\partial x} \tag{D.13}$$

Summing forces on each constraining layer gives

$$\frac{\partial P_1}{\partial x} = -\tau \quad \text{and} \quad \frac{\partial P_3}{\partial x} = \tau \tag{D.14}$$

Therefore,

$$Et_1 \frac{\partial^2 u_1}{\partial x^2} + \frac{2G}{t_2}(u_3 - u_1) = -G\left(1+\frac{t_1}{t_2}\right)\frac{\partial w}{\partial x} \tag{D.15}$$

$$Et_1 \frac{\partial^2 u_3}{\partial x^2} - \frac{2G}{t_2}(u_3 - u_1) = G\left(1+\frac{t_1}{t_2}\right)\frac{\partial w}{\partial x} \tag{D.16}$$

Remember that we are considering the deformation of the sandwich beam to be the superposition of the direct shear quasi-static case and the *total* bending case (quasi-static plus dynamic). Since the effects of the external axial forces have already been considered, the axial load will be assumed to be zero. Consequently, for no axial loading and a symmetric layup,

$$\frac{\partial u_1}{\partial x} = -\frac{\partial u_3}{\partial x} \tag{D.17}$$

Subtracting (D.16) from (D.15) yields

$$\frac{\partial^2 u_1}{\partial x^2} - \frac{2G}{Et_1t_2}u_1 = \frac{-G}{Et_1}\left(1+\frac{t_1}{t_2}\right)\frac{\partial w}{\partial x} \tag{D.18}$$

Rearranging (D.11) gives

$$\frac{\partial^4 w}{\partial x^4} - \frac{Gt_2}{D}\left(1+\frac{t_1}{t_2}\right)^2\frac{\partial^2 w}{\partial x^2} - \frac{2G}{D}\left(1+\frac{t_1}{t_2}\right)\frac{\partial u_1}{\partial x} + (\rho t)\frac{\partial^2 w}{\partial t^2} = 0 \tag{D.19}$$

We can use (D.18) and (D.19) to solve for w by taking derivatives to eliminate u_1. Differentiate (D.19) once and (D.18) twice to obtain

$$\frac{\partial^3 u_1}{\partial x^3} = \frac{2G}{Et_1t_2}\frac{\partial u_1}{\partial x} - \frac{G}{Et_1}\left(1+\frac{t_1}{t_2}\right)\frac{\partial^2 w}{\partial x^2} \tag{D.20}$$

$$\frac{\partial^6 w}{\partial x^6} - \frac{Gt_2}{D}\left(1+\frac{t_1}{t_2}\right)^2\frac{\partial^4 w}{\partial x^4} - \frac{2G}{D}\left(1+\frac{t_1}{t_2}\right)\frac{\partial^3 u_1}{\partial x^3} + (\rho t)\frac{\partial^4 w}{\partial x^2 \partial t^2} = 0 \tag{D.21}$$

Substitution of (D.20) into (D.21) gives

$$\frac{\partial^6 w}{\partial x^6} - \frac{Gt_2}{D}\left(1+\frac{t_1}{t_2}\right)^2\frac{\partial^4 w}{\partial x^4} - \frac{2G}{D}\left(1+\frac{t_1}{t_2}\right)\left[\frac{2G}{Et_1t_2}\frac{\partial u_1}{\partial x} - \frac{G}{Et_1}\left(1+\frac{t_1}{t_2}\right)\frac{\partial^2 w}{\partial x^2}\right] + (\rho t)\frac{\partial^4 w}{\partial x^2 \partial t^2} = 0 \tag{D.22}$$

We can determine u_1' in terms of w by using (D.19) as

$$\frac{\partial u_1}{\partial x} = -\frac{2G}{Et_1t_2}\frac{\partial^4 w}{\partial x^4} + \frac{2G^2}{Et_1D}\left(1+\frac{t_1}{t_2}\right)^2\frac{\partial^2 w}{\partial x^2} - \frac{2G(\rho t)}{Et_1t_2D}\frac{\partial^2 w}{\partial t^2} \qquad \text{(D.23)}$$

Substitution of (D.23) into (D.22) yields

$$\frac{\partial^6 w}{\partial x^6} - \frac{Gt_2}{D}\left(1+\frac{t_1}{t_2}\right)^2\frac{\partial^4 w}{\partial x^4} - \frac{2G}{Et_1t_2}\frac{\partial^4 w}{\partial x^4} - \frac{2G(\rho t)}{Et_1t_2D}\frac{\partial^2 w}{\partial t^2} + \frac{(\rho t)}{D}\frac{\partial^4 w}{\partial x^2 \partial t^2} = 0 \qquad \text{(D.24)}$$

We now define the shear and geometric parameters to be

$$g = \frac{2G}{Et_1t_2} \quad \text{and} \quad Y = \frac{Et_1(t_1+t_2)^2}{2D}$$

which simplify (D.24) to

$$\frac{\partial^6 w}{\partial x^6} - g(1+Y)\frac{\partial^4 w}{\partial x^4} + \frac{(\rho t)}{D}\left(\frac{\partial^4 w}{\partial x^2 \partial t^2} - g\frac{\partial^2 w}{\partial t^2}\right) = 0 \qquad \text{(D.25)}$$

This is the sixth-order, homogeneous differential equation of motion for transverse displacement of a three-layer sandwich beam.

Appendix E - *Development of the Volume Specific Energy Dissipation Per Cycle D*

For this development, we define the complex quantity τ^* as

$$\tau^* = G^* \gamma^* \tag{E.1}$$

where

$$G^* = G' + iG'' \text{ and } \gamma^* = (\gamma' + i\gamma'')e^{i\omega t}.$$

The volume specific energy dissipation per cycle D is

$$D = \int_0^{2\pi/\omega} \tau^* \dot{\gamma}^* \, dt \tag{E.2}$$

We must integrate the *real* parts of each term over one cycle of oscillation (equal to $2\pi/\omega$).

$$\begin{aligned}
D &= \int_0^{2\pi/\omega} \mathrm{Re}\{G^* \gamma^*\} \mathrm{Re}\{i\omega \gamma^* e^{i\omega t}\} \, dt \\
&= \int_0^{2\pi/\omega} \mathrm{Re}\{(G' + iG'')(\gamma' + i\gamma'')\} \mathrm{Re}\{i\omega(\gamma' + i\gamma'')(\cos\omega t + i\sin\omega t)\} \, dt \\
&= \int_0^{2\pi/\omega} \mathrm{Re}\{G'\gamma'\cos\omega t + iG'\gamma'\sin\omega t + iG'\gamma''\cos\omega t + i^2 G'\gamma''\sin\omega t + iG''\gamma'\cos\omega t \\
&\quad + i^2 G''\gamma'\sin\omega t + i^2 G''\gamma''\cos\omega t + i^3 G''\gamma''\sin\omega t\} \mathrm{Re}\{i\omega\gamma'\cos\omega t + i^2\omega\gamma'\sin\omega t \\
&\quad + i^2\omega\gamma''\cos\omega t + i^3\omega\gamma''\sin\omega t\} \, dt \\
&= \int_0^{2\pi/\omega} (G'\gamma'\cos\omega t - G'\gamma''\sin\omega t - G''\gamma'\sin\omega t - G''\gamma''\cos\omega t)(-\omega\gamma'\sin\omega t - \omega\gamma''\cos\omega t) \, dt \\
&= \int_0^{2\pi/\omega} \omega[-G'\gamma'^2\cos\omega t\sin\omega t + G'\gamma'\gamma''\sin^2\omega t + G''\gamma'^2\sin^2\omega t + G''\gamma'\gamma''\cos\omega t\sin\omega t \\
&\quad - G'\gamma'\gamma''\cos^2\omega t + G'\gamma''^2\cos\omega t\sin\omega t + G''\gamma'\gamma''\cos\omega t\sin\omega t + G''\gamma''^2\cos^2\omega t] \, dt \\
&= \int_0^{2\pi/\omega} \omega[(G'\gamma'\gamma'' + G''\gamma'^2)\sin^2\omega t + (-G'\gamma'\gamma'' + G''\gamma''^2)\cos^2\omega t \\
&\quad + (-G'\gamma'^2 + G''\gamma'\gamma'' + G'\gamma''^2 + G''\gamma'\gamma'')\cos\omega t\sin\omega t] \, dt \\
&= \omega\left(\frac{\pi}{\omega}\right)[G''\gamma'^2 + G''\gamma''^2] \\
&= \pi G''(\gamma'^2 + \gamma''^2) \\
&= \pi G''|\gamma|^2
\end{aligned} \tag{E.3}$$

The energy dissipated per cycle D_S is

$$D_s = \int_{Volume} \pi G'' |\gamma|^2 dV$$
$$= \pi G'' b t_2 \int_0^1 |\gamma|^2 dx \qquad \text{(E.4)}$$

Appendix F - *Determinaton of the Shear Strain Due to Bending* γ_b

From Appendix D, we know that

$$\gamma_b = (1 + t_1/t_2)\frac{\partial w}{\partial x} + \frac{u_1 - u_3}{t_2} \tag{F.1}$$

and

$$Et_1\left(\frac{\partial^2 u_1}{\partial x^2} - \frac{\partial^2 u_3}{\partial x^2}\right) - 2G\left(\frac{u_1 - u_3}{t_2}\right) = 2G(1 + t_1/t_2)\frac{\partial w}{\partial x} \tag{F.2}$$

Solving for γ_b,

$$\frac{Et_1}{2G}\left(\frac{\partial^2 u_1}{\partial x^2} - \frac{\partial^2 u_3}{\partial x^2}\right) = (1 + t_1/t_2)\frac{\partial w}{\partial x} + \frac{u_1 - u_3}{t_2} = \gamma_b \tag{F.3}$$

Also from Appendix D,

$$\frac{\partial u_1}{\partial x} = -\frac{\partial u_3}{\partial x} = \frac{D}{gEt_1t_2(1 + t_1/t_2)}\left[\frac{\partial^4 w}{\partial x^4} + gY\frac{\partial^2 w}{\partial x^2} - \frac{(\rho t)}{D}\frac{\partial^2 w}{\partial t^2}\right] \tag{F.4}$$

Differentiating this quantity gives

$$\frac{\partial^2 u_1}{\partial x^2} = -\frac{\partial^2 u_3}{\partial x^2} = \frac{D}{gEt_1t_2(1 + t_1/t_2)}\left[\frac{\partial^5 w}{\partial x^5} + gY\frac{\partial^3 w}{\partial x^3} - \frac{(\rho t)}{D}\frac{\partial^2 w}{\partial t^2}\frac{\partial w}{\partial x}\right] \tag{F.5}$$

Subtracting $-\frac{\partial^2 u_3}{\partial x^2}$ from $\frac{\partial^2 u_1}{\partial x^2}$,

$$\frac{Et_1}{2G}\frac{2D}{gEt_1t_2(1 + t_1/t_2)}\left[\frac{\partial^5 w}{\partial x^5} + gY\frac{\partial^3 w}{\partial x^3} - \frac{(\rho t)}{D}\frac{\partial^2 w}{\partial t^2}\frac{\partial w}{\partial x}\right] = \gamma_b \tag{F.6}$$

Rewriting the displacement $w(x,t)$ in a convenient shorthand form,

$$w(x,t) = \sum_{n=1}^{\infty}\left[C_n \sin\frac{n\pi x}{L}\frac{M_b}{\omega_{SB_n}}\left(\frac{\omega_T \sin\omega_{SB_n}t - \omega_{SB_n}\sin\omega_T t}{\omega_T^2 - \omega_{SB_n}^2}\right)\right] \qquad \text{(F.7)}$$
$$+ M_b \sin\omega_T t\left(a_1 x + a_2 x^2 + a_3 x^3 + a_4 x^4\right)$$

where

$$C_n = \left\{\omega_T^2\left[gL\left(\frac{L}{\pi}\right)\left(\frac{gYL^3 - 12L}{24D}\right) + \left[\left(\frac{L}{\pi}\right)\left(gL^2 + 4\right) + 4g\left(\frac{L}{\pi}\right)^3\right]\frac{1}{2D}\right.\right.$$
$$-\left[\left(6L - gL^3\right)\left(\frac{L}{\pi}\right) + 6gL\left(\frac{L}{\pi}\right)^3\right]\frac{gYL}{12D} + \left[\left(12L^2 - gL^4\right)\left(\frac{L}{\pi}\right) + \left(12gL^2 - 48\right)\left(\frac{L}{\pi}\right)^3\right.$$
$$\left.\left.\left.-48g\left(\frac{L}{\pi}\right)^5\right]\left(\frac{gY}{24D}\right)\right] + (1+Y)\left[\frac{2g^2Y}{D}\left(\frac{L}{\pi}\right)\right]\right\}$$

$$a_1 = \frac{12L - gYL^3}{24D}$$

$$a_2 = -\frac{1}{2D}$$

$$a_3 = \frac{gYL}{12D}$$

$$a_4 = -\frac{gY}{24D}$$

At this point, we are ready to take derivatives and find an expression for γ_b.

$$\frac{\partial}{\partial x}\frac{\partial^2 w}{\partial t^2} = \frac{\partial}{\partial x}\sum_{n=1}^{\infty}\left[C_n \sin\frac{n\pi x}{L}\frac{M_b}{\omega_{SB_n}}\left(\frac{-\omega_{SB_n}{}^2\omega_T \sin\omega_{SB_n}t + \omega_T{}^2\omega_{SB_n}\sin\omega_T t}{\omega_T^2 - \omega_{SB_n}^2}\right)\right]$$
$$- \omega_T{}^2 M_b \sin\omega_T t\left(a_1 x + a_2 x^2 + a_3 x^3 + a_4 x^4\right)$$

$$= \sum_{n=1}^{\infty}\left[\frac{n\pi}{L}C_n \cos\frac{n\pi x}{L}\frac{M_b}{\omega_{SB_n}}\left(\frac{-\omega_{SB_n}{}^2\omega_T \sin\omega_{SB_n}t + \omega_T{}^2\omega_{SB_n}\sin\omega_T t}{\omega_T^2 - \omega_{SB_n}^2}\right)\right] \qquad \text{(F.8)}$$
$$-\omega_T{}^2 M_b \sin\omega_T t\left(a_1 + 2a_2 x + 3a_3 x^2 + 4a_4 x^3\right)$$

$$\frac{\partial^3 w}{\partial x^3} = \sum_{n=1}^{\infty}\left[-\left(\frac{n\pi}{L}\right)^3 C_n \cos\frac{n\pi x}{L}\frac{M_b}{\omega_{SB_n}}\left(\frac{\omega_T \sin\omega_{SB_n}t - \omega_{SB_n}\sin\omega_T t}{\omega_T^2 - \omega_{SB_n}^2}\right)\right] \qquad \text{(F.9)}$$
$$+ M_b \sin\omega_T t\left(6a_3 + 24a_4 x\right)$$

$$\frac{\partial^5 w}{\partial x^5} = \sum_{n=1}^{\infty}\left[\left(\frac{n\pi}{L}\right)^5 C_n \cos\frac{n\pi x}{L}\frac{M_b}{\omega_{SB_n}}\left(\frac{\omega_T \sin\omega_{SB_n} t - \omega_{SB_n}\sin\omega_T t}{\omega_T^2 - \omega_{SB_n}^2}\right)\right] \qquad \text{(F.10)}$$

Substitution of these terms into (F.6) gives

$$\begin{aligned}\gamma_b = \frac{Et_1}{2G}\left(\frac{2D}{gEt_1t_2(1+t_1/t_2)}\right)\Bigg\{&\sum_{n=1}^{\infty} C_n \cos\frac{n\pi x}{L}\Bigg[\frac{\rho t}{D}\frac{n\pi}{L}\frac{M_b}{\omega_{SB_n}} \times \\ &\left[\frac{-\omega_{SB_n}^2\,\omega_T \sin\omega_{SB_n} t + \omega_T^2\,\omega_{SB_n}\sin\omega_T t}{\omega_T^2 - \omega_{SB_n}^2}\right] \\ &+\left[\left(\left(\frac{n\pi}{L}\right)^5 - gY\left(\frac{n\pi}{L}\right)^3\right)\frac{M_b}{\omega_{SB_n}}\left[\frac{\omega_T \sin\omega_{SB_n} t - \omega_{SB_n}\sin\omega_T t}{\omega_T^2 - \omega_{SB_n}^2}\right]\right]\Bigg] \\ &+M_b \sin\omega_T t\left[-gY(6a_3 + 24a_4x) - \frac{\rho t}{D}\omega_T^2\left(a_1 + 2a_2x + 3a_3x^2 + 4a_4x^3\right)\right]\Bigg\}\end{aligned} \qquad \text{(F.11)}$$

Appendix G - *Determination of Improved Treatment Parameters h, s, t, and the Cross-Section*

In designing the improved treatment, one of the limiting constraints was that "off-the-shelf" parts must be used. This requirement limits the number of choices of constraining layer thickness t and the cross-section to the following choices:

t: Since aluminum was chosen, the reasonable choices for thickness were 0.025", 0.032", and 0.040". Thinner sheets required special ordering, and thicknesses greater than 0.040" possess unacceptably high bending stiffnesses.

cross-section: The AFIT shop had several thick sheet sizes and a beam whose cross-section measured 0.125" x 0.75". The sheet sizes considered to be reasonable were 0.062", 0.080", and 0.090". Of course, the other dimension could be arbitrarily chosen, so there were actually an infinite number of choices. Since the task of choosing a cross-section was considered peripheral, the field of choices was arbitrarily narrowed to the following:

Cross-Section 1: 0.062" x 0.75"
Cross-Section 2: 0.080" x 0.75"
Cross-Section 3: 0.090" x 0.75"
Cross-Section 4: 0.090" x 1.0"
Cross-Section 5: 0.125" x 0.75".

Some rough calculations showed that the optimal range of values for h and s were 4"-8" and 1.0"-1.5", respectively. The choices for h and s were chosen to be the following:

h: 5", 6", and 7"
s: 1.0", 1.25", and 1.5"

The total number of configurations, then, was 135. The total width of the sandwich beams was backed out by using the constraint of maximum weight of (levers + sandwich beams) = 1.0 lb. However, the proportion of the width in each bay is another variable, which complicates matters even further.

The general approach of choosing the "best" configuration was the elimination of one variable at a time. Finite element modeling was chosen as the tool for the process. Basically, one parameter was varied in a nominal configuration while all other variables (except b_i) were held constant. The particular widths b_1 and b_2 were assigned widths of

$0.7b_{total}$ and $0.3b_{total}$, respectively. The key parameter in the elimination of each variable was the ratio of

$$r = \frac{\sum \text{elastic strain energy in the sandwich beam elements}}{\sum \text{elastic strain energy in all other elements (levers + truss)}}$$

To fix parameter i, several configurations were tested where the only difference between them was the value of parameter i. The configuration which had the highest value of r was chosen, and the process was repeated for next parameter. Parameter i was then held constant for the remainder of the study.

One of the peculiarities of the I-DEAS software is its inability to allow the user to bring two beam elements together to a pin-jointed connection. The use of multi-point degree-of-freedom constraints is required, which involves the creation of nearly coincident nodes that are constrained to have the same values for the desired DOF. The software continued to show a non-zero moment at the end of a simply supported beam (intuitively an impossibility). The result of this discrepancy was a linearly varying value of strain energy in the eight elements that comprise the sandwich beam. This makes no sense, so a moment of equal magnitude and opposite sense had to be administered to enforce the condition of zero moment at the lever tip. This correction resulted in a uniform distribution of strain energy over the length of the sandwich beam. Although the actual distribution of strain energy is non-uniform (governed by the beam-column effect of the sec $^{kL}/_{2}$ phenomenon), the expected result from the model is uniform because the solver uses linear strength of materials theory (which assumes circular curvature for equal moments applied at both ends of an element).

Some configuration choices, upon closer review, were ruled out immediately or were eliminated because of too high a value of $^{kL}/_{2}$ (which produces unacceptable asymmetry of cycle halves). A discussion of the $^{kL}/_{2}$ phenomenon is in Chapter 5.

The following is a list of judgments that eliminated possible configurations. For t, the choice was rather simple. $t = 0.025$" caused excessive deflections ($^{kL}/_{2}$ was too high), while 0.040" was too stiff, not allowing adequate bending deflections. Hence, $t = 0.032$" was chosen.

In choosing the cross-section, it was determined that 4 and 5 were excessively beefy and merely reduced the sandwich beam widths because of their weight. Cross-section 1 was eliminated because it is dubiously flimsy in bending out of its own plane. A combined torsion-bending motion might easily cause lateral instability of such a thin cross-section.

Cross-sections 2 and 3 were tested in I-DEAS, and number 2 resulted in a higher value of the ratio r.

Since the choices of h and s are so heavily coupled, they were varied simultaneously. Two test case finite element models were run to investigate the extreme values of $h = 5"$ and $s = 1"$. The solution indicated that choosing $h = 5"$ does not offer enough lever tip displacement, while choosing $s = 1"$ results in unacceptably high values of $^{kL}/_{2}$ for h equal to 6" or 7". Therefore, the following five models were chosen as candidate configurations based on the individual advantages of each. The models were the following:

Model 1: $h = 5"$, $s = 1"$,
Model 2: $h = 6"$, $s = 1"$,
Model 3: $h = 6"$, $s = 1.25"$,
Model 4: $h = 7"$, $s = 1.25"$, and
Model 5: $h = 7"$, $s = 1.5"$.

Model 4 produced the highest ratio r and was thus declared the winner. Finally, a simple test was run between three models (configured like model 4) whose only difference was the distribution of the total sandwich beam width b_{tot} between bays 1 and 2. The three distributions were $^{65}/_{35}$ (65% in bay 1 and 35% in bay 2), $^{70}/_{30}$, and $^{75}/_{25}$. The $^{70}/_{30}$ configuration produced the highest ratio r, although this particular test produced very small differences in the strain energy distribution in the system. The final configuration is then

long lever length $h = 7$ in.
short lever length $s = 1.25$ in.
sandwich plate thickness $t_1 = 0.032$ in.
cross – section $= 0.75$ in. $\times$ 0.080 in.
wide sandwich beam width $b_1 = 5.4$ in.
slim sandwich beam width $b_2 = 2.3$ in.

Appendix H - *MATLAB function file LOSS*

For this program, the input *P* represents the tip load given by the finite element model. The FE model was loaded like the figure shown at the beginning of chapter 5.

```
function [sse,energy]=loss(z)
% LOSS(z) calculates the energy dissipated per cycle in a sandwich beam due to
% induced shear and moment. For a 1 X 12 vector z whose inputs are [E, G*, t1, t2, s, P,
% omegsb, omegt, L, rhot, b, 4-digit model#], LOSS(z) returns the value of the definite
% integral of total (shear strain)^2 over the area of the SB and the corresponding energy
% dissipated per cycle.

E=z(1);
G=z(2);
t1=z(3);
t2=z(4);
s=z(5);
P=z(6);
omegsb=z(7);
omegt=z(8);
L=z(9);
rhot=z(10);
b=z(11);

g=2*G/(E*t1*t2)
D=E*t1^3/(6*.8911)
Y=(t1+t2)^2*E*t1/(2*D)

a1=(12*L-g*Y*L^3)/(24*D)
a2=-1/(2*D)
a3=g*Y*L/(12*D)
a4=-g*Y/(24*D)

vnsq=2/(L*((pi/L)^2+g))

capc1=-g*L^2/pi*a1
capc2=-a2*(L/pi*(g*L^2+4)+4*g*(L/pi)^3)
capc3=-a3*((6*L-g*L^3)*L/pi+6*g*L*(L/pi)^3)
capc4=-a4*((12*L^2-g*L^4)*L/pi+(12*g*L^2-48)*(L/pi)^3-48*g...
*(L/pi)^5)
capc5=(1+Y)*L/pi*2*g^2*Y/D

capc=vnsq*(omegt^2*(capc1+capc2+capc3+capc4)+capc5)

gamtco1=D*(P*s/b)/(G*g*(t1+t2))
gamtco2=((pi/L)^5-g*Y*(pi/L)^3)/(omegt^2-omegsb^2)
gamtco3=rhot*omegt^2/D

gamsco=(P/b)/(sqrt(g)*E*t1*t2)/((-tanh(sqrt(g)*L/2)...
*cosh(sqrt(g)*L)+sinh(sqrt(g)*L)))

hiterm=gamtco1*g*Y*6*a3
```

```
dx=.2;
n=1;
x=.1;
uintgrl=0;
intgrl=0;


while n<65

 gamt(n)=gamtco1*(capc*gamtco2*cos(pi*x/L)-g*Y*(6*a3+24*a4*x)...
    +gamtco3*(capc*pi/(L*(omegt^2-omegsb^2))*cos(pi*x/L)...
     -(a1+2*a2*x+3*a3*x^2+4*a4*x^3)));
 gams(n)=gamsco*(cosh(sqrt(g)*x)-tanh(sqrt(g)*L/2)...
    *sinh(sqrt(g)*x));
 gamtotal(n)=gamt(n)+gams(n);
 uenrgy(n)=dx*(real(gamtotal(n)))^2;
 senrgy(n)=dx*(abs(gamtotal(n)))^2;
 uintgrl=uintgrl+uenrgy(n);
 intgrl=intgrl+senrgy(n);
 uruntot(n)=uintgrl;
 runtotal(n)=intgrl;
 x=x+dx;
 n=n+1;
end


enrgy1=uenrgy';
enrgy2=senrgy';
enrgymat=[enrgy1 enrgy2];
urun=uruntot';
run=runtotal';
runmat=[urun run];

energy=pi*imag(G)*t2*intgrl
benergy=b*energy
uenergy=.5*real(G)*t2*uintgrl
buenergy=b*uenergy

gamt(1)
gamt(32)
gamt(64)
r=.1:.2:12.7;
clg;
plot(r,gamt)
grid
title(['Bending Shear Strain (rad), t2 = ',num2str(z(4)),' in.'])
```

Appendix I - *Experimental Results of Damping Tests - Raw Data*

Test	Resp.	Excit.	f1	% 1	f2	% 2	f3	% 3	f4	% 4	f5	% 5	f6	% 6	details
1	1R	0.8	1.247	1.38	5.72	0.717	7.623	0.7697	14.77	1.425			27.3	1.877	4K,4,sharp 0-50
2	1R	1	1.251	1.948	5.798	0.993	7.477	0.2479	14.41	1.761					2K,3,slow,0-20
3	1R	1	1.252	1.95	5.799	0.997	7.482	0.1968	14.41	0.162					2K,3,sharp,0-20
4	1R	0.6	1.28	2.714	5.795	0.916	7.472	0.2492	14.5	2.351					2K,3,sharp,0-20
5	1R	0.4	1.296	2.32	5.796	0.802	7.481	0.2055	14.56	2.391					2K,5,sharp,0-20
6	1R	-0.2			5.797	0.92	7.443	0.1064	14.61	2.136			26.16	1.236	4K,4,sharp,0-50
7	1R	MSB1	1.3	2.915	5.802	0.918	7.563	0.1126	14.59	2.382	20.825	0.6642	26.12	1.311	4K,4,sharp,0-50
8	1R	.4R	1.238	2.224	5.8	0.891	7.483	0.2068	14.52	1.824	20.528	0.9765	26.69	1.841	4K,4,sharp,0-50
9	1R	.6R	1.258	2.028	5.796	0.868	7.486	0.1981	14.4	1.406	20.265	0.6698	25.95	0.6085	4K,4,sharp,0-50
10	1	.6R			5.662	0.611	7.594	0.1826	14.41	1.571			26.19	0.865	4K,4,sharp,0-50
11	1	0.6	1.24	2.179	5.801	0.9			14.4	1.599			26.12	1.538	4K,4,sharp,0-50
12	1	0.4	1.275	2.01	5.807	0.936			14.41	1.402			26.15	1.663	4K,4,sharp,0-50
13	1	0.6	1.25	2.128	5.799	0.971			14.38	1.49					4K,3,slow,0-20
14	1	0.4	1.251	2.265	5.8	0.976			14.41	1.652					4K,3,slow,0-20
15	1	0.2	1.257	2.32	5.799	0.972	7.574	0.162	14.4	1.301					4K,3,slow,0-20
16	1	0.8	1.254	1.921	5.807	0.864			14.4	1.474					2K,3,slow,0-20
17	1	0.8	1.253	2.012	5.813	0.886			14.4	1.475			26.09	1.305	2K,3,slow,0-50
18	1	1	1.257	1.889	5.807	0.851			14.4	1.484					2K,3,slow,0-20
19	1	1	1.254	1.954	5.807	0.869			14.41	1.554			26.39	0.2693	2K,3,sharp,0-50
20	1	1			5.811	0.738			14.36	1.238			26.12	1.451	2K,3,sharp,0-50
21	1	0.6	1.261	1.89	5.81	0.854			14.43	1.329			26.11	1.372	2K,3,sharp,0-50
22	1	0.6	1.259	1.789	5.809	0.842			14.43	1.184					2K,3,slow,0-20
23	1	-0.4	1.26	1.849	5.811	0.854			14.37	1.101					2K,3,slow,0-20
24	1	-0.4			5.829	0.819			14.42	1.298			26.14	1.206	4K,3,sharp,0-50
25	0.8	0.8							14.44	1.239			26.12	1.521	4K,3,sharp,0-50
26	0.8	0.8	1.258	1.684					14.45	1.425					2K,3,slow,0-20
27	0.6	0.6			5.823	0.862			14.49	1.572					2K,3,slow,0-20
28	0.6	0.6			5.827	0.93			14.46	1.8			26.28	1.435	4K,3,sharp,0-50
29	0.4	0.4			5.83	0.871			14.48	1.493			26.15	1.345	4K,3,sharp,0-50
30	1R	1R	1.258	1.865	5.806	0.856	7.493	0.2691	14.44	1.847					2K,3,slow,0-20
31	1R	1R			5.81	0.869	7.5	0.2277	14.47	1.698			26.27	1.383	4K,3,sharp,0-50
32	1R	.6R	1.249	2.101	5.82	0.64	7.497	0.218	14.38	1.309			26.61	0.4365	4K,3,sharp,0-50
33	1R	.6R	1.261	1.948	5.812	0.878	7.491	0.2489	14.42	1.278					2K,3,slow,0-20
34	1R	BSB1Y					7.504	0.2133							2K,3,slow,0-20
35	1R	BSB1Y					7.506	0.2166					26.31	1.187	4K,3,sharp,0-50
36	BSB1Y	.6R					7.527	0.237					26.46	0.5405	4K,3,sharp,0-50
37	BSB1Y	.6R	1.261	1.513			7.523	0.2701							2K,3,slow,0-20
38	BSB1Y	BSB1Y					7.53	0.2173							2K,3,slow,0-20
39	BSB1Y	BSB1Y													

Table I.1 Damping Tests, Improved Treatment, t2 = 0.005"

Test	Resp.	Excit.	f1	% 1	f2	% 2	f3	% 3	f4	% 4	f5	% 5	f6	% 6	details
1	1	0.6	1.219	1.518	5.719	1.138			14.17	2.581					1K,5,slow,0-20
2	1	0.8	1.219	1.72	5.741	1.026			14.19	2.421			25.77	3.436	1K,5,slow,0-50
3	1	0.4	1.22	1.612	5.718	1.148			14.18	2.23			26.05	2.716	2K,5,slow,0-50
4	1	MSB1	1.222	1.656	5.718	1.115			14.16	2.48			25.98	3.2	2K,5,slow,0-50
5	1	0.6	1.22	1.527	5.718	1.109			14.18	2.419			25.82	2.867	2K,5,sharp,0-50
6	1	MSB1	1.222	1.628	5.719	1.116			14.18	2.508			25.92	2.811	2K,5,sharp,0-50
7	1	0.2	1.216	1.346	5.716	1.096			14.18	2.451			26.04	3.235	2K,5,sharp,0-50
8	.2R	.6R			5.755	1.015	7.543	0.16	14.2	2.052	22.08	0.2302	25.62	2.456	2K,5,sharp,0-50
9	.2R	1R			5.74	1.145	7.502	0.1776	14.19	1.55					2K,5,sharp,0-20
10	.2R	1R			5.748	1.203	7.504	0.1987	14.17	1.617			25.9	0.6736	2K,5,sharp,0-50
11	.2R	1			5.748	1.125	7.477	0.0708	14.22	2.504			25.85	2.723	2K,5,sharp,0-50
12	SB1M	0.8	1.228	1.599	5.772	0.758			14.22	2.504					2K,5,slow,0-50
13	SB1M	1	0.123	1.555	5.751	1.142			14.23	2.515					2K,5,slow,0-50
14	SB1M	1	0.122	1.34	5.748	1.14			14.26	2.573			25.96	3.323	2K,5,sharp,0-50
15	0.2	1			5.746	1.096			14.23	2.4			26.04	3.068	2K,5,sharp,0-50
16	.6RY	1RY		IN PLANE BENDING 1, f = 21.556, % = .1852											2K,5,sharp,0-50
17	.6R	.4R			5.791	0.73	7.505	0.1987	14.13	2.706	20.278	0.2937	25.97	0.6751	2K,5,sharp,0-50
18	.6R	.4R	1.206	1.614	5.773	0.997	7.499	0.1811	14.11	2.571	20.294	0.2755	25.97	0.666	2K,5,sharp,0-50
19	.6R	.2R			5.762	0.885	7.501	0.1753	14.16	2.53	20.317	0.2649	26.02	0.4231	2K,5,sharp,0-50
20	1R	.6R			5.838	1.114	7.513	0.1628	14.23	2.073	20.187	0.2859	25.95	0.524	2K,5,sharp,0-50
21	1R	.4R	1.186	3.636	5.754	1.245	7.489	0.1655	14.22	1.509	20.247	0.4452	25.94	0.4773	2K,5,sharp,0-50
22	1R	1L			5.778	1.256	7.486	0.1796	14.26	1.391	20.235	0.4097	25.93	0.4235	2K,5,sharp,0-50
23	1R	1L	1.221	1.834	5.732	1.207	7.475	0.2025	14.26	1.58	20.137	0.2625	25.93	0.4821	2K,5,slow,0-50
24	1R	.4R	1.221	1.751	5.743	1.155	7.482	0.1799	14.25	2.507	20.262	1.146	25.91	0.6057	2K,5,slow,0-50

Table I.2 Damping Tests, Improved Treatment, t2 = 0.015"

Test	Resp.	Excit.	f1	% 1	f2	% 2	f3	% 3	f4	% 4	f5	% 5	f6	% 6	details
1	1	0.8	1.235	1.855	5.741	1.119			14.154	2.706					2K,3,slow,0-20
2	1	0.8	1.242	1.112	5.779	0.894			14.103	2.547			25.983	3.036	4K,3,sharp,0-50
3	1	1	1.178	0.977	5.737	0.946			14.236	2.49			26.393	2.763	4K,3,sharp,0-50
4	1	1	1.236	1.729	5.731	1.247			14.176	3.022					2K,3,slow,0-20
5	1	1	1.236	1.689	5.729	1.192			14.217	2.885			26.638	0.777	4K,3,sharp,0-50
6	1	0.6	1.238	1.677	5.733	1.196			14.109	2.834					2K,3,slow,0-20
7	1	0.6	1.246	1.405	5.729	1.712			14.209	2.65					2K,3,slow,0-20
8	1	-0.4	1.251	1.097	5.72	1.11			14.179	2.561			25.944	2.862	4K,3,sharp,0-50
9	1	-0.4	1.239	1.683	5.732	1.133			14.074	2.134					2K,3,slow,0-20
10	0.8	0.8	1.245	2.118					14.105	3.037					2K,3,slow,0-20
11	0.8	0.8							14.199	3.359			26.033	2.001	4K,3,sharp,0-50
12	0.6	0.6							14.028	2.052					2K,3,slow,0-20
13	0.6	0.6	1.239	1.522	5.744	1.126			14.27	1.763					2K,3,slow,0-20
14	0.4	0.4			5.748	1.495			14.308	2.394			25.813	2.881	4K,3,sharp,0-50
15	1R	1R	1.239	1.468	5.742	1.187			14.313	2.355			25.977	0.961	4K,3,sharp,0-50
16	1R	1R	1.241	1.696	5.727	0.898	7.47	0.179	14.093	3.064	20.534	0.482	25.431	0.374	4K,3,sharp,0-50
17	1R	.6R	1.237	1.885	5.272	1.042	7.474	0.219	14.029	0.307					2K,3,slow,0-20
18	1R	.6R	1.246	1.868	5.747	0.859	7.477	0.184	14.309	2.204	20.427	0.367	25.357	0.554	4K,3,sharp,0-50
19	1R	BSB1Y			5.739	1.028	7.48	0.18	13.644	0.738	20.392	0.363	25.308	0.679	4K,3,sharp,0-50
20	1R	BSB1Y			5.721	1.176	7.475	0.178	13.61	0.687					2K,3,slow,0-20
21	BSB1Y	.6R					7.504	0.166	13.498	0.762					2K,3,slow,0-20
22	BSB1Y	.6R					7.505	0.179	13.51	0.705			25.164	0.84	4K,3,sharp,0-50
23	1R	BSB2Y			5.728	1.097	7.478	0.178	13.555	1.379	20.526	0.136	25.205	0.801	4K,3,sharp,0-50
24	1R	BSB2Y	1.254	1.641	5.727	1.15	7.477	0.175	13.685	0.687					2K,3,slow,0-20

Table I.3 Damping Tests, Improved Treatment, t2 = 0.030"

Test	Resp.	Excit.	f1	% 1	f2	% 2	f3	% 3	f4	% 4	f5	% 5	f6	% 6	details
1	1	1	1.053	4.766	6.318	6.644			18.061	8.085					1K,3,slow,0-20
2	1	1			6.317	5.948			17.912	6.579			33.905	7.532	2K,3,sharp,0-50
3	1	1	1.051	4.663	6.352	6.864			19.239	4.193					1K,3,slow,0-20
4	1	1	1.05	4.881	6.345	6.838			18.467	8.279					1K,3,slow,0-20
5	1	1			6.375	6.177			17.927	6.933			34.082	7.477	2K,3,sharp,0-50
6	1	1			6.331	6.707			17.971	6.951			34.101	7.422	2K,3,sharp,0-50
7	1	0.8	1.056	4.51					17.97	5.693					1K,3,slow,0-20
8	1	0.6	1.073	3.272	6.339	6.441			17.887	7.265					2K,3,sharp,0-50
9	1	0.4			6.367	6.845			17.958	6.848			34.01	7.616	2K,3,sharp,0-50
10	1	0.2			6.377	6.475			17.968	6.994			33.989	7.342	2K,3,sharp,0-50
11	0.8	0.4	1.064	4.082					17.776	6.655					1K,3,slow,0-20
12	0.6	1	0.862	4.56	6.368	6.676			17.958	7.177			33.968	7.349	2K,3,sharp,0-50
13	0.4	0.2			6.318	6.302			17.966	7.064			33.794	7.493	2K,3,sharp,0-50
14	0.8	0.2							17.964	7.106			33.983	7.353	2K,3,sharp,0-50
15	1R	1R	1.052	4.135			6.544	1.021							1K,3,slow,0-20
16	1R	1R	1.053	4.365			6.545	1.002							1K,3,slow,0-20
17	1R	.77R	1.081	5.257			6.54	0.578	17.994	5.774	20.127	1.763	35.262	2.524	2K,3,sharp,0-50
18	1R	.77R	1.083	4.358			6.553	0.634	18.043	6.113	20.142	1.488	35.205	5.2	2K,3,sharp,0-50
19	1R	.5R	1.074	4.812			6.553	0.628	18.193	6.539	20.192	1.575	35.13	4.867	2K,3,sharp,0-50
20	1R	.52R	1.075	5.16			6.545	0.468			20.106	1.677			2K,3,sharp,0-50
21	1R	.52R	1.099	4.965			6.542	0.491			20.108	1.73	34.933	1.477	2K,3,sharp,0-50
22	.7R	1R	1.056	2.602			6.549	0.578	17.994	6.06	19.954	2.096	35.407	3.155	2K,3,sharp,0-50
23	.5R	1R					6.55	0.526			20.053	1.888	35.099	1.132	2K,3,sharp,0-50
24	1Y	1RY		IN PLANE BENDING - f = 20.394 HZ, % = .7562											
25	1Y	1RY		IN PLANE BENDING - f = 20.390 HZ, % = .7376											

Table I.4 Damping Tests, Conventional Treatment, t2 = 0.005"

Bibliography

[1] Torvik, P. J. and B. J. Lazan. "A Corrugated Addition for Increased Damping in Flexure," AFML-TR-64-73, Air Force Materials Laboratory, Wright-Patterson Air Force Base, Ohio, 1964.

[2] Torvik, P. J. "The Analysis and Design of Constrained Layer Damping Treatments," AFIT-TR-80-4, Air Force Institute of Technology, Wright-Patterson Air Force Base, Ohio, 1980.

[3] Soovere, J. and M. L. Drake. *Aerospace Structures Technology Damping Design Guide, Volume I - Technology Review.* Technical Report AFWAL-TR-84-3089, Air Force Wright Aeronautical Laboratories, Wright-Patterson Air Force Base, Ohio, 1984.

[4] Soovere, J. and M. L. Drake. *Aerospace Structures Technology Damping Design Guide, Volume II - Design Guide.* Technical Report AFWAL-TR-84-3089, Air Force Wright Aeronautical Laboratories, Wright-Patterson Air Force Base, Ohio, 1984.

[5] Kerwin, E. M. "Damping of Flexural Waves by a Constrained Viscoelastic Layer," *Journal of the Acoustical Society of America, 31:* 952-962 (July 1959).

[6] Ungar, E. E. "Loss Factors of Viscoelastically Damped Beam Structures," Journal of the Acoustical Society of America, 34: 1082-1089 (August 1962).

[7] DiTaranto, R. A. "Theory of Vibratory Bending for Elastic and Viscoelastic Layered Finite Length Beams," *Journal of Applied Mechanics, 32:* 881-886 (December 1965).

[8] Mead, D. J. and S. Markus. "The Forced Vibration of a Three-Layer Damped Sandwich Beam With Arbitrary Boundary Conditions," *Journal of Sound and Vibration, 10:* 163-175 (September 1969).

[9] Yan, M. J. and E. H. Dowell. "Governing Equations for Vibrating Constrained Layer Damping Plates and Beams," *Journal of Applied Mechanics, 39:* 1041-1046 (October1972).

[10] Rao, D. K. "Static Response of Stiff-Cored Unsymmetric Sandwich Beams," *Journal of Engineering for Industry, 98:* 391-396 (April 1976).

[11] Rao, D. K. "Vibration of Short Sandwich Beams," *Journal of Sound and Vibration, 52:* 253-263 (May 1977).

[12] Whittier, J. S. "The Effect of Configurational Additions Using Viscoelastic

Interfaces on the Damping of a Cantilever Beam," Wright Air Development Center Technical Report 58-568, Wright-Patterson Air Force Base, Ohio (May 1959).

[13] Lazan, B. J. *et al.* "Multiple-Band Surface Treatments for High Damping," AFML-TR-65-269, Air Force Materials Laboratory, Wright Patterson Air Force Base, Ohio (September 1965).

[14] Plunkett, R. and Lee, C. T. "Length Optimization for Constrained Viscoelastic Layer Damping," JASA Vol. 48, No. 1, Part 2, 150-161 (July 1970).

[15] Bagley, R. L. and P. J. Torvik. "Fractional Calculus-A Different Approach to the Analysis of Viscoelastically Damped Structures," *AIAA Journal, 21:* 741-748 (May 1983).

[16] Morgenthaler, Daniel R. *Passive and Active Control of Space Structures, Volume 1: Damping Design Methodology.* WRDC-90-3044, Volume 1, Wright Research and Development Center, Wright-Patterson Air Force Base, Ohio (September 1990).

[17] Torvik, P. J. "Damping of Layered Materials." *30th AIAA/ASME/ASME/-ASCE/AHS/ASC Structures, Structural Dynamics and Materials Conference,* AIAA, April 1989. AIAA 89-1422.

[18] Mantena, P. Raju *et al.* "Optimal Constrained Viscoelastic Tape Lengths for Maximizing Damping in Laminated Composites," *AIAA Journal, 29:* 1678-1685 (October 1991).

[19] Gere, James M. and Stephen P. Timoshenko. *Mechanics of Materials* (Second Edition). Boston: PWS-KENT, 1984.

[20] Mindlin, R. D. and L. E. Goodman. "Beam Vibrations With Time-Dependent Boundary Conditions," *Journal of Applied Mechanics, 17:* 377-380 (December 1950).

[21] Meirovitch, Leonard. *Analytical Methods in Vibrations.* New York: Macmillan, 1967.

[22] Cottle, E. T. *Damping of Layered Beams with Mixed Boundary Conditions.* MS thesis, AFIT/GAE/ENY/90D-5. School of Engineering, Air Force Institute of Technology (AU), Wright-Patterson AFB, OH, December 1990 (AAE-3352).

[23] Nokes, David S. and Fredrick C. Nelson. "Constrained Layer Damping With Partial Coverage," *Shock and Vibration Bulletin, 38,Part 3:* 5-12 (November 1968).

Vita

Lt. Mark A. Scharpen was born on 20 Nov 1966 at Vandenberg AFB, California. He graduated from Columbia High School, Troutdale, Oregon in 1985 and entered the U. S. Air Force Academy that same year. He took a leave of absence for the 1987-88 school year and returned to graduate in May 1990 with a Bachelor of Science degree in engineering mechanics.

Upon leaving the Air Force Academy, he was assigned to Detachment 1, Ballistic Missile Organization at F. E. Warren Air Force Base, WY as a deployment engineer for the Peacekeeper Rail Garrison Program. Budget cuts resulted in the cancellation of the program in October 1990. He entered the School of Engineering, Air Force Institute of Technlogy, in May 1991.

Permanent Address:
5600 Peach Blossom Court
Springfield, OH 45502

REPORT DOCUMENTATION PAGE

Form Approved
OMB No. 0704-0188

1. AGENCY USE ONLY *(Leave blank)*	2. REPORT DATE	3. REPORT TYPE AND DATES COVERED
	Dec 92	Master's Thesis

4. TITLE AND SUBTITLE

Passive Damping of a Solar Array

5. FUNDING NUMBERS

6. AUTHOR(S)

Mark A. Scharpen, Lt, USAF

7. PERFORMING ORGANIZATION NAME(S) AND ADDRESS(ES)

Air Force Institute of Technology, WPAFB OH 45433-6583

8. PERFORMING ORGANIZATION REPORT NUMBER

AFIT/GA/ENY/92D-13

9. SPONSORING / MONITORING AGENCY NAME(S) AND ADDRESS(ES)

10. SPONSORING / MONITORING AGENCY REPORT NUMBER

11. SUPPLEMENTARY NOTES

12a. DISTRIBUTION / AVAILABILITY STATEMENT

Approved for Public Release; distribution unlimited

12b. DISTRIBUTION CODE

13. ABSTRACT *(Maximum 200 words)*

This study was an attempt to conceptualize, design, build, and test a constrained layer damping device that uses mechanical advantage for the purpose of increasing the damping of transient vibration of a five-bay planar truss. The aluminum truss was clamped to a fixed support and simulated a solar array. A conventional constrained layer treatment was designed, built, and tested to serve as a benchmark for comparison. For the conventional treatment, Plunkett and Lee's segmented constraining layer technique was used.

The improved device, two three-layer sandwich beams spanning the two bays nearest the built-in end, were supported several inches away from the truss plane by a series of levers that were designed to impart a combined shear and bending load to the beam ends. Mindlin and Goodman's method was used to solve a sixth-order, homogeneous differential equation of motion with time-dependent boundary conditions.

Experimental results showed that the sandwich beam device did not exceed the loss factors for any of the first four out-of-plane bending modes. However, measurable levels of system damping were achieved for all modes of interest, particularly at the mode whose frequency coincided with that of the sandwich beams.

14. SUBJECT TERMS

Damping, Viscoelasticity, Vibration, Dynamics, Solar Array, Structural Dynamics

15. NUMBER OF PAGES

138

16. PRICE CODE

17. SECURITY CLASSIFICATION OF REPORT	18. SECURITY CLASSIFICATION OF THIS PAGE	19. SECURITY CLASSIFICATION OF ABSTRACT	20. LIMITATION OF ABSTRACT
Unclassified	Unclassified	Unclassified	UL